

## GEOLOGY

# Reevaluating the evidence for a Hadean-Eoarchean dynamo

Cauê S. Borlina<sup>1\*</sup>, Benjamin P. Weiss<sup>1</sup>, Eduardo A. Lima<sup>1</sup>, Fengzai Tang<sup>2</sup>, Richard J. M. Taylor<sup>2</sup>, Joshua F. Einsle<sup>2,3,4</sup>, Richard J. Harrison<sup>2</sup>, Roger R. Fu<sup>5</sup>, Elizabeth A. Bell<sup>6</sup>, Ellen W. Alexander<sup>6</sup>, Heather M. Kirkpatrick<sup>6</sup>, Matthew M. Wielicki<sup>7</sup>, T. Mark Harrison<sup>6</sup>, Jahandar Ramezani<sup>1</sup>, Adam C. Maloof<sup>8</sup>

The time of origin of the geodynamo has important implications for the thermal evolution of the planetary interior and the habitability of early Earth. It has been proposed that detrital zircon grains from Jack Hills, Western Australia, provide evidence for an active geodynamo as early as 4.2 billion years (Ga) ago. However, our combined paleomagnetic, geochemical, and mineralogical studies on Jack Hills zircons indicate that most have poor magnetic recording properties and secondary magnetization carriers that postdate the formation of the zircons. Therefore, the existence of the geodynamo before 3.5 Ga ago remains unknown.

## INTRODUCTION

Determining the history of the geodynamo before 3.5 Ga ago is limited by the lack of a well-preserved Archean-Hadean rock record. However, the discovery of Hadean detrital zircon grains in metasediments of the Jack Hills, Western Australia (1), opens up the possibility of studying the magnetic history of Earth during its first billion years. In particular, primary ferromagnetic inclusions (e.g., magnetite) in the zircons may contain a thermoremanent magnetization (TRM) that records the paleointensity of the ancient field during primary cooling (2–5).

To preserve such a record, magnetite-bearing zircon crystals must have avoided being heated above magnetite's 580°C Curie temperature over their subsequent histories (3, 6). Furthermore, obtaining accurate paleointensity studies with well-determined ages for bulk zircon grains requires that the grains' natural remanent magnetization (NRM) be dominated by a TRM rather than a secondary crystallization remanent magnetization (CRM) carried by ferromagnetic inclusions formed or altered during aqueous alteration events after zircon crystallization (3, 6).

Two recent studies (7, 8) using single-crystal paleointensity analyses of Jack Hills zircon grains suggested that a geodynamo existed as early as 4.2 Ga ago with a surface field ~0.1 to 1 times that of present-day Earth. However, those studies (7, 8) had three main limitations: (i) The ages of the NRMs in the grains analyzed are unknown (3, 9); (ii) the grains were not shown to contain a TRM rather than a secondary CRM (6, 10, 11); (iii) the studies' grain selection criteria, which targeted grains with NRM intensities  $>10^{-12}$  Am<sup>2</sup>, might inadvertently have excluded zircons that would have recorded the absence of a dynamo (i.e., that carry no magnetization). In addition, there have been no independent studies corroborating their paleomagnetic measurements. The latter issue is particularly important

because Jack Hills zircons have some of the weakest magnetic NRMs measured in the history of paleomagnetism and therefore require exceptionally sensitive magnetometry techniques and stringent contamination controls. To further evaluate the evidence of an early dynamo and address these limitations, we conducted coupled paleomagnetic, geochemical, and mineralogical analyses on Jack Hills detrital zircon grains.

We extracted the zircon crystals from the pebble conglomerate that we sampled in 2012 at the Hadean zircon discovery locality at Erawandoo Hill [site W74 (3, 9)] using nonmagnetic techniques (see Materials and Methods). From these samples, 3754 zircons were washed with HCl acid and mounted in nonmagnetic epoxy, polished to approximately their midplanes, and dated using U-Pb chronometry. Grains found to have U-Pb ages older than 3.5 Ga (a total of 250) were analyzed using backscattered scanning electron (BSE) microscopy, cathodoluminescence (CL) imaging, and Li-ion imaging. BSE and CL images were used to assess the likelihood of secondary CRM by identifying zircon overgrowths, recrystallization zones, metamictization, cracks, and secondary deposits of minerals in void spaces (12). The goal of Li-ion imaging was to constrain the possibility of secondary TRM by providing estimates of the peak metamorphic temperatures experienced by zircons (11).

We defined a set of selection criteria that enables the identification of detrital zircon grains minimally affected by secondary TRM and CRM overprints (Fig. 1): (1) U-Pb age discordance <10% (see Materials and Methods); (2) lack of visible cracks, metamictization, and secondary deposits in BSE images and the presence of zonation in CL images interpreted as a primary igneous texture; and (3) presence of detectable primary Li zoning with thickness of <20 μm as observed by Li-ion imaging (11). Criterion (3) indicates the absence of TRM overprints acquired during  $\gtrsim$ 1 million years (Ma) long,  $\gtrsim$ 550°C metamorphic events under the assumption that natural Li diffusivity is similar to experimentally determined values (13). Note that these three criteria are based on measurements that only probe the polished surface of the grain (i.e., do not survey the full grain volume). Furthermore, the analytical methods used for criterion (2) are unable to resolve the <1-μm-diameter single-domain magnetite grains that would carry stable primary magnetization. Thus, these criteria likely are necessary but not sufficient requirements for identifying a zircon with primary NRM.

Of a total of 250 zircon grains, only 3 grains passed all of the above selection criteria. We selected these 3 grains, along with 53 grains

Copyright © 2020  
The Authors, some  
rights reserved;  
exclusive licensee  
American Association  
for the Advancement  
of Science. No claim to  
original U.S. Government  
Works. Distributed  
under a Creative  
Commons Attribution  
NonCommercial  
License 4.0 (CC BY-NC).

<sup>1</sup>Department of Earth, Atmospheric and Planetary Sciences, Massachusetts Institute of Technology (MIT), Cambridge, MA, USA. <sup>2</sup>Department of Earth Sciences, University of Cambridge, Cambridge, UK. <sup>3</sup>Department of Materials Science and Metallurgy, University of Cambridge, Cambridge, UK. <sup>4</sup>Department of Earth Science and Engineering, Imperial College London, London, UK. <sup>5</sup>Department of Earth and Planetary Sciences, Harvard University, Cambridge, MA, USA. <sup>6</sup>Department of Earth, Planetary, and Space Sciences, University of California, Los Angeles, Los Angeles, CA, USA. <sup>7</sup>Department of Geological Sciences, University of Alabama, Tuscaloosa, AL, USA. <sup>8</sup>Department of Geosciences, Princeton University, Princeton, NJ, USA.

\*Corresponding author. Email: caue@mit.edu

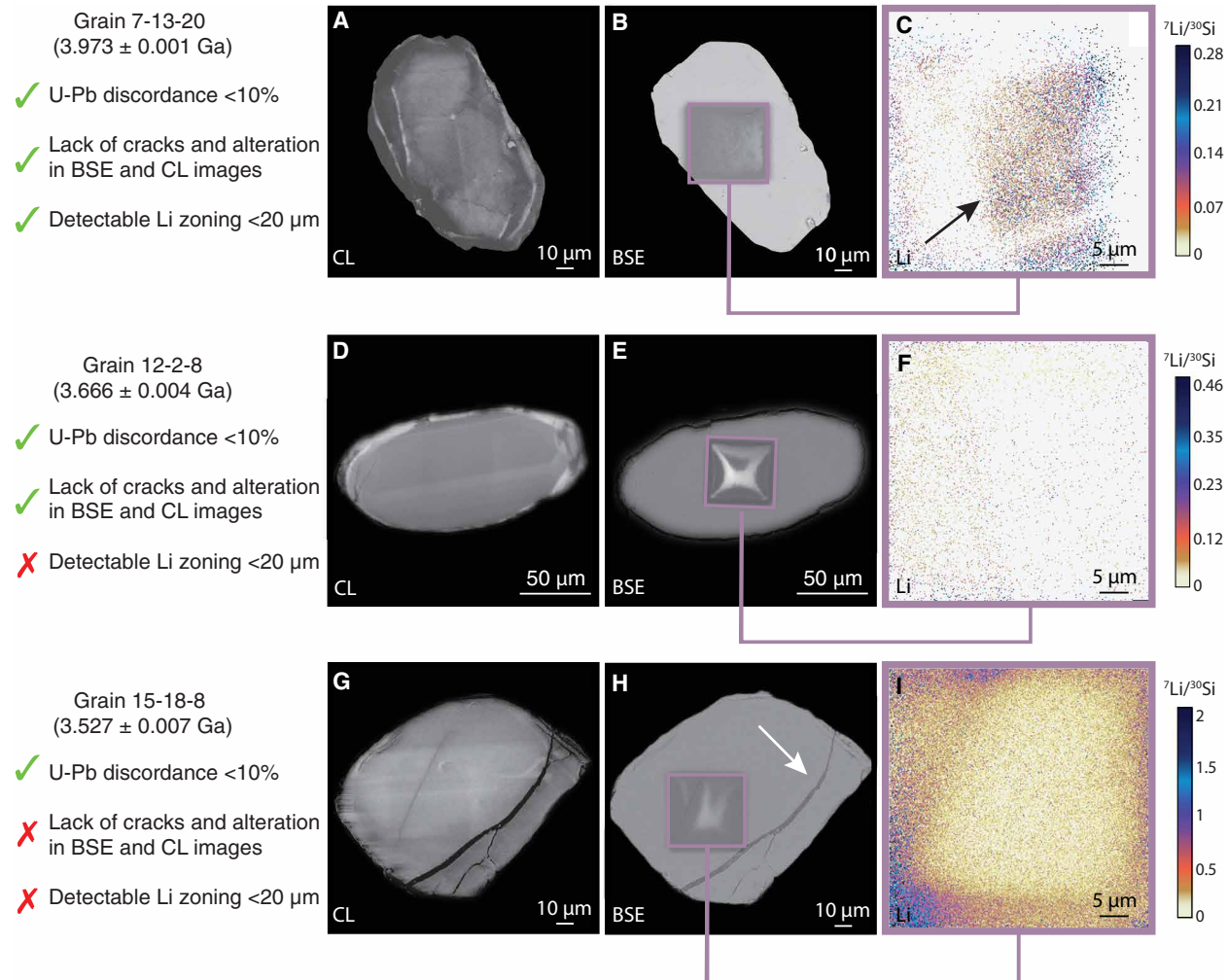


**Fig. 1. Examples of grains that pass and fail the selection criteria.** (A to C) Example of a zircon grain (7-13-20;  $3.973 \pm 0.001$  Ga) that passes all selection criteria: U-Pb age discordance <10%, presence of zonation in CL (A), no signs of secondary deposits on the exposed surface from BSE (B), and <20- $\mu\text{m}$ -thick Li zoning banding (black arrow), indicating that the sample may not have been fully thermally remagnetized since crystallization (C). (D to F) Example of a zircon grain (12-2-8;  $3.666 \pm 0.004$  Ga) that passes some of the selection criteria: U-Pb age discordance <10%, presence of zonation in CL (D), no signs of secondary deposits on the exposed surface from BSE (E), and no observed Li zonation (F). (G to I) Example of a zircon grain (15-18-8;  $3.527 \pm 0.007$  Ga) that fails most of the selection criteria: U-Pb age discordance <10%, absence of igneous zonation (G), presence of secondary mineral filling cracks at the lower right side of the grain (white arrow) (H), and no observed Li zonation (I).

that failed one or more criteria (including 13 subsamples from 6 grains; see Materials and Methods), for subsequent paleomagnetic studies. As a control to confirm that our polishing and ion and electron microprobe measurements do not fundamentally alter the zircons' NRMs, we also analyzed an additional 21 grains in their natural unpolished forms from the same host rocks using nonmagnetic methods, 4 of which were acid-washed. We conducted paleomagnetic analyses on a total of 77 grains.

Given the weak NRMs of the zircons (ranging between  $6.05 \times 10^{-15}$  and  $4.15 \times 10^{-12}$  Am $^2$  before demagnetization), their magnetic moments were analyzed using superconducting quantum interference device (SQUID) microscopy (see Materials and Methods) (14, 15). Following methods previously developed for the Bishop Tuff zircons (2), we obtained paleointensity estimates for the 77 grains using the in-field zero-field zero-field in-field (IZZI) double-heating protocol (16) with partial TRM (pTRM) alteration checks at every other heating step starting at 300°C.

We defined paleomagnetic quality criteria that are permissive compared with those of typical paleointensity studies of younger rocks (see the Supplementary Materials). This is because the overall goal of this study was to establish the presence or absence of a geodynamo at >3.5 Ga ago, which only requires paleointensities with order-of-magnitude uncertainties. Therefore, paleointensity estimates were considered acceptable when a sample (a) had a difference ratio sum  $\leq 25\%$  (17) and (b) gained a moment in the direction of the laboratory field during in-field steps with a maximum angular deviation  $\leq 15^\circ$  (18). Criterion (a) indicates that minimal thermochemical alteration occurred during the paleointensity experiments, while criterion (b) provides evidence that the sample can record an ancient field's direction and intensity (while not requiring the presence or absence of such a field when the zircon acquired its magnetic record). In summary, samples that pass our initial selection criteria and paleomagnetic criteria are candidates for providing a robust constraint on the dynamo at the time of their crystallization. Conversely, samples

with unstable NRM would either indicate the absence of a dynamo (if the sample passes the selection and paleomagnetic criteria) or that the sample is unsuitable for paleointensity experiments (either because of poor magnetic recording properties and/or sample alteration during laboratory heating). Following the paleointensity experiments, we analyzed selected grains with quantum diamond magnetometry (QDM) (19) coupled with transmission electron microscopy (TEM) to elucidate the origin of the magnetic sources within the grains.

## RESULTS

Of the 77 zircon grains analyzed for paleointensity estimations, only a total of 6 grains passed the two paleomagnetic criteria. We found that 63 of the 77 samples failed paleomagnetic criterion (a), indicating alteration during our experiments. In addition, we found that 54 samples have poor magnetic recording properties, as indicated by their failure of paleomagnetic criterion (b). Among the six grains that passed both paleomagnetic criteria, only two passed all five combined selection and paleomagnetic criteria (Fig. 2). Even if we were to exclude Li zonation as one of the selection criteria, there would be no additional grains that would pass the other selection and paleomagnetic criteria (13). In addition, our analyses of the unpolished control grains confirm that polishing the grains did not increase the incidence of alteration

during experiments or the magnetic recording quality (see the Supplementary Materials).

The two grains that passed the five combined criteria were sample 7-13-20, with a U-Pb age of  $3.973 \pm 0.001$  Ga, and sample 8-2-11, with a U-Pb age of  $3.979 \pm 0.007$  Ga. Figure 2 summarizes the selection process starting from the initial 3754 grains and ending at these 2 grains. Figures 3 and 4 show BSE, CL, Li, and paleomagnetic data for these two grains. The two grains each have at least two NRM components. Sample 7-13-20 (Fig. 3) has a low-temperature component that unblocked between room temperature and 200°C, a medium-temperature component that unblocked between 200° and 300°C, and a high-temperature component that unblocked between 300° and 580°C. Sample 8-2-11 (Fig. 4) has a low-temperature component that unblocked between room temperature and 510°C and a high temperature component that unblocked between 510° and 580°C. The 580°C peak demagnetization temperature of the NRMs for both samples indicates that the high-temperature components are carried by nearly pure magnetite.

Figure 5 shows an example of a grain that passes all of the selection criteria but fails all of the paleomagnetic criteria. Most of our grains present NRM demagnetization similar to the one in Fig. 5: unstable demagnetization, thermochemical alteration in the laboratory, and no in-field acquisition of remanence.

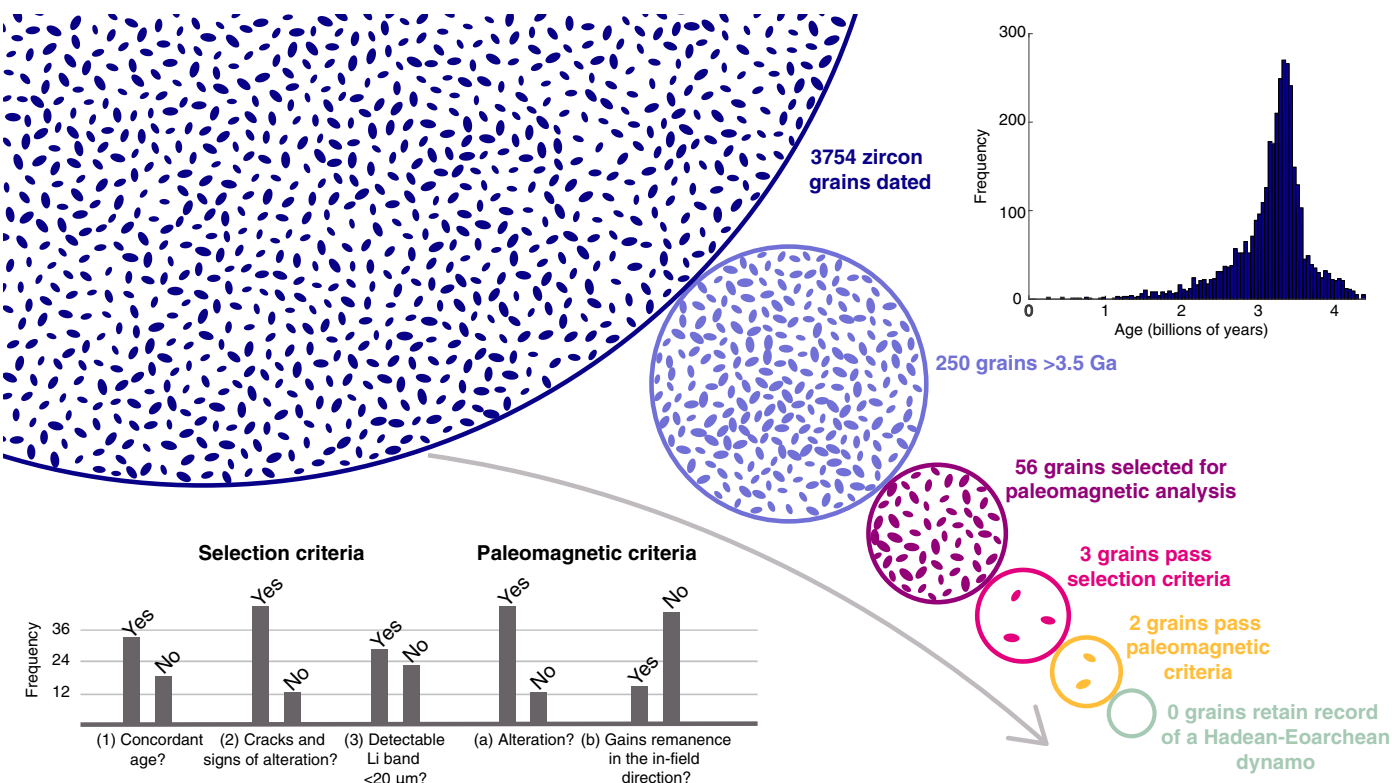


**Fig. 2. Summary of zircon selection from the initial 3754 dated grains.** Each circle shows the number of zircon grains remaining after each selection step. The histogram on the top right shows the measured age distribution of the 3754 grains. From the 250 grains that were older than 3.5 Ga, we selected all grains that passed all the selection criteria (3 grains) and an additional set of 53 grains. The histograms at the bottom left show the number of grains that satisfy the various selection criteria [(1) U-Pb age discordance  $<10\%$ ; (2) lack of visible cracks, metamictization, and secondary deposits; and (3) detectable primary Li zoning with thickness of  $<20 \mu\text{m}$ ] and paleomagnetic criteria [(a) the NRM component had a difference ratio sum  $\leq 25\%$ , and (b) the sample gained a moment in the direction of the laboratory field during in-field steps with a maximum angular deviation  $\leq 15^\circ$  over the same temperature range as the NRM component] for the 56 grains selected for paleomagnetic analysis. Only two grains pass all the selection and paleomagnetic criteria. In addition to the 56 polished grains shown here, 21 whole grains were also analyzed paleomagnetically as a control. No grain showed evidence for a Hadean-Eoarchean dynamo.

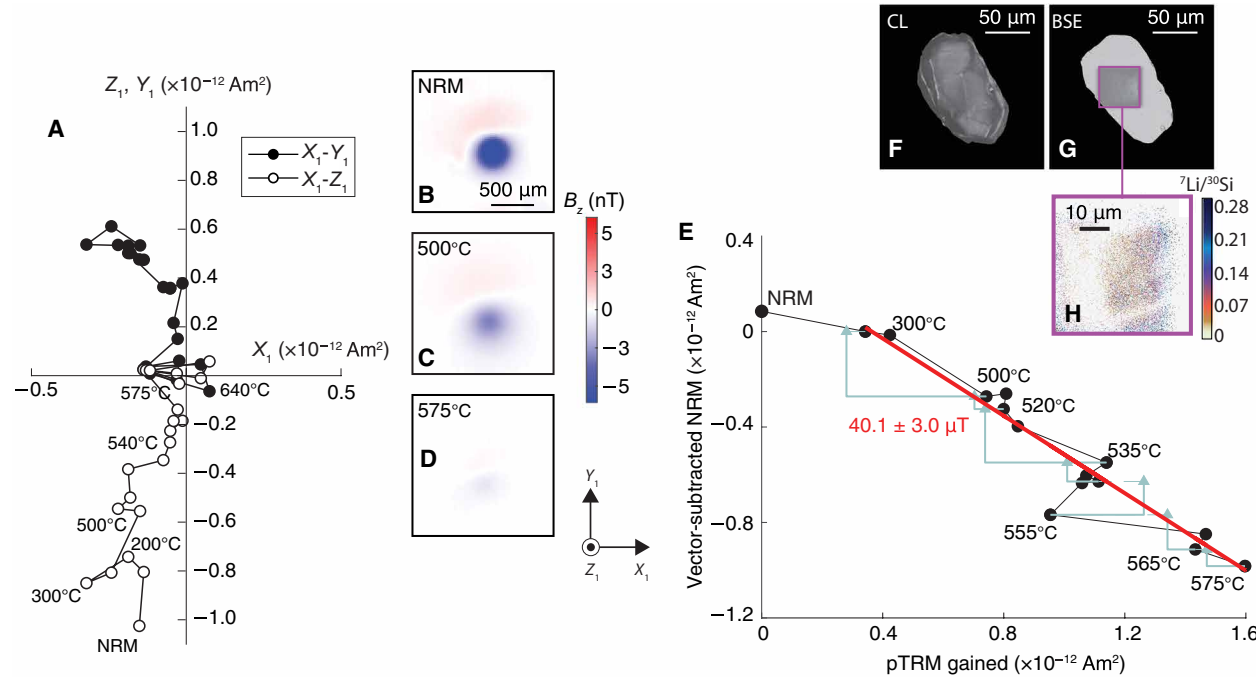


**Fig. 3. Paleomagnetic data for zircon grain 7-13-20 ( $3.973 \pm 0.001$  Ga) that passes all selection and paleomagnetic criteria. (A)** Orthographic projection of NRM vector endpoints during thermal demagnetization. Closed symbols show the  $X_1$ - $Y_1$  projection of the magnetization; open symbols show  $Z_1$ - $Y_1$  projection of the magnetization. Selected demagnetization steps are labeled. **(B to D)** Out-of-the-page magnetic field component ( $B_z$ ) maps measured at a height of  $\sim 360$   $\mu\text{m}$  above the grains obtained with the SQUID microscope for the NRM, 500°C, and 575°C steps. We use a “1” subscript on  $X_1$ ,  $Y_1$ , and  $Z_1$  to denote the fact that the grain orientations during the thermal demagnetization and paleointensity experiments are different from the grain orientations during the BSE, CL, and Li measurements and during the QDM measurements (Fig. 6). **(E)** Vector-subtracted NRM from the 300°C step versus pTRM grained during progressive laboratory heating. Blue triangles show pTRM checks. The red line shows the measurements used to compute paleointensity values (300° to 580°C). **(F to H)** CL, BSE, and Li images of the grains.

Subsequent to the paleointensity studies, grains 7-13-20 and 8-2-11 were analyzed in more detail to elucidate the nature and origin of their ferromagnetic inclusions. First, the isothermal remanent magnetization (IRM) of the samples was imaged with QDM (19) to determine the location of the magnetization sources (Fig. 6). Following this, we used TEM to investigate internal regions with the strongest magnetization. We found no evidence of primary ferromagnetic inclusions. Instead, we observed magnetite crystals (identified using Moiré diffraction interferometry) (10) growing inside voids fed by iron that diffused along the regions of intersecting dislocations. We also identified magnetite crystals with high aspect ratios, crystallographically aligned with the host zircon, and growing along dislocation cores [Fig. 6; see also (10)]. The alignment, aspect ratios, and locations of the magnetite grains within regions of recovery from accumulated radiation damage demonstrate that the grains are secondary in origin (20–22). No evidence has been put forth to support the speculation that they formed by exsolution and/or vapor deposition (8). The presence of secondary magnetite is not linked to alteration during laboratory heating steps, as demonstrated by the fact that these two grains passed paleomagnetic criterion (a) and that they contain voids with a diversity of shapes and sizes that commonly are empty or filled with phases other than magnetite, most commonly baddeleyite and ilmenite (23). The magnetite apparently formed as a result of natural fluid alteration at an unknown time during the last 3.9 Ga, at which time their bulk host zircons would have acquired a secondary CRM.

## DISCUSSION

The data presented here suggest that the vast majority of Jack Hills zircons are not suitable for paleointensity studies of the Hadean-Eoarchean magnetic field. In particular, only 2 of 77 grains passed our five selection and paleomagnetic criteria. These two grains yielded results similar to those previously reported for Jack Hills zircons (7, 8) and that were interpreted to be a record of a Hadean-Eoarchean dynamo: initial NRM intensities of  $\sim 1 \times 10^{-12}$   $\text{Am}^2$ , no signs of alteration, and stable NRM demagnetization exhibiting multiple components. However, close examination of both of our grains shows that their magnetic carriers are most likely secondary in origin. Therefore, the ages of their NRMs are unknown and certainly younger than their U-Pb ages. Their multicomponent NRMs are consistent with being CRMs overprinted by pTRMs because of heating events in the Jack Hills outcrop or else by younger CRMs. The presence of a CRM means that the thermal paleointensity experiments, which implicitly assume that the NRM is a TRM, will yield unreliable paleointensity values. We also note that unlike the previous studies (7, 8), we found that the majority of grains analyzed paleomagnetically have poor demagnetization and remagnetization behavior. In conclusion, the existence of the dynamo before 3.5 Ga has yet to be established.

We suggest that the difference in results between our study and that of (7, 8) may be due to our different measurement protocol, in which we washed the grains using concentrated (6 M) HCl to remove considerable amounts of secondary magnetic deposits before paleomagnetic

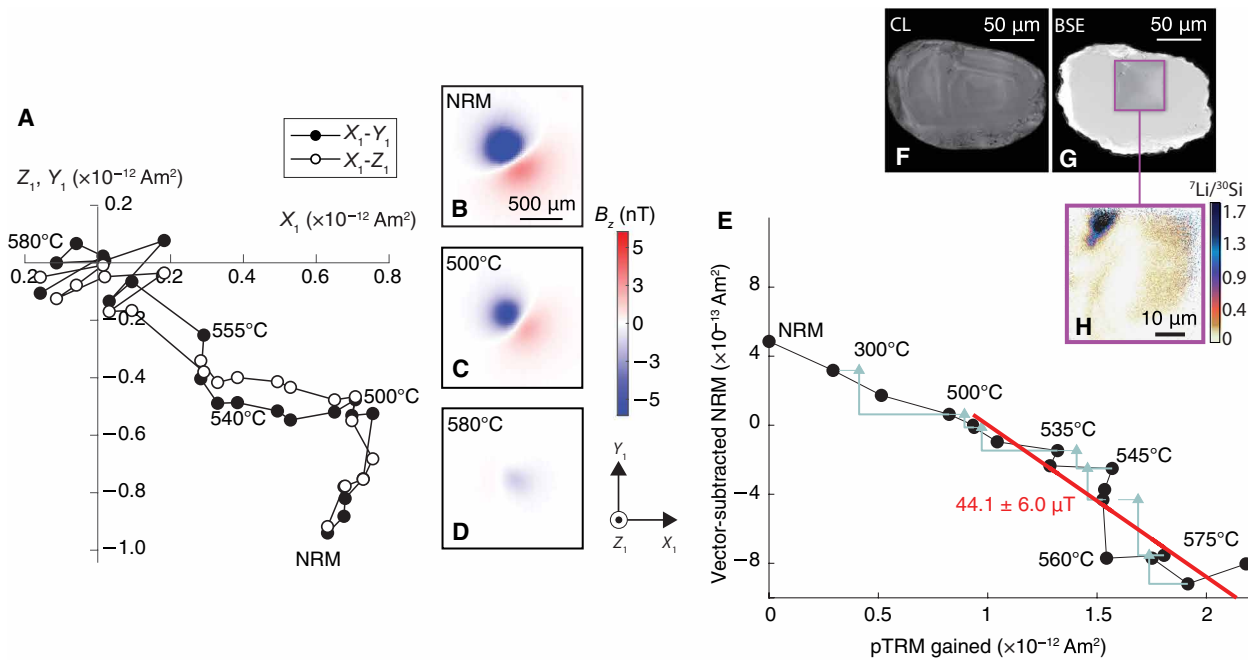


**Fig. 4. Paleomagnetic data for zircon grain 8-2-11 ( $3.979 \pm 0.007$  Ga) that passes all selection and paleomagnetic criteria.** (A) Orthographic projection of NRM vector endpoints during thermal demagnetization. Closed symbols show  $X-Y$  projection of the magnetization; open symbols show  $Z-Y$  projection of the magnetization. Selected demagnetization steps are labeled. (B to D) Out-of-the-page magnetic field component ( $B_z$ ) maps measured at a height of  $\sim 360$  μm above the grains obtained with the SQUID microscope for the NRM, 500°C, and 575°C steps. We use a “1” subscript on  $X_1$ ,  $Y_1$ , and  $Z_1$  to denote the fact that the grain orientations during the thermal demagnetization and paleointensity experiments are different from those during the BSE, CL, and Li measurements and during the QDM measurements (Fig. 6). (E) Vector-subtracted NRM from the 510°C step versus pTRM grained during progressive laboratory heating. Blue triangles show pTRM checks. The red line shows the measurements used to compute paleointensity values (510° to 580°C). (F to H) CL, BSE, and Li images of the grains.

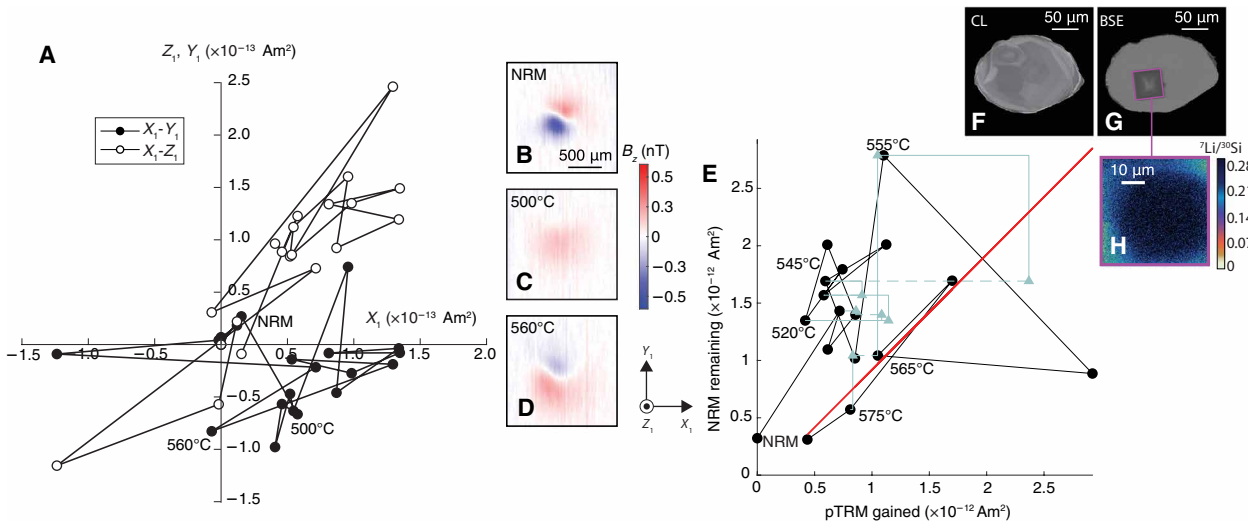


**Fig. 5. Paleomagnetic data for zircon grain 15-1-7 ( $4.094 \pm 0.005$  Ga) that passes the selection criteria but fails the paleomagnetic criteria.** (A) Orthographic projection of NRM vector endpoints during thermal demagnetization. Closed symbols show  $X-Y$  projection of the magnetization; open symbols show  $Z-Y$  projection of the magnetization. Selected demagnetization steps are labeled. (B to D) Out-of-the-page magnetic field component ( $B_z$ ) maps at a height of  $\sim 360$  μm above the grains obtained with the SQUID microscope for the NRM, 500°C and 580°C steps. We use a “1” subscript on  $X_1$ ,  $Y_1$  and  $Z_1$  to denote the fact that the grain orientations during the thermal demagnetization and paleointensity experiments are different from the grain orientations during the BSE, CL, and Li measurements. (E) NRM lost versus pTRM grained during progressive laboratory heating. Blue triangles show pTRM checks. Red line shows the measurements used to compute paleointensity values (550° to 580°C). (F to H) CL, BSE, and Li images of the grains.

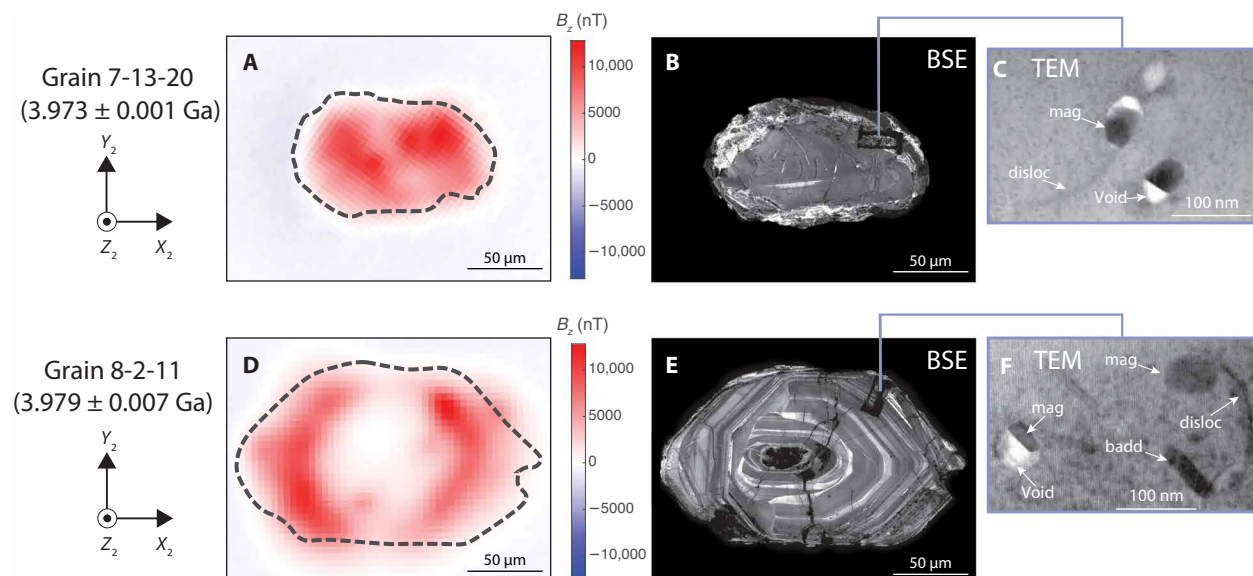


**Fig. 6. Magnetite grains located in dislocations and filling parts of voids postdating igneous formation of the zircon host.** (A to C) Zircon grain 7-13-20. (D to F) Zircon grain 8-2-11. (A and D) QDM maps of the out-of-the-page magnetic field component ( $B_z$ ) of an IRM applied to the grain used to locate magnetic sources at a height of  $\sim 5 \mu\text{m}$  above the samples. We use  $X_2$ ,  $Y_2$ , and  $Z_2$  to denote that the grain orientations for these measurements differ from those during the paleointensity experiments (Figs. 3 to 5). (B and E) BSE images of the grains. The grains were repolished after the paleomagnetic experiments and before these BSE images. Note the difference when compared with the earlier BSE images of the same grains in Figs. 3 and 4; the images here expose several cracks that were not previously visible. (C and F) TEM analyses conducted in the vicinity of the strongest magnetic region of the grain by extracting rectangular focused ion beam sections (from rectangular regions visible in the BSE images). Magnetite ("mag") grains are seen to be forming inside voids that intersect dislocations ("disloc") and growing along dislocation cores that formed during recovery. Magnetite commonly is associated with baddeleyite ("badd"), a secondary product formed after recovery from radiation damage (23), pointing to the fact that the magnetite crystals were not present in the zircon structure when the zircon crystal formed.

measurements, used high-sensitivity magnetic microscopy that enabled measurements of samples with up to 1000 times weaker NRMs, and used QDM and TEM to constrain whether the magnetic carriers are primary in origin. Elucidating the early evolution of the geodynamo may require as yet unidentified detrital minerals that are less prone to radiation damage.

## MATERIALS AND METHODS

### Source location of the samples

Our field work was conducted in the Jack Hills in 2002 and 2012. We separated zircons from five rock samples (named D175C, D175H, D175L, and Cong14c) collected at the Hadean zircon discovery site, location W74 (24), in the Jack Hills, Western Australia, Australia (1), during the 2012 field trip. Table S1 shows the sampling information about the bulk samples and the source material for the grains.

### Zircon separation from host rocks

The five rock samples were manually sledged to gravel size fragments in the Massachusetts Institute of Technology (MIT) Isotope Laboratory. These fragments then were pulverized in a Shatterbox using an all-ceramic grinding vessel and sieved to  $<500 \mu\text{m}$  grain size. The material then was mixed in water in a 4-liter beaker, and the suspended material ( $<5 \mu\text{m}$ ) was decanted; this wash process was repeated 15 times. The remaining sand- and silt-size fraction then was dried under a heat lamp (maximum temperature of  $45^\circ\text{C}$ ). The heavy-mineral aliquot was separated by immersion in a high-density liquid (methylene iodide; specific gravity, 3.32), followed by rinsing in acetone and air drying. Zircon grains then were handpicked under

a binocular microscope using nonmagnetic tweezers. Note that our separation procedures did not involve the standard use of a Frantz isodynamic separator for removing paramagnetic and ferromagnetic minerals, as the high magnetic field of the Frantz would otherwise alter any original NRM that might have been present in the grains.

### Ion and electron microprobe measurements

U and Pb isotopes, backscattered electron microscopy (BSE microscopy), CL, and Li-ion measurements were carried out in the UCLA Secondary Ion Mass Spectrometry (SIMS) Laboratory at the University of California, Los Angeles (UCLA). The samples were transported between MIT and UCLA in magnetically shielded cans. Approximately 400 grains were placed in 10 separate 2.5-cm-diameter epoxy EPO-TEK 301 mounts and polished to approximately their midplanes. Information about bulk rock source for the zircon grains and their respective mount number are compiled in table S1. U and Pb isotopes were measured on a CAMECA IMS 1270 SIMS, using an  $^{16}\text{O}^-$  primary beam, with beam currents of 12 to  $15 \text{nA}$ . A beam diameter of  $\sim 20$  to  $30 \mu\text{m}$  was used. Isotopes measured were  $^{94}\text{Zr}^{2+}$ ,  $^{204}\text{Pb}$ ,  $^{206}\text{Pb}$ ,  $^{207}\text{Pb}$ ,  $^{208}\text{Pb}$ ,  $^{232}\text{Th}$ ,  $^{238}\text{U}$ , and  $^{238}\text{U}^{16}\text{O}$ . The mass-resolving power was  $\geq 5500$ . We used oxygen flooding for improved Pb ionization (25). For the common Pb correction, we used a  $^{204}\text{Pb}$  correction assuming laboratory contamination with environmental Pb from southern California, specifically the San Diego sewage (26), with common  $^{206}\text{Pb}/^{204}\text{Pb} = 18.86$ , common  $^{207}\text{Pb}/^{204}\text{Pb} = 15.62$ , and common  $^{208}\text{Pb}/^{204}\text{Pb} = 38.34$ . An initial  $^{206}\text{Pb}/^{207}\text{Pb}$  ratio survey on 3754 grains was used to identify grains older than 3.5 Ga for all mounts except UCLA 1, 2, and 3; the latter were instead surveyed for grains older than 3.8 Ga. U-Pb measurements and BSE, CL, and

Li images were then acquired from grains that passed this criterion. We calculated the  $^{207}\text{Pb}/^{206}\text{Pb}$  and  $^{206}\text{Pb}/^{238}\text{U}$  dates and inferred the  $^{207}\text{Pb}/^{235}\text{U}$  using the known U isotope ratio ( $^{238}\text{U}/^{235}\text{U} = 137.88$ ). We assigned ages using  $^{207}\text{Pb}/^{206}\text{Pb}$  ratios.  $^{207}\text{Pb}/^{206}\text{Pb}$  and  $^{206}\text{Pb}/^{238}\text{U}$  were used to compute the discordance (27, 28)

$$\left| \frac{\frac{^{207}\text{Pb}}{^{206}\text{Pb}}}{\frac{^{206}\text{Pb}}{^{238}\text{Pb}}} - 1 \right| \times 100\% \quad (1)$$

Table S2 compiles U-Pb measurements for the grains that passed the initial  $^{206}\text{Pb}/^{207}\text{Pb}$  survey. Table S3 contains age and uncertainties for the 77 grains selected for the paleomagnetic experiments. BSE and CL images were acquired with a TESCAN VEGA3 scanning electron microscope equipped with a TESCAN three-channel color CL detector and TESCAN retractable BSE detector (29).

Li-ion images were acquired using a CAMECA IMS 1290 SIMS at the UCLA SIMS Laboratory. We used the Hyperion II radio frequency plasma primary ion source (30) with a 250 to 300 pA  $^{16}\text{O}^-$  beam focused to a  $<1\text{-}\mu\text{m}$  spot size. We rastered the beam over a  $50 \times 50\text{-}\mu\text{m}$  area and recorded 10 frames of ion images of  $^7\text{Li}$  and  $^{30}\text{Si}$ . We used the program WinImage to accumulate the 10 frames each of  $^7\text{Li}$  and  $^{30}\text{Si}$  (image intensity was integrated over all 10 frames), and computed the ratio of the two to get an image of  $^7\text{Li}/^{30}\text{Si}$  intensity. We normalized  $^7\text{Li}$  to  $^{30}\text{Si}$  to account for charging (where the ionization rate may be heterogeneous because of accumulation of charge in the sample as it is continually bombarded with negative secondary ions). The spatial resolution of the images is equivalent to the spot size, so any feature  $>1\text{ }\mu\text{m}$  is not an artifact. Because boundaries on zones are resolved to  $\leq 1\text{ }\mu\text{m}$ , blurring of zones by more than this value means they are actually physically smooth over that length scale. A detectable Li zoning with thickness of  $<20\text{ }\mu\text{m}$  provides evidence that the sample has not been heated  $>550^\circ\text{C}$  for more than 1 million years (11). However, this method might provide an underestimation of the peak temperature experienced by the grains in some cases (13). As discussed in the main text, whether or not the Li band criterion is used to filter our samples does not change the overall outcome of this study. In the Supplementary Materials, we provide evidence that the ion and electron microprobe work measurements did not remagnetize the samples. We also provide the complete set of images taken from all measured grains.

### Acid washing

We previously showed that most Jack Hills zircon grains, when untreated with concentrated (6 M) hydrochloric acid (HCl) acid, have magnetization likely dominated by secondary minerals coating the zircons (6). Therefore, before paleomagnetic measurements, all grains analyzed here (with the exception of four whole grains; see section S5 of the Supplementary Materials) were washed with a 6 M HCl solution for 12 min at room temperature, followed by rinsing in Milli-Q water and air drying. Zircon crystals from samples D175C and D175H were washed with HCl before U-Pb measurements, while grains from D175L and Cong14C were washed with HCl after U-Pb measurements. All grains selected for paleomagnetic measurements were extracted from the epoxy mounts using nonmagnetic tools (Semprex probe needle, lot 18) and washed in 70% sulfuric acid ( $\text{H}_2\text{SO}_4$ ) for 3 hours to remove any residual epoxy deposits before magnetic measurements. During extraction, five samples (18-8-12, 18-15-18, 18-4-8, 1-1-9, and 18-2-12) fragmented into two pieces

and one sample (18-11-13) fragmented into three pieces. All acid washing steps were performed in the MIT Isotope Laboratory clean-room facilities.

### Paleomagnetism

Following HCl and  $\text{H}_2\text{SO}_4$  acid-washing, grains were mounted in pits drilled into Corning Eagle XG glass slides, following similar procedures previously developed for analyzing zircons from the Bishop Tuff (2). Figure S3 shows the overall measuring setup. Optical and magnetic field images of the four glass holders with the grains mounted in the pits before demagnetization are shown in fig. S4. The absolute orientation of the grains was not maintained between mounting in the epoxy for the electron microscopy and ion probe measurements and in the glass mount for paleomagnetic measurements. However, the orientation of the grains and the glass mount was kept fixed throughout the paleomagnetic measurements.

Heating steps were conducted with an ASC Scientific TD48-SC thermal demagnetizer, which provides temperature control with accuracy of better than  $\pm 5^\circ\text{C}$ . An IZZI protocol was used in this experiment (16). The in-field step used a  $50\text{-}\mu\text{T}$  laboratory magnetic field.

Because of the overall weak magnetic moments of the samples (between  $6.05 \times 10^{-15}$  and  $4.15 \times 10^{-12}\text{ Am}^2$ ), NRM measurements were conducted with the SQUID microscope (14) in the MIT Paleomagnetism Laboratory. The configuration used in these experiments, including the sample holder and the mount with the zircon crystals, yields an approximate distance from the SQUID sensor to the midplane of the sample of  $\sim 360\text{ }\mu\text{m}$  (fig. S3). This distance includes the sensor to the window separation ( $\sim 200\text{ }\mu\text{m}$ ), the thickness of the Corning Eagle XG glass left at the bottom of the wells ( $\sim 60\text{ }\mu\text{m}$ ), and half of the size of the grain ( $\sim 100\text{ }\mu\text{m}$ ).

Using SQUID microscopy, we mapped the out-of-the-plane component of the magnetic field of individual zircons at a fixed distance above the sample. Maps were  $3\text{ mm} \times 3\text{ mm}$  in size with spatial sampling of  $25\text{ }\mu\text{m}$ . Magnetic field maps were subsequently inverted for the magnetic moment using previously validated techniques (2, 15). At each demagnetization/remagnetization step, zircon grains with moments  $<1 \times 10^{-13}\text{ Am}^2$  were measured four times and the inverted moments averaged to obtain accurate estimates of their net moments, while stronger magnetic samples were measured only once. When magnetic sources were not observed in our measurements, we assumed a maximum magnetic moment of  $\sim 6 \times 10^{-15}\text{ Am}^2$ , which is the noise floor of the MIT SQUID microscope at this sensor-sample distance. All magnetic measurements, including magnetic maps and processed data, are located in the dataset (see the Supplementary Materials) and will be uploaded to the Magetics Information Consortium (MagiC) database.

### Quantum diamond microscopy

After paleomagnetic measurements, select grains were extracted from the glass mount, placed in epoxy EPO-TEK 301, and polished again. We used the QDM (19) in the Harvard Paleomagnetics Laboratory to constrain the location of the magnetization carriers within the grains. Samples were measured in contact with the sensing diamond after a 0.4-T IRM was applied in the out-of-plane direction using an ASC model IM-10-3 impulse magnetizer. We measured the magnetic field intensity at a height of  $\sim 5\text{ }\mu\text{m}$  above the sample along the [111] direction of the diamond crystal lattice using projective magnetic microscopy with a resolution of 1.17 micrometers per

pixel (19). We isolated the remanent field signal of ferromagnetic grains by measuring the sample successively under two mutually antiparallel 0.9-mT bias fields and computing the out-of-plane magnetic field using a spectral algorithm (15). Figure 6 shows the QDM measurements. The absolute orientation of the grains differed between the SQUID microscopy measurements and these QDM measurements.

### Transmission electron microscopy

TEM was conducted in the Wolfson Electron Microscopy Suite at the University of Cambridge. Our TEM analysis targeted locations based on the QDM maps previously measured. The TEM foil was prepared using a dual-beam focused ion beam microscope FEI Helios NanoLab (Hillsboro, OR, USA) with an area of  $\sim 60 \mu\text{m}^2$  and a depth of  $\sim 7 \mu\text{m}$ . An in-situ lift-out technique was used to site-specifically extract the foil from the place with magnetic signals mapped with the QDM, and a cleanup procedure with low acceleration voltage was used to reduce surface damage of the foil. The TEM sample was examined using a FEI Tecnai Osiris TEM with an extreme Schottky field emission gun. The instrument was equipped with four large-area energy-dispersive x-ray spectrometer detectors, providing a fast chemical compositional measurement. The analysis was carried out at scanning TEM mode at 200 kV, where both bright-field and high-angle annular dark-field images were acquired.

### SUPPLEMENTARY MATERIALS

Supplementary material for this article is available at <http://advances.sciencemag.org/cgi/content/full/6/15/eaav9634/DC1>

### REFERENCES AND NOTES

- W. Compston, R. T. Pidgeon, Jack Hills, evidence of more very old detrital zircons in Western Australia. *Nature* **321**, 766–769 (1986).
- R. R. Fu, B. P. Weiss, E. A. Lima, P. Kehayias, J. F. D. F. Araujo, D. R. Glenn, J. Gelb, J. F. Einsle, A. M. Bauer, R. J. Harrison, G. A. H. Ali, R. L. Walsworth, Evaluating the paleomagnetic potential of single zircon crystals using the Bishop Tuff. *Earth Planet. Sci. Lett.* **458**, 1–13 (2017).
- B. P. Weiss, A. C. Maloof, N. Tailby, J. Ramezani, R. R. Fu, V. Hanus, D. Trail, E. Bruce Watson, T. M. Harrison, S. A. Bowring, J. L. Kirschvink, N. L. Swanson-Hysell, R. S. Coe, Pervasive remagnetization of detrital zircon host rocks in the Jack Hills, Western Australia and implications for records of the early geodynamo. *Earth Planet. Sci. Lett.* **430**, 115–128 (2015).
- J. A. Tarduno, E. G. Blackman, E. E. Mamajek, Detecting the oldest geodynamo and attendant shielding from the solar wind: Implications for habitability. *Phys. Earth Planet. Inter.* **233**, 68–87 (2014).
- M. Sato, S. Yamamoto, Y. Yamamoto, Y. Okada, M. Ohno, H. Tsunakawa, S. Maruyama, Rock-magnetic properties of single zircon crystals sampled from the Tanzawa tonalitic pluton, central Japan. *Earth Planets Space* **67**, 150 (2015).
- B. P. Weiss, R. R. Fu, J. F. Einsle, D. R. Glenn, P. Kehayias, E. A. Bell, J. Gelb, J. F. D. F. Araujo, E. A. Lima, C. S. Borlina, P. Boehnke, D. N. Johnstone, T. M. Harrison, R. J. Harrison, R. L. Walsworth, Secondary magnetic inclusions in detrital zircons from the Jack Hills, Western Australia, and implications for the origin of the geodynamo. *Geology* **46**, 427–430 (2018).
- J. A. Tarduno, R. D. Cottrell, W. J. Davis, F. Nimmo, R. K. Bono, A Hadean to Paleoarchean geodynamo recorded by single zircon crystals. *Science* **349**, 521–524 (2015).
- J. A. Tarduno, R. D. Cottrell, R. K. Bono, H. Oda, W. J. Davis, M. Fayek, O. van 't Erve, F. Nimmo, W. Huang, E. R. Thern, S. Fearn, G. Mitra, A. V. Smirnov, E. G. Blackman, Paleomagnetism indicates that primary magnetite in zircon records a strong Hadean geodynamo. *Proc. Natl. Acad. Sci.* **117**, 2309–2318 (2020).
- B. P. Weiss, A. C. Maloof, T. M. Harrison, N. L. Swanson-Hysell, R. R. Fu, J. L. Kirschvink, E. Bruce Watson, R. S. Coe, S. M. Tikoo, J. Ramezani, Reply to comment on “Pervasive remagnetization of detrital zircon host rocks in the Jack Hills, Western Australia and implications for records of the early dynamo”. *Earth Planet. Sci. Lett.* **450**, 409–412 (2016).
- F. Tang, R. J. M. Taylor, J. F. Einsle, C. S. Borlina, R. R. Fu, B. P. Weiss, H. M. Williams, W. Williams, L. Nagy, P. A. Midgley, E. A. Lima, E. A. Bell, T. M. Harrison, E. W. Alexander, R. J. Harrison, Secondary magnetite in ancient zircon precludes analysis of a Hadean geodynamo. *Proc. Natl. Acad. Sci. U.S.A.* **116**, 407–412 (2018).
- D. Trail, D. J. Cherniak, E. B. Watson, T. M. Harrison, B. P. Weiss, I. Szumila, Li zoning in zircon as a potential geospeedometer and peak temperature indicator. *Contrib. Mineral. Petro.* **171**, 1–15 (2016).
- F. Corfu, J. M. Hanchar, P. W. O. Hoskin, P. Kinny, Atlas of zircon textures. *Rev. Mineral. Geochemistry* **53**, 469–500 (2003).
- M. Tang, R. L. Rudnick, W. F. McDonough, M. Bose, Y. Goreva, Multi-mode Li diffusion in natural zircons: Evidence for diffusion in the presence of step-function concentration boundaries. *Earth Planet. Sci. Lett.* **474**, 110–119 (2017).
- B. P. Weiss, E. A. Lima, L. E. Fong, F. J. Baudenbacher, Paleomagnetic analysis using SQUID microscopy. *J. Geophys. Res.* **112**, 1–20 (2007).
- E. A. Lima, B. P. Weiss, Ultra-high sensitivity moment magnetometry of geological samples using magnetic microscopy. *Geochem. Geophys. Geosyst.* **17**, 3754–3774 (2016).
- Y. Yu, L. Tauxe, A. Genevey, Toward an optimal geomagnetic field intensity determination technique. *Geochem. Geophys. Geosyst.* **5**, Q02H07 (2004).
- L. Tauxe, H. Staudigel, Strength of the geomagnetic field in the cretaceous normal superchron: New data from submarine basaltic glass of the Troodos Ophiolite. *Geochem. Geophys. Geosyst.* **5**, Q02H06 (2004).
- J. L. Kirschvink, The least-squares line and plane and the analysis of paleomagnetic data. *Geophys. J. Roy. Astron. Soc.* **62**, 699–718 (1980).
- D. R. Glenn, R. R. Fu, P. Kehayias, D. Le Sage, E. A. Lima, B. P. Weiss, R. L. Walsworth, Micrometer-scale magnetic imaging of geological samples using a quantum diamond microscope. *Geochem. Geophys. Geosyst.* **18**, 3254–3267 (2017).
- L. F. White, J. R. Darling, D. E. Moser, D. A. Reinhard, T. J. Prosa, D. Bullen, D. Olson, D. J. Larson, D. Lawrence, I. Martin, Atomic-scale age resolution of planetary events. *Nat. Commun.* **8**, 15597 (2017).
- N. E. Timms, S. M. Reddy, J. D. Fitzgerald, L. Green, J. R. Muhling, Inclusion-localised crystal-plasticity, dynamic porosity, and fast-diffusion pathway generation in zircon. *J. Struct. Geol.* **35**, 78–89 (2012).
- S. Piazolo, A. La Fontaine, P. Trimby, S. Harley, L. Yang, R. Armstrong, J. M. Cairney, Deformation-induced trace element redistribution in zircon revealed using atom probe tomography. *Nat. Commun.* **7**, 10490 (2016).
- T. Geisler, U. Schaltegger, F. Tomaschek, Re-equilibration of zircon in aqueous fluids and melts. *Elements* **3**, 43–50 (2007).
- A. J. Cavosie, S. A. Wilde, D. Liu, P. W. Weiblen, J. W. Valley, Internal zoning and U-Th-Pb chemistry of Jack Hills detrital zircons: A mineral record of early Archean to Mesoproterozoic (4348–1576 Ma) magmatism. *Precambrian Res.* **135**, 251–279 (2004).
- X. Quidelleur, M. Grove, O. M. Lovera, T. M. Harrison, A. Yin, F. J. Ryerson, Thermal evolution and slip history of the Renbu Zedong thrust, southeastern Tibet. *J. Geophys. Res.* **102**, 2659–2679 (1997).
- C. Patterson, D. Settle, B. Glover, Analysis of lead in polluted coastal seawater. *Mar. Chem.* **4**, 305–319 (1976).
- C. J. Spencer, C. L. Kirkland, R. J. M. Taylor, Strategies towards statistically robust interpretations of in situ U-Pb zircon geochronology. *Geosci. Front.* **7**, 581–589 (2016).
- Q. Wang, S. A. Wilde, New constraints on the Hadean to Proterozoic history of the Jack Hills belt, Western Australia. *Gondw. Res.* **55**, 74–91 (2018).
- E. A. Bell, P. Boehnke, M. D. Hopkins-Wielicki, T. M. Harrison, Distinguishing primary and secondary inclusion assemblages in Jack Hills zircons. *Lithos* **234–235**, 15–26 (2015).
- M.-C. Liu, K. D. McKeegan, T. M. Harrison, G. Jarzebinski, L. Vltava, The Hyperion-II radio-frequency oxygen ion source on the UCLA ims1290 ion microprobe: Beam characterization and applications in geochemistry and cosmochemistry. *Int. J. Mass Spectrom.* **424**, 1–9 (2018).
- E. A. Bell, T. M. Harrison, M. T. McCulloch, E. D. Young, Early Archean crustal evolution of the Jack Hills zircon source terrane inferred from Lu-Hf,  $^{207}\text{Pb}/^{206}\text{Pb}$ , and  $\delta^{18}\text{O}$  systematics of Jack Hills zircons. *Geochim. Cosmochim. Acta* **75**, 4816–4829 (2011).
- T. Berndt, A. R. Muxworthy, K. Fabian, Does size matter? Statistical limits of paleomagnetic field reconstruction from small rock specimens. *J. Geophys. Res. Solid Earth* **121**, 15–26 (2016).
- G. A. Paterson, L. Tauxe, A. J. Biggin, R. Shaar, L. C. Jonestrask, On improving the selection of Thellier-type paleointensity data. *Geochem. Geophys. Geosyst.* **15**, 1180–1192 (2014).
- P. W. Reiners, R. W. Carlson, P. R. Renne, K. M. Cooper, D. E. Granger, N. M. McLean, B. Schoene, *Geochronology and Thermochronology* (Wiley, 2017).

**Acknowledgments:** We acknowledge R. L. Walsworth for developing the QDM and T. F. Peterson Jr. for support. **Funding:** This study was supported by the NSF (grants EAR 1647504, EAR 1847042, and DMS 1521765) and the European Research Council under the European Union’s Seventh Framework Programme (Grant FP/2007–2013)/European Research Council Grant Agreement 320750, Natural Environment Research

Council Grant NE/P002498/1. The UCLA ion microprobe facility is partly supported by a grant from the Instrumentation and Facilities Program, Division of Earth Sciences, NSF (1339051). **Author contributions:** C.S.B. conducted paleomagnetic measurements, analyzed the data, and prepared the manuscript. B.P.W. conceived the project and carried out the advising. E.A.L. provided support on data analysis. F.T., R.J.M.T., J.F.E., and R.J.H. conducted measurements. R.R.F. conducted QDM measurements. E.A.B., E.W.A., H.M.K., M.M.W., and T.M.H. conducted microprobe measurements. J.R. separated the samples and provided support with acid washing. A.C.M. provided help with the manuscript preparation. **Competing interests:** The authors declare that they have no competing interests. **Data and materials availability:** All data needed to evaluate the conclusions in the paper are present in

the paper and/or the Supplementary Materials. Additional data related to this paper may be requested from the authors.

Submitted 5 November 2018  
Accepted 19 December 2019  
Published 8 April 2020  
10.1126/sciadv.aav9634

**Citation:** C. S. Borlina, B. P. Weiss, E. A. Lima, F. Tang, R. J. M. Taylor, J. F. Einsle, R. J. Harrison, R. R. Fu, E. A. Bell, E. W. Alexander, H. M. Kirkpatrick, M. M. Wielicki, T. M. Harrison, J. Ramezani, A. C. Maloof, Reevaluating the evidence for a Hadean-Eoarchean dynamo. *Sci. Adv.* **6**, eaav9634 (2020).

# Science Advances

## Reevaluating the evidence for a Hadean-Eoarchean dynamo

Cauê S. Borlina, Benjamin P. Weiss, Eduardo A. Lima, Fengzai Tang, Richard J. M. Taylor, Joshua F. Einsle, Richard J. Harrison, Roger R. Fu, Elizabeth A. Bell, Ellen W. Alexander, Heather M. Kirkpatrick, Matthew M. Wielicki, T. Mark Harrison, Jahandar Ramezani and Adam C. Maloof

Sci Adv 6 (15), eaav9634.  
DOI: 10.1126/sciadv.aav9634

### ARTICLE TOOLS

<http://advances.sciencemag.org/content/6/15/eaav9634>

### SUPPLEMENTARY MATERIALS

<http://advances.sciencemag.org/content/suppl/2020/04/06/6.15.eaav9634.DC1>

### REFERENCES

This article cites 33 articles, 3 of which you can access for free  
<http://advances.sciencemag.org/content/6/15/eaav9634#BIBL>

### PERMISSIONS

<http://www.sciencemag.org/help/reprints-and-permissions>

Use of this article is subject to the [Terms of Service](#)

---

Science Advances (ISSN 2375-2548) is published by the American Association for the Advancement of Science, 1200 New York Avenue NW, Washington, DC 20005. The title *Science Advances* is a registered trademark of AAAS.

Copyright © 2020 The Authors, some rights reserved; exclusive licensee American Association for the Advancement of Science. No claim to original U.S. Government Works. Distributed under a Creative Commons Attribution NonCommercial License 4.0 (CC BY-NC).

[advances.sciencemag.org/cgi/content/full/6/15/eaav9634/DC1](https://advances.sciencemag.org/cgi/content/full/6/15/eaav9634/DC1)

## Supplementary Materials for

### **Reevaluating the evidence for a Hadean-Eoarchean dynamo**

Cauê S. Borlina\*, Benjamin P. Weiss, Eduardo A. Lima, Fengzai Tang, Richard J. M. Taylor, Joshua F. Einsle, Richard J. Harrison, Roger R. Fu, Elizabeth A. Bell, Ellen W. Alexander, Heather M. Kirkpatrick, Matthew M. Wielicki, T. Mark Harrison, Jahandar Ramezani, Adam C. Maloof

\*Corresponding author. Email: caue@mit.edu

Published 8 April 2020, *Sci. Adv.* **6**, eaav9634 (2020)

DOI: 10.1126/sciadv.aav9634

#### **The PDF file includes:**

Sections S1 to S4

Figs. S1 to S6

Tables S1 to S7

References

#### **Other Supplementary Material for this manuscript includes the following:**

(available at [advances.sciencemag.org/cgi/content/full/6/15/eaav9634/DC1](https://advances.sciencemag.org/cgi/content/full/6/15/eaav9634/DC1))

Databases S1 and S2

## 1. Introduction

Here we present more details about our methodology and further discuss their implications. This includes our ion and electron microprobe measurements (Section 2), paleomagnetic measurements (Section 3), paleomagnetic data analysis (Section 4), and the effects of sample polishing (Section 5). We also present data tables containing source blocks and sampling locations for the zircons (Table S1), U-Pb measurements (Table S2), and paleomagnetic analyses (Tables S3-S7).

Throughout this manuscript we have used “ $X_n$ ”, “ $Y_n$ ” and “ $Z_n$ ”, where  $n = 1, 2, 3$ , to represent three different coordinate systems. The grain orientations used during the SQUID microscopy measurements ( $n = 1$ ; Figs. 3-5 and Fig. S6) are different from the orientations during the QDM measurements ( $n = 2$ ; Fig. 6), which are also different than the orientations during the BSE, CL, Li measurements ( $n = 3$ ; Fig. S2).

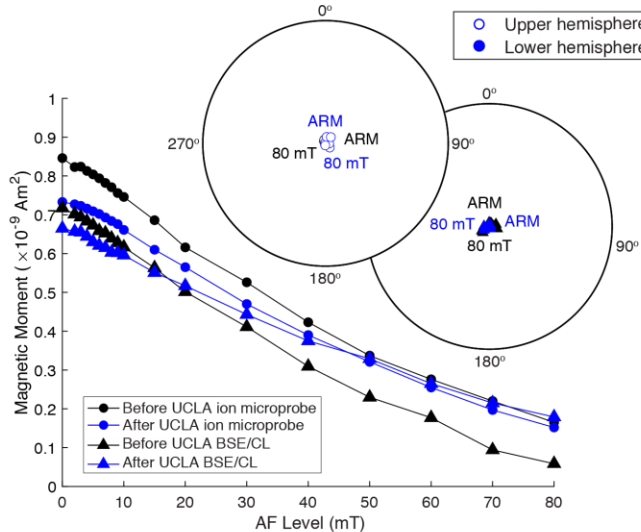
## 2. Ion and electron microprobe measurements do not remagnetize samples

Prior to conducting the U-Pb, BSE, CL and Li measurements, we verified that these measurements do not detectably overprint the natural remanent magnetization (NRM) in the grains. In particular, four zircon crystals from the Mud Tank carbonatite outcrop (31), Northern Territory, Australia, were imparted with an anhysteretic remanent magnetization (ARM) using an alternating field of 200 mT and a 0.4 mT bias field in the Massachusetts Institute of Technology (MIT) Paleomagnetism Laboratory (Figure S1). The samples were then progressively alternating-field (AF) demagnetized to a peak field of 80 mT and their magnetic moments measured using a 2G Enterprises Superconducting Rock Magnetometer model 755 at MIT to infer their ARM coercivity spectra (black circles; Fig. S1). They were then again imparted with the same ARM as before, sent to UCLA to be measured with the ion microprobe and shipped back to MIT. Samples were kept in magnetic shielding cans during transport. At MIT, the samples were again AF demagnetized (blue circles; Fig. S1). Following this, the same procedure was conducted for the BSE and CL measurements (black and blue triangles; Fig. S1).

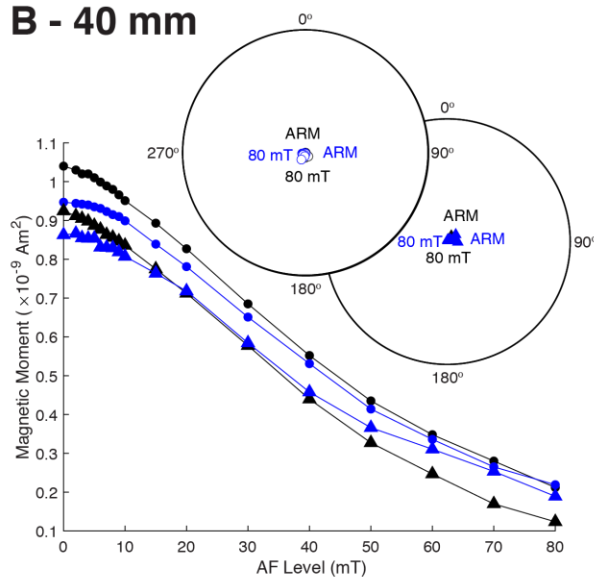
Ion microprobe, BSE and CL measurements of grains A and C were conducted at a measurement height of 20 and 60 mm, respectively, gold coated while grains B and D were measured at a height of 40 and 90 mm, respectively (Figure S1). No magnetic overprint was observed to have been acquired at UCLA (only a slight decay of the magnetization was observed and likely due to viscous decay of the ARM in the shielded can and shielded room). Before the ion microprobe and BSE/CL measurements, the samples were polished resulting in weaker ARM acquisition between the steps (i.e., for each grain, compare first black dot with first black triangle).

We also conducted a second test to assess the effects on the sample’s magnetization of U-Pb measurements and Li imaging using the ion microprobe. The out of the page component ( $B_z$ ) of the NRM of holders UCLA 3 and 7 were measured with the MIT superconducting quantum interference device (SQUID) microscope (14) before and after measurements with the ion microprobe at UCLA (Fig. S2). Samples were kept in magnetic shielding cans during transport as before. No variation in the overall NRM of the samples was observed. These experiments collectively demonstrate that our U-Pb, Li, BSE, and CL measurements do not detectably overprint the NRM of the samples. Section 5 provides further evidence for this.

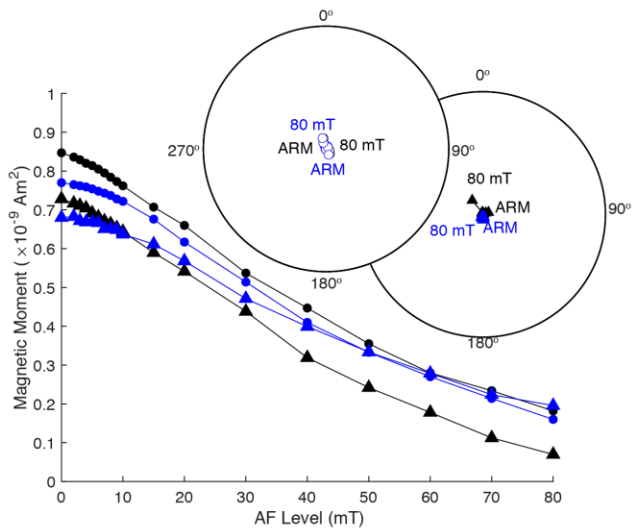
### A - 20 mm - gold coated



### B - 40 mm



### C - 60 mm - gold coated



### D - 90 mm

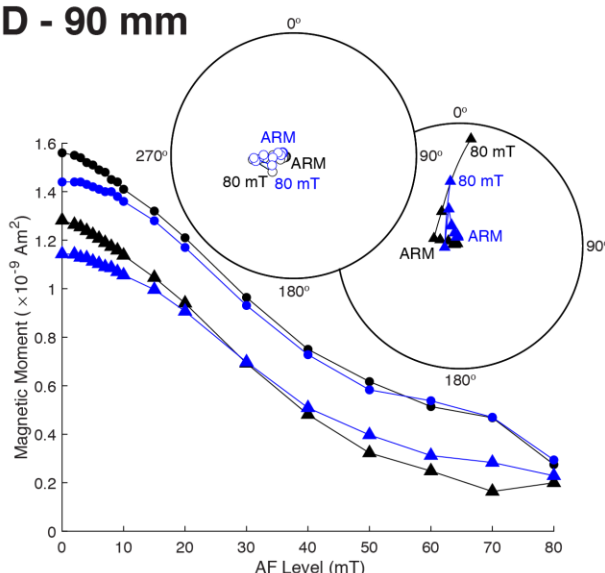


**Fig. S1. Test for remagnetization of Jack Hills zircon mounts from electron microscopy and ion probe measurements.** Shown Four zircons from the Mud Tank carbonatite outcrop, Northern Territory, Australia, demagnetization curves, and their respective equal area plots. Samples were initially imparted an anhysteretic remanent magnetization (ARM) using an alternating field of 200 mT and a 0.4 mT bias field, then progressively alternating-field (AF) demagnetized to a peak field of 800 mT and measured using a 2G Enterprises Superconducting Rock Magnetometer 755 in the MIT Paleomagnetism Laboratory (black circles). They were then again imparted with the same ARM as before, sent to UCLA for ion microprobe measurements, and shipped back to MIT. At MIT, the samples were again AF demagnetized (blue circles). The same procedure was conducted for backscattered electron microscopy (BSE) and cathodoluminescence (CL) measurements (black and blue triangles). The demagnetization curves show no significant difference in magnetic behavior before and after the measurements.

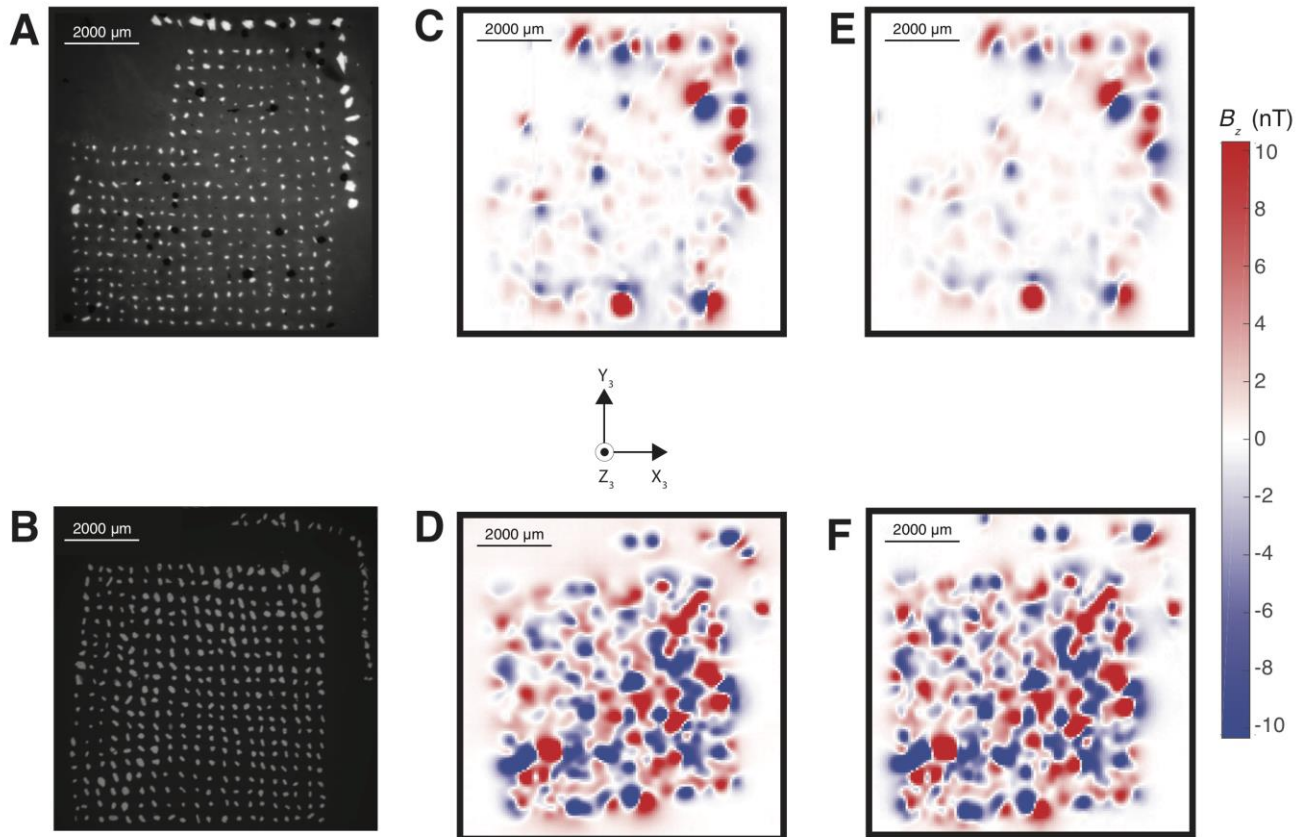


**Fig. S2. Test for remagnetization of Jack Hills zircon mounts from ion microprobe measurements.** (A, B) BSE image of epoxy mounts UCLA 3 and UCLA 7 containing 325 and 400 Jack Hills zircon grains, respectively. (C, D) Out-of-the-page magnetic field component ( $B_z$ ) maps of the NRM of two zircon-bearing quartz holders obtained with the SQUID microscope measured at a height of ~250  $\mu\text{m}$  above the grains. We use  $X_3$ ,  $Y_3$  and  $Z_3$  to denote that the grain orientations in the epoxy mount are not the same as those during the thermal demagnetization and paleointensity experiments (Figs. 3-5). (E, F) Magnetic field ( $B_z$ ) of the NRM of two holders obtained with the SQUID microscope at a height of ~250  $\mu\text{m}$  after U-Pb, BSE, CL and Li measurements obtained at UCLA. There are no significant differences in the magnetization before and after imaging the grains.

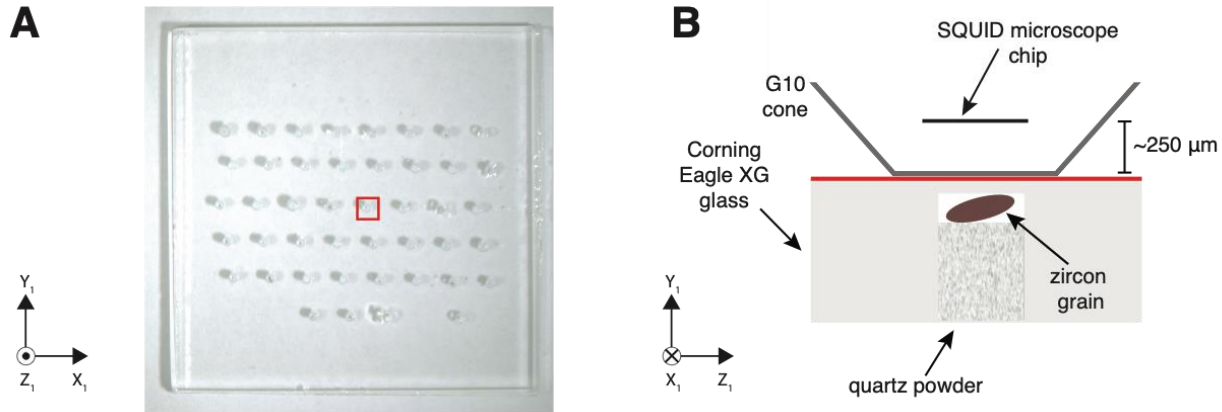


**Fig. S3. Setup for magnetic measurements using SQUID microscopy.** (A) Photograph of one of the quartz holders. (B) Cross-sectional view of the measurement setup referenced to the coordinate system presented in (A). Figure shows the SQUID microscope chip, the G10 cone, the glass used to mount samples (Corning Eagle XG glass), the quartz powder and the zircon grain. The distance from the SQUID microscope chip to the top of the sample is  $\sim 250 \mu\text{m}$ . The red line represents the top of the glass as shown in (A). We use a “1” subscript on  $X_1$ ,  $Y_1$  and  $Z_1$  to denote this figure orientation is the same as the data shown in Figs. 3, 4 and 5.

### 3. Paleomagnetism

In this section, we discuss general aspects of the grain orientation during the paleointensity experiments, the inversion of non-dipolar magnetic sources, the structure of the supplementary datasets available with this paper, and paleomagnetic criteria. Figure S3 shows the setup for the holders and the samples with respect to the SQUID microscope.

Figure S4 shows photographs of the 4 sample holders used in this experiment overlain with their respective SQUID microscope magnetic maps ( $B_z$ ). Each dark circle represents a hole used to mount one of the 77 zircon grains. The white circles identify non-acid washed zircon grains that were given an isothermal remanent magnetization (IRM) in a field of 0.4 T with an ASC Scientific IM-10 Pulse Magnetizer. Because of their high magnetic moment, these grains were used as references for the location and orientation of the other zircon grains during the experiments.

Figure S5 shows the demagnetization of the IRM of the markers along with Curie temperature indicators for goethite (“goeth”), pyrrhotite (“pyrr”), magnetite (“mag”) and hematite (“hem”). We observe goethite (grains “B” and “L”), pyrrhotite (grains “C”, “H”, “I”, “J”, “K”), magnetite (“C”, “D”) and hematite (grains “A”, “E”, “F”, “G”, “I”) as the major magnetic carriers among the markers. A similar assemblage of ferromagnetic minerals was previously observed in an IRM study of Jack Hills zircons (6) as well as in the pebble conglomerate that hosts the zircons (3). Alteration, characterized by increase of remanence during demagnetization, can also be observed in grains “B”, “H” and “L”. These interpretations are based on the characteristic thermal unblocking temperature of the remanence.

We obtained net magnetic moments from the SQUID microscope maps using a net moment dipole-fitting technique (15). Some of the grains’ magnetic fields were modestly non-dipolar and these data were ignored due to the restrictions of our net moment dipole-fitting technique (15) [18-15-18 (h04) (pTRM check at 555 °C), 18-20-14 (h20) (pTRM check at 555 °C), 18-2-12 (h22) (560 °C Z step, 560 °C I step), 11-12-2 (h24) (560 °C Z step, 565 °C Z step), 15-3-15 (h14) (535 °C I step)]. The exception was sample WGNAW3, for which the majority of measurements were non-dipolar. We fit for dipolar sources for this sample to provide an order-of-magnitude estimate of the magnetic moment variation of the grain.

Included with the supplementary material of this article is a compiled dataset that includes

BSE, CL, Li images, calibrated SQUID microscope maps and fitted data. The dataset is also available in the MagiC database.

Jack Hills detrital zircon grains are among of the weakest-moment samples ever measured in paleomagnetism. Previous studies have shown that grains with NRMs below  $\sim 10^{-14}$  Am<sup>2</sup> are likely to exhibit noisy demagnetization due to statistics of small numbers of ferromagnetic grains and measurement noise (15, 32). Because we are mainly interested in an order-of-magnitude paleointensity estimate to establish the presence or absence of a dynamo, standard paleomagnetic quality criteria will provide an overly conservative selection of the dataset. For example, none of the samples analyzed here have all  $\delta pTRM_{i,j} \leq 25\%$ , where  $\delta pTRM_{i,j}$  is the difference between the pTRM check in the  $i^{\text{th}}$  temperature step after heating to the  $j^{\text{th}}$  temperature step and pTRM gained in the  $i^{\text{th}}$  temperature step. The exception is sample 080201 (which fails our selection criteria due to the presence of cracks; Fig. S6). Most of the samples have demagnetization similar to what we show in main text Fig. 5. Thus, we considered that a sample could be a reliable paleomagnetic recorder if it did not alter during lab experiments and if it gained magnetic moment in the direction of the bias field during in-field steps of the IZZI protocol. To quantify laboratory-heating alteration, we used the difference ratio sum (DRATS) parameter (17, 33), defined as:

$$DRATS = \frac{|\sum_{i=1}^{end} \delta pTRM_{i,j}|}{x_{end}} \times 100, \quad (2)$$

where  $x_{end}$  is the last pTRM gained step. This parameter is an aggregate measure of the success of all the pTRM checks used for the paleointensity estimate. This is useful for considering the effects of low temperature steps for which little pTRM may be gained and, as a result, might yield a large fractional discrepancy between the pTRM check step and the pTRM gained at the same temperature step. We used a threshold value of DRATS  $\leq 25\%$  to identify samples that did not alter during the experiments. Values for all samples are compiled in Table S4.

We used principal component analysis (PCA) (18) to determine whether the in-field components acquired by the grains trend towards Y, as expected from the in-field application during heating steps (which pointed Y in the reference frame in which the paleomagnetic data are presented). This would indicate that the samples acquired magnetization, suggesting that they may be robust paleomagnetic recorders. Zero-field and in-field PCA of the components are presented in Tables S5 and S6. We considered a maximum angular deviation (MAD)  $< 25^\circ$  (18) as indication that the field was adequately recorded. For reference, we also computed the modified PICRIT03 paleomagnetic statistics (33) for all samples analyzed.

In the studies that previously reported paleomagnetism of Jack Hills detrital zircon grains (7,8), only grains with NRM  $> 1 \times 10^{-12}$  Am<sup>2</sup> were subjected to their paleointensity protocol. We did not use the magnitude of the NRM as a selection criterion for three reasons: (i) ref. (2) obtained reliable paleomagnetic records from the Bishop Tuff zircon crystals with NRM moments as low as  $1.8 \times 10^{-13}$  Am<sup>2</sup> and 40% of our samples have NRM moments above this threshold; (ii) such weak moments are at least 30 times stronger than the sensitivity of our magnetometer (2); (iii) such data selection would be biased against a no-dynamo scenario.

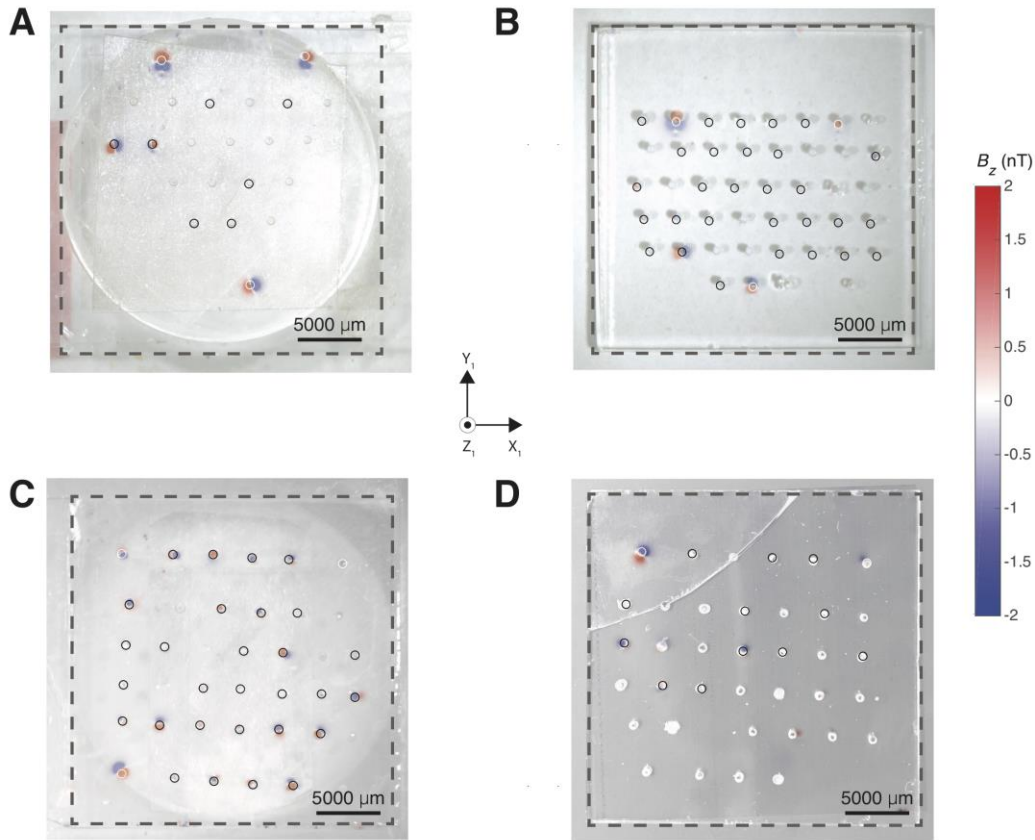


**Fig. S4. Maps of the NRMs of Jack Hills zircons in quartz mounts.** Out-of-the-page field component ( $B_z$ ) of the NRMs of the four sample holders used in this study. (A) Holder C2. (B) Holder E1. (C) Holder F1. (D) Holdeer T1. Measurements were obtained with the SQUID microscope at a height of  $\sim 360$   $\mu\text{m}$  above the top of the grains (Fig. S3). The grain orientations, shown by the compass in the center of the figure, are the same as those shown in Figs. 3-5 and S6. Black circles show where zircon grains were mounted; white circles show where marker zircons were mounted to constrain the location and orientation of each grain analyzed paleomagnetically. The white circles are non-acid washed zircon grains that were given an isothermal remanent magnetization (IRM) in a field of 0.4 T with an ASC Scientific IM-10 Pulse Demagnetizer and used as reference for the location and orientation of the zircon grains during the experiments. We use a “1” subscript on  $X_1$ ,  $Y_1$  and  $Z_1$  to denote the fact that the grain orientations during the thermal demagnetization and paleointensity experiments are different from the grain orientations during the BSE, CL and Li measurements.

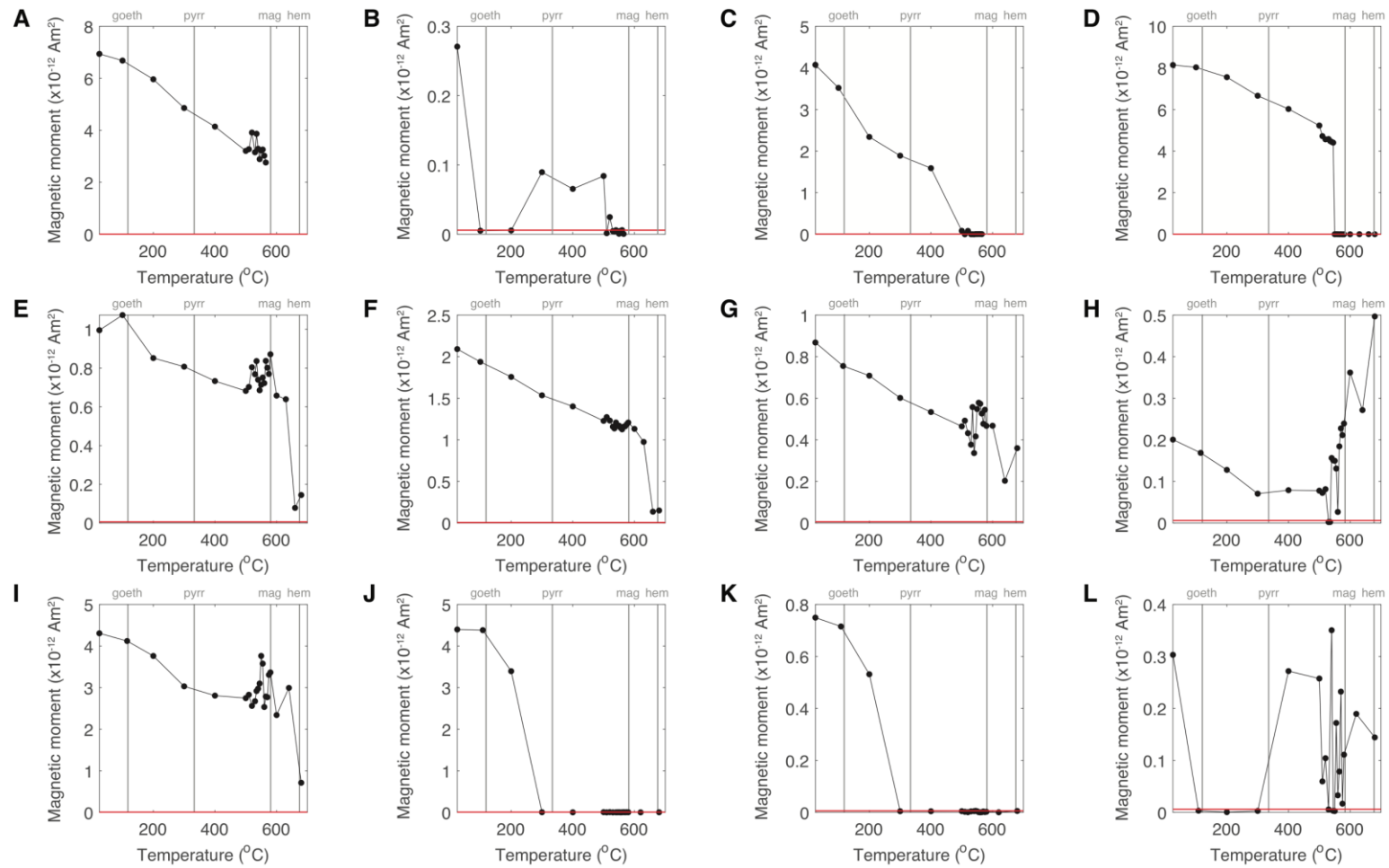


**Fig. S5. Compilation of IRM demagnetization of markers used in this study.** Starting from the left, the grey lines denote the Curie temperatures for goethite (“goeth”), pyrrhotite (“pyrr”), magnetite (“mag”) and hematite (“hem”). We observe goethite (grains “B” and “L”), pyrrhotite (grains “C”, “H”, “I”, “J”, “K”), magnetite (“C”, “D”) and hematite (grains “A”, “E”, “F”, “G”, “I”) as the major magnetic carriers among the markers. Thermochemical alteration, characterized by increase of remanence during demagnetization, can also be observed in grains “B”, “H” and “L”. Red line shows the detection limit of our instrument.

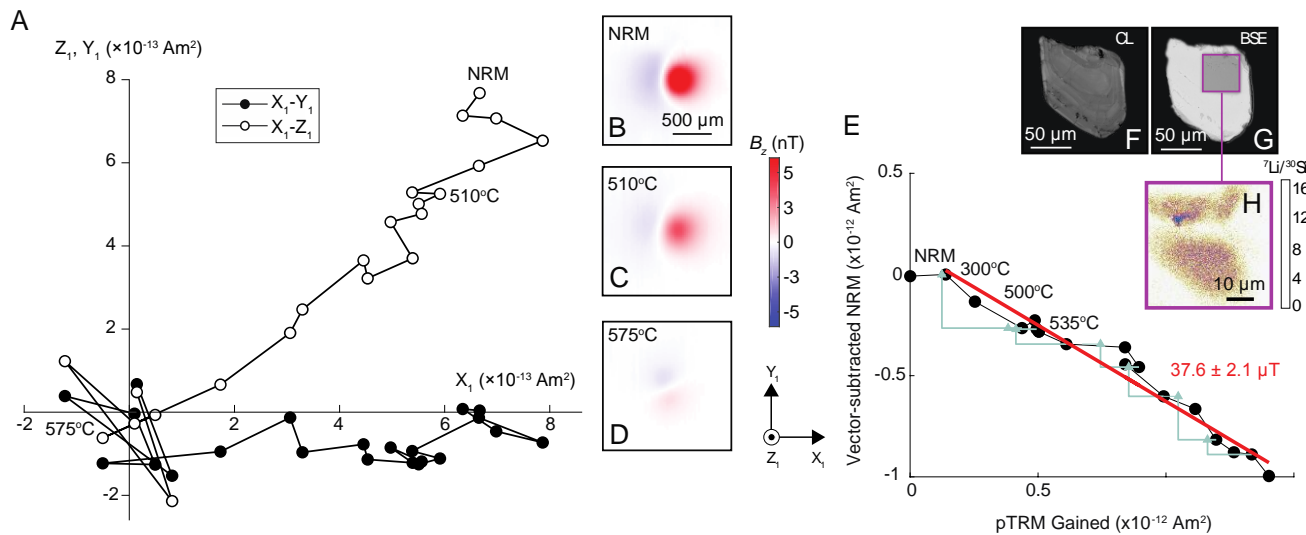


**Fig. S6. Paleomagnetic data for zircon grain 8-2-1 ( $3.117 \pm 0.006$  Ga).** (A) Orthographic projection of NRM vector endpoints during thermal demagnetization. Closed symbols show X-Y projection of the magnetization; open symbols show Z-Y projection of the magnetization. (B-D) Out-of-the page magnetic field component ( $B_z$ ) maps at a height of  $\sim 360 \mu\text{m}$  above the grains obtained with the SQUID microscope for NRM, 500°C and 575°C steps. We use  $X_1$ ,  $Y_1$  and  $Z_1$  to denote the fact that the grain orientations during the thermal demagnetization and paleointensity experiments are different from the grain orientations during the BSE, CL and Li measurements. (E) Vector-subtracted NRM from the 300°C step versus pTRM grained during progressive laboratory heating. Blue triangles show pTRM checks. Red line shows the measurements used to compute paleointensity values (300-580°C). (F-H) CL, BSE, and Li images of the grains.

## 5. Effects of polishing samples

A factor that might enhance thermochemical alteration during our paleointensity experiments is the polishing of the grains required for the imaging and dating procedures that occurred prior to beginning the magnetic measurements. Such polishing may have exposed magnetic minerals in the original interior of the zircons to alteration in air, which otherwise would be encapsulated in whole grains. We tested for this effect by conducting double-heating IZZI paleointensity experiments on 21 whole grains zircons (of which 4 were non-acid-washed and the remaining acid-washed) following the same heating and measurement schedule as that used for polished grains. These whole grains were randomly selected from separates from rock sample Cong14c without the use of any selection criteria (see Table S1). We observed that 19 grains altered during experiments (by failing the DRATS requirement described in Section 4), 12 were poor magnetic field recorders (did not gain moment in the direction of the reference field during in-field steps by failing the MAD requirement as in Section 4), and no grain passed the paleomagnetic criteria.

Table S5 provides a comparison of results from non-polished and polished grains. As before, grains that had DRATS values  $\leq 25\%$  were considered to not have significantly altered, while grains that had MAD values  $\leq 15^\circ$  for the in-field magnetic component were considered robust paleomagnetic recorders. Because 0% of unpolished and 11% of polished grains pass the paleomagnetic criteria, we conclude that there is no systematic difference between the suitability of polished grains and non-polished grains for paleointensity analyses.

We can also compare the NRM components of polished and non-polished grains (18). While Section 2 provides evidence that the U-Pb, BSE, CL and Li measurements do not overprint the NRMs of our polished samples, we can use the unpolished grain paleomagnetic dataset (which did not undergo U-Pb, BSE, CL and Li measurements) to further test that conclusion. In particular, we searched for NRM components with MAD values  $\leq 15^\circ$ , obtained from PCA (18). Grains that had a single NRM component with MAD values  $\leq 15^\circ$  totaled 12 (20%) out of 56 for the polished grains, versus 2 (10%) out of 21 for the non-polished grains. Therefore, similarly small fractions of polished and unpolished grains have identifiable NRM components. PCAs of all grains are compiled in Tables S6 (zero-field steps) and S7 (in-field steps).

**Table S1. Information about source blocks for analyzed zircon grains from Jack Hills, Western Australia.** Table includes block sample names, mass, mount names, sampling location (Australian Map Grid 1984 datum) and sampling date.

Block Name	Mass (kg)	Mounts	Sample Location		Sampling Date (MM/DD/YYYY)
			Latitude (°)	Longitude (°)	
D175C	2.6	UCLA 1, 2, 3	-26.16664	116.99148	7/31/2012
D175H	8.6	UCLA 6, 7, 8	-26.16664	116.99148	8/3/2012
D175L	2.0	UCLA 11, 12	-26.16664	116.99148	8/3/2012
Cong14c	2.8	UCLA 15, 18	-26.16674	116.99134	7/31/2012

**Table S2. Compilation of U-Pb ages for grains that passed initial  $^{207}\text{Pb}/^{206}\text{Pb}$  survey.** The first column gives the samples name. The second and third columns give the  $^{207}\text{Pb}/^{206}\text{Pb}$  age in million years (Ma) and the standard error (1 sigma). The fourth and fifth columns give the  $^{206}\text{Pb}/^{238}\text{U}$  in million years (Ma) and the standard error (1 sigma). The sixth and seventh columns give the  $^{207}\text{Pb}/^{235}\text{U}$  in million years (Ma) and the standard error (1 sigma). The eighth column gives the percentage of radiogenic  $^{206}\text{Pb}$ . The ninth and tenth columns show the ratio of  $^{206}\text{Pb}/^{238}\text{U}$  values corrected for common Pb ( $^{206}\text{Pb}^*/^{238}\text{U}$ ) and the standard error (1 sigma). The eleventh and twelfth columns show the ratio of  $^{207}\text{Pb}/^{235}\text{U}$  values corrected for common Pb ( $^{207}\text{Pb}^*/^{235}\text{U}$ ) and the standard error (1 sigma). The thirteenth and fourteenth columns show the ratio of  $^{207}\text{Pb}/^{206}\text{Pb}$  values corrected for common Pb ( $^{207}\text{Pb}^*/^{206}\text{Pb}^*$ ) and the standard error (1 sigma). The fifteenth column shows the correlation of concordia ellipses of the grains that passed the initial  $^{206}\text{Pb}/^{207}\text{Pb}$  ratio survey calculated according to ref. (34). Dashed values ("--") represent no measurements were obtained. AS3 standards are the standard measured for each mount.

Sample name	$^{207}\text{Pb}/^{206}\text{Pb}$ Age (Ma)	1 s.e. (Ma)	$^{206}\text{Pb}/^{238}\text{U}$ Age (Ma)	1 s.e. (Ma)	$^{207}\text{Pb}/^{235}\text{U}$ Age (Ma)	1 s.e. (Ma)	% radiogenic $^{206}\text{Pb}$	$^{206}\text{Pb}^*/^{238}\text{U}$ 1 s.e.	$^{207}\text{Pb}^*/^{235}\text{U}$ 1 s.e.	$^{207}\text{Pb}^*/^{206}\text{Pb}^*$ 1 s.e.	Correlation of concordia ellipses			
1-10-11	3564	4.0	4174	252.0	3772	81.4	99.97	0.9108	0.07480	40.040	3.2900	0.31880	0.000837	1.000
1-10-14	3414	26.6	-	-	-	-	100.00	-	-	-	-	0.28940	0.004950	0.991
1-13-11	3445	1.6	2955	188.0	3255	77.3	99.97	0.5816	0.04600	23.670	1.8800	0.29520	0.000295	1.000
1-13-3	3498	10.6	2483	190.0	3081	91.1	99.92	0.4698	0.04330	19.790	1.8700	0.30550	0.002090	0.998
1-13-6	3402	3.4	3049	188.0	3266	75.4	99.95	0.6048	0.04670	23.940	1.8500	0.28710	0.000619	1.000
1-14-16	3708	26.7	411	34.8	1451	69.6	99.68	0.0658	0.00576	3.175	0.2860	0.35020	0.006150	0.981
1-14-9	4054	7.5	4224	270.0	4109	87.0	99.86	0.9255	0.08070	56.230	4.9000	0.44070	0.002210	0.998
1-15-12	3510	18.4	-	-	-	-	99.64	-	-	-	-	0.30770	0.003670	1.000
1-15-4	3097	92.2	701	59.7	1582	95.9	97.23	0.1149	0.01030	3.750	0.4480	0.23660	0.013700	0.886
1-17-10	3464	19.1	1580	132.0	2560	86.9	98.63	0.2778	0.02610	11.440	1.0600	0.29880	0.003690	0.991
1-17-15	3771	18.3	3452	299.0	3657	112.0	98.14	0.7083	0.07920	35.640	4.0300	0.36500	0.004400	0.994
1-18-7	3988	11.1	2855	250.0	3562	108.0	99.32	0.5572	0.06030	32.400	3.5500	0.42170	0.003130	0.998
1-19-16	3884	37.9	-	-	-	-	100.00	-	-	-	-	0.39350	0.009900	0.980
1-2-13	3364	13.1	2463	233.0	2988	107.0	99.84	0.4654	0.05290	17.980	2.0000	0.28010	0.002350	0.997
1-20-3	4116	9.2	3010	301.0	3712	124.0	99.84	0.5950	0.07440	37.700	4.7400	0.45960	0.002850	0.999
1-20-6	2777	163.0	-	-	-	-	98.12	-	-	-	-	0.19400	0.019300	0.905
1-3-20	3382	13.1	3167	296.0	3300	116.0	99.88	0.6344	0.07510	24.790	2.9400	0.28340	0.002380	0.998
1-5-13	4043	10.1	2508	177.0	3443	86.7	99.88	0.4756	0.04050	28.690	2.5300	0.43750	0.002960	0.998

1-7-14	3896	3.5	831	52.3	2176	60.0	99.88	0.1375	0.00922	7.523	0.5040	0.39670	0.000911	0.999	
1-8-11	3408	12.6	1222	103.0	2264	86.0	99.92	0.2087	0.01920	8.294	0.7880	0.28820	0.002330	0.997	
1-8-6	2912	74.9	-	-	-	-	99.67	-	-	-	-	0.21080	0.009750	0.993	
1-8-7	3448	2.7	3716	237.0	3544	82.5	99.97	0.7797	0.06540	31.800	2.6600	0.29580	0.000520	1.000	
1-9-11	3426	30.0	-	-	-	-	99.64	-	-	-	-	0.29150	0.005620	0.993	
AS3 standard	1008	18.3	1365	203.0	1233	118.0	99.92	0.2358	0.03890	2.367	0.3900	0.07278	0.000655	0.999	
AS3 standard	1108	10.5	988	110.0	1026	77.7	99.97	0.1656	0.02000	1.746	0.2100	0.07650	0.000404	0.999	
AS3 standard	1074	11.9	1066	157.0	1068	106.0	99.99	0.1797	0.02880	1.864	0.2990	0.07521	0.000446	0.999	
AS3 standard	1103	10.6	1018	112.0	1045	78.1	99.91	0.1710	0.02040	1.799	0.2150	0.07629	0.000405	0.999	
AS3 standard	1089	11.7	1170	115.0	1142	74.1	99.93	0.1991	0.02150	2.080	0.2250	0.07576	0.000442	0.999	
AS3 standard	1116	13.2	1054	104.0	1075	71.3	99.94	0.1777	0.01900	1.881	0.2020	0.07679	0.000509	0.998	
AS3 standard	1140	19.1	1018	106.0	1058	74.2	99.93	0.1711	0.01920	1.835	0.2070	0.07775	0.000747	0.996	
AS3 standard	1428	153.0	766	112.0	958	110.0	100.00	0.1262	0.01950	1.569	0.2790	0.09014	0.007230	0.893	
AS3 standard	944	37.4	1487	343.0	1279	188.0	99.85	0.2594	0.06700	2.522	0.6520	0.07053	0.001290	0.998	
AS3 standard	1298	15.4	1141	163.0	1196	110.0	99.95	0.1936	0.03020	2.248	0.3510	0.08424	0.000668	0.999	
AS3 standard	1252	17.7	1203	247.0	1221	160.0	99.96	0.2051	0.04610	2.327	0.5250	0.08228	0.000743	0.999	
AS3 standard	1090	12.7	1141	130.0	1123	84.9	99.94	0.1936	0.02410	2.024	0.2530	0.07583	0.000483	0.999	
AS3 standard	1090	14.8	990	113.0	1021	79.5	99.98	0.1659	0.02050	1.734	0.2140	0.07580	0.000558	0.998	
AS3 standard	1077	17.0	1131	101.0	1113	66.1	99.98	0.1919	0.01860	1.992	0.1950	0.07531	0.000639	0.996	
AS3 standard	1146	6.0	1210	123.0	1187	78.0	99.99	0.2064	0.02300	2.218	0.2470	0.07796	0.000235	1.000	
AS3 standard	1100	6.0	1020	113.0	1046	77.9	99.99	0.1714	0.02050	1.801	0.2150	0.07620	0.000229	1.000	
AS3 standard	1109	13.2	988	103.0	1026	73.0	99.97	0.1657	0.01870	1.748	0.1980	0.07652	0.000507	0.998	
AS3 standard	1102	5.5	1047	117.0	1065	79.7	100.00	0.1763	0.02130	1.854	0.2240	0.07628	0.000208	1.000	
2-1-6	4010	50.4	-	-	-	-	99.37	-	-	-	-	0.42780	0.014400	0.994	
2-1-7	3660	7.2	1756	301.0	2793	186.0	99.96	0.3132	0.06120	14.650	2.8700	0.33930	0.001590	1.000	
2-10-5	4164	3.6	3548	339.0	3952	123.0	99.97	0.7339	0.09110	48.020	5.9600	0.47450	0.001160	1.000	
2-12-19	3803	22.0	-	-	-	-	99.92	-	-	-	-	0.37280	0.005420	0.998	
2-2-1	4251	3.4	2521	222.0	3587	105.0	99.94	0.4786	0.05100	33.220	3.5400	0.50350	0.001150	1.000	
2-2-4	3893	28.4	-	-	-	-	99.74	-	-	-	-	0.39580	0.007470	0.988	
2-9-19	3738	9.7	3076	389.0	3491	157.0	99.74	0.6116	0.09730	30.120	4.8000	0.35720	0.002280	0.999	

AS3 standard	1089	5.3	1184	129.0	1151	82.0	99.99	0.2020	0.02400	2.110	0.2510	0.07578	0.000202	1.000	
AS3 standard	1087	9.4	953	135.0	995	96.4	99.98	0.1590	0.02420	1.660	0.2530	0.07571	0.000356	1.000	
AS3 standard	1133	15.5	923	131.0	987	96.1	99.96	0.1540	0.02340	1.640	0.2500	0.07744	0.000603	0.999	
AS3 standard	1072	25.8	2677	2890.0	1874	1130.0	99.87	0.5150	0.68000	5.330	7.0500	0.07514	0.000963	1.000	
AS3 standard	1139	12.7	955	195.0	1013	141.0	99.95	0.1600	0.03510	1.710	0.3760	0.07768	0.000495	1.000	
AS3 standard	1087	16.6	1028	257.0	1047	177.0	99.95	0.1730	0.04680	1.800	0.4880	0.07569	0.000628	1.000	
AS3 standard	1093	12.2	1006	124.0	1034	86.3	99.92	0.1690	0.02250	1.770	0.2350	0.07591	0.000461	0.999	
AS3 standard	1061	10.1	1210	163.0	1157	102.0	99.96	0.2060	0.03050	2.130	0.3140	0.07471	0.000373	0.999	
3-1-10	5389	539.0	10400	8140.0	6525	1550.0	-452.00	4.0160	6.33000	616.800	942.0000	1.11400	0.430000	0.970	
3-13-14	4171	5.0	4700	386.0	4336	116.0	99.93	1.0730	0.12400	70.560	8.1600	0.47680	0.001600	1.000	
3-14-18	3968	22.8	-	-	-	-	99.64	-	-	-	-	0.41590	0.006330	0.992	
3-20-14	4050	7.3	4392	403.0	4160	126.0	99.91	0.9766	0.12400	59.190	7.5000	0.43960	0.002160	0.999	
3-3-2	4061	14.4	4490	476.0	4198	147.0	99.86	1.0070	0.14800	61.460	9.0600	0.44280	0.004270	0.998	
3-5-16	3749	4.0	3994	357.0	3832	119.0	99.92	0.8582	0.10300	42.560	5.1200	0.35970	0.000955	1.000	
s3-8-14	3959	98.2	-	-	-	-	99.87	-	-	-	-	0.41350	0.027100	0.952	
AS3 standard	1118	45.1	1056	119.0	1076	81.5	99.53	0.1780	0.02170	1.887	0.2320	0.07687	0.001740	0.983	
AS3 standard	1264	60.8	1164	155.0	1200	104.0	99.44	0.1979	0.02890	2.259	0.3350	0.08276	0.002570	0.978	
AS3 standard	918	111.0	1002	152.0	976	104.0	99.68	0.1681	0.02750	1.615	0.2690	0.06966	0.003750	0.947	
AS3 standard	974	102.0	943	93.5	952	70.5	99.66	0.1575	0.01680	1.554	0.1770	0.07157	0.003600	0.899	
AS3 standard	947	202.0	1061	154.0	1024	121.0	98.42	0.1788	0.02810	1.742	0.3270	0.07065	0.006970	0.851	
6-13-2	3571	8.9	1513	96.2	2579	66.5	98.90	0.2646	0.01890	11.680	0.8310	0.32020	0.001850	0.997	
6-15-17	3737	4.6	3158	227.0	3523	89.1	99.90	0.6320	0.05740	31.110	2.8200	0.35700	0.001070	1.000	
6-2-12	1897	17.8	5395	70.2	3136	19.7	96.90	1.3090	0.02510	20.950	0.4260	0.11610	0.001150	0.876	
6-2-20	3942	7.1	3574	247.0	3813	89.3	99.90	0.7408	0.06680	41.760	3.7600	0.40880	0.001930	0.999	
6-20-10	1779	47.6	445	26.9	740	34.7	93.10	0.0715	0.00448	1.072	0.0708	0.10880	0.002840	0.919	
6-20-12	3693	9.2	2887	194.0	3384	81.2	99.80	0.5650	0.04720	27.020	2.2400	0.34690	0.002100	0.997	
6-20-16	4035	6.6	4128	295.0	4065	96.3	100.00	0.8972	0.08670	53.800	5.2000	0.43490	0.001920	0.999	
6-5-19	3785	17.8	3677	260.0	3747	92.1	99.70	0.7690	0.07150	39.070	3.6300	0.36850	0.004320	0.992	
6-7-11	3899	14.2	1099	60.5	2451	56.3	97.00	0.1859	0.01110	10.180	0.6200	0.39730	0.003760	0.988	

6-7-7	3275	6.8	1020	63.7	2013	59.8	98.30	0.1715	0.01160	6.258	0.4270	0.26470	0.001140	0.998		
6-8-10	1435	35.0	987	75.5	1137	57.8	95.70	0.1655	0.01360	2.064	0.1750	0.09045	0.001660	0.976		
AS3 standard	1073	39.1	1057	96.6	1062	64.8	99.70	0.1781	0.01760	1.846	0.1820	0.07517	0.001460	0.981		
AS3 standard	1046	18.7	1027	87.6	1033	59.9	99.90	0.1727	0.01590	1.766	0.1630	0.07418	0.000689	0.995		
AS3 standard	1041	41.8	952	91.2	979	68.3	99.50	0.1591	0.01640	1.623	0.1760	0.07399	0.001530	0.982		
AS3 standard	1088	16.1	1086	95.2	1087	63.5	99.90	0.1836	0.01750	1.917	0.1830	0.07575	0.000609	0.996		
AS3 standard	1099	30.8	1077	92.9	1084	63.3	99.90	0.1818	0.01700	1.909	0.1810	0.07614	0.001170	0.987		
AS3 standard	1077	15.4	1085	93.8	1083	62.6	99.90	0.1834	0.01720	1.904	0.1790	0.07533	0.000577	0.997		
7-10-1	4162	2.4	3418	118.0	3903	44.8	99.94	0.6993	0.03120	45.700	2.0600	0.47400	0.000754	0.999		
7-10-15	3387	4.0	3325	461.0	3364	174.0	100.00	0.6749	0.12000	26.460	4.7000	0.28440	0.000731	1.000		
7-10-17	2824	26.5	541	84.5	1246	117.0	99.96	0.0876	0.01430	2.413	0.3940	0.19980	0.003240	0.995		
7-10-18	3543	11.2	3399	113.0	3490	40.0	99.74	0.6944	0.02960	30.110	1.2300	0.31450	0.002290	0.986		
7-10-20	3487	10.3	2922	71.5	3267	29.8	99.67	0.5735	0.01750	23.980	0.7330	0.30320	0.002020	0.976		
7-11-12	3633	5.3	3384	129.0	3543	47.9	99.87	0.6904	0.03370	31.750	1.5500	0.33360	0.001160	0.997		
7-12-3	3420	10.5	2915	134.0	3223	56.3	99.53	0.5718	0.03260	22.900	1.3300	0.29050	0.001960	0.993		
7-13-10	3463	11.7	2550	148.0	3090	68.2	98.87	0.4852	0.03410	19.980	1.4100	0.29860	0.002260	0.994		
7-13-20	3973	1.0	3899	121.0	3948	41.1	99.95	0.8309	0.03440	47.820	1.9800	0.41740	0.000289	1.000		
7-13-4	4180	5.4	3717	144.0	4023	51.0	99.95	0.7799	0.03970	51.580	2.6400	0.47970	0.001730	0.998		
7-14-10	1873	46.0	1424	233.0	1615	150.0	99.96	0.2472	0.04510	3.905	0.7230	0.11460	0.002920	0.991		
7-14-12	3560	7.1	2011	54.9	2880	30.8	96.22	0.3662	0.01160	16.050	0.5170	0.31800	0.001470	0.990		
7-14-17	4115	5.2	2343	85.9	3410	43.4	99.71	0.4383	0.01920	27.750	1.2300	0.45910	0.001600	0.997		
7-15-16	4091	2.1	3949	127.0	4043	43.0	99.89	0.8451	0.03640	52.630	2.2700	0.45170	0.000651	0.999		
7-15-4	3677	14.4	2973	107.0	3410	45.5	99.21	0.5860	0.02640	27.730	1.2900	0.34320	0.003240	0.979		
7-15-6	4276	2.7	4183	205.0	4246	66.7	99.96	0.9134	0.06100	64.460	4.3000	0.51180	0.000924	1.000		
7-15-7	4197	4.2	3596	113.0	3992	41.3	99.90	0.7468	0.03070	49.960	2.0700	0.48520	0.001360	0.998		
7-16-18	3841	1.3	3153	88.0	3588	34.8	99.94	0.6308	0.02230	33.240	1.1700	0.38220	0.000339	1.000		
7-17-16	3809	3.9	1107	29.5	2404	27.5	99.92	0.1873	0.00543	9.669	0.2890	0.37440	0.000958	0.997		
7-17-18	4216	2.2	2414	56.6	3512	27.7	99.95	0.4542	0.01280	30.770	0.8680	0.49140	0.000742	0.999		
7-17-8	4227	4.1	3236	106.0	3877	41.6	99.91	0.6521	0.02720	44.530	1.8600	0.49530	0.001390	0.998		
7-18-15	4003	4.4	4050	149.0	4019	48.9	99.83	0.8742	0.04340	51.340	2.5200	0.42590	0.001240	0.998		

7-19-1	4100	4.2	3603	118.0	3930	42.1	99.92	0.7489	0.03190	46.940	1.9900	0.45460	0.001280	0.998		
7-19-20	3500	4.5	3629	490.0	3547	174.0	99.99	0.7559	0.13300	31.880	5.6300	0.30590	0.000898	1.000		
7-19-3	3470	10.0	3823	482.0	3595	165.0	99.88	0.8096	0.13500	33.490	5.6000	0.30000	0.001940	0.999		
7-19-7	3836	1.5	3719	136.0	3795	48.0	99.95	0.7804	0.03760	41.010	1.9900	0.38110	0.000372	1.000		
7-2-13	3575	6.3	3558	481.0	3569	173.0	99.97	0.7367	0.12900	32.610	5.7300	0.32110	0.001310	1.000		
7-2-20	3597	3.9	3547	103.0	3579	36.9	99.94	0.7336	0.02770	32.950	1.2300	0.32580	0.000822	0.998		
7-2-4	3746	7.0	3515	501.0	3664	183.0	99.98	0.7251	0.13400	35.900	6.6400	0.35910	0.001650	1.000		
7-2-9	4088	3.8	3450	135.0	3865	50.1	99.87	0.7078	0.03590	44.000	2.2200	0.45090	0.001150	0.999		
7-20-6	2183	22.1	1286	46.1	1665	34.5	98.97	0.2208	0.00873	4.156	0.1750	0.13650	0.001740	0.954		
7-3-10	4219	3.0	3803	125.0	4080	43.2	99.90	0.8039	0.03500	54.610	2.3600	0.49260	0.000994	0.999		
7-3-12	3975	2.2	2187	49.1	3238	25.7	99.97	0.4039	0.01070	23.270	0.6140	0.41780	0.000600	0.999		
7-3-14	2102	17.1	821	133.0	1254	124.0	99.98	0.1358	0.02350	2.439	0.4200	0.13030	0.001270	0.998		
7-3-15	3534	7.2	3427	117.0	3495	43.3	99.69	0.7017	0.03100	30.250	1.3300	0.31260	0.001450	0.995		
7-3-20	3543	6.8	3454	491.0	3510	181.0	99.98	0.7087	0.13000	30.730	5.6500	0.31450	0.001380	1.000		
7-3-4	4231	3.6	4119	165.0	4195	54.4	99.89	0.8945	0.04860	61.250	3.3400	0.49670	0.001210	0.999		
7-3-8	4153	2.7	2763	85.8	3632	37.4	99.95	0.5352	0.02040	34.750	1.3200	0.47100	0.000849	0.999		
7-4-12	3524	6.6	3460	120.0	3501	43.0	99.81	0.7104	0.03180	30.430	1.3300	0.31070	0.001320	0.996		
7-4-13	3400	3.1	3306	470.0	3365	178.0	99.99	0.6700	0.12200	26.480	4.8200	0.28670	0.000573	1.000		
7-4-18	3325	8.4	3009	429.0	3202	173.0	99.93	0.5948	0.10600	22.420	4.0000	0.27330	0.001470	1.000		
7-4-5	4011	4.0	3345	109.0	3774	41.4	99.78	0.6802	0.02830	40.150	1.6800	0.42820	0.001160	0.998		
7-5-12	2690	33.9	1231	55.5	1875	31.6	98.92	0.2104	0.01040	5.339	0.1970	0.18410	0.003780	0.928		
7-5-17	3937	4.8	1961	56.3	3091	31.7	99.95	0.3556	0.01180	19.990	0.6550	0.40760	0.001290	0.996		
7-5-3	4083	2.9	3078	86.0	3718	35.1	99.95	0.6120	0.02150	37.910	1.3400	0.44920	0.000877	0.999		
7-6-14	4012	1.8	1998	49.6	3160	27.8	99.96	0.3634	0.01050	21.480	0.6160	0.42860	0.000510	0.999		
7-6-19	3597	9.9	1847	58.8	2809	35.0	99.95	0.3318	0.01220	14.900	0.5480	0.32570	0.002090	0.985		
7-7-1	4078	2.5	3682	132.0	3943	46.3	99.89	0.7702	0.03620	47.570	2.2200	0.44790	0.000755	0.999		
7-7-10	2903	6.5	1291	207.0	2034	155.0	99.99	0.2218	0.03920	6.412	1.1300	0.20970	0.000836	1.000		
7-7-13	3631	4.9	2424	83.7	3137	40.4	99.55	0.4564	0.01890	20.960	0.8740	0.33310	0.001070	0.997		
7-7-19	3419	8.2	2474	76.0	3028	35.9	99.47	0.4679	0.01730	18.720	0.6970	0.29020	0.001540	0.990		
7-7-20	4123	2.3	3881	121.0	4042	41.4	99.89	0.8260	0.03430	52.580	2.1800	0.46170	0.000713	0.999		
7-7-6	1688	96.4	434	21.2	701	38.3	86.15	0.0697	0.00352	0.995	0.0752	0.10350	0.005410	0.724		

7-8-1	3575	6.2	3476	468.0	3539	171.0	99.98	0.7145	0.12400	31.630	5.5100	0.32110	0.001300	1.000		
7-8-16	4198	2.1	4063	125.0	4154	41.5	99.94	0.8783	0.03650	58.790	2.4400	0.48550	0.000700	0.999		
7-8-17	4227	9.6	4011	137.0	4156	45.8	99.69	0.8631	0.03970	58.940	2.7100	0.49520	0.003240	0.990		
7-8-19	4194	4.2	4018	163.0	4136	53.7	99.73	0.8649	0.04700	57.760	3.1100	0.48430	0.001360	0.999		
7-8-3	3683	5.5	3229	439.0	3516	170.0	100.00	0.6503	0.11200	30.890	5.3400	0.34450	0.001230	1.000		
7-8-9	3760	11.1	3490	548.0	3663	201.0	99.96	0.7183	0.14600	35.880	7.2900	0.36230	0.002640	0.999		
7-9-17	4149	6.7	2070	247.0	3289	136.0	99.99	0.3786	0.05280	24.520	3.4200	0.46970	0.002110	1.000		
7-9-19	3968	4.9	3821	117.0	3918	40.5	99.87	0.8089	0.03290	46.410	1.8900	0.41610	0.001350	0.997		
7-9-8	4047	1.5	2259	78.0	3323	39.8	99.98	0.4197	0.01720	25.380	1.0300	0.43860	0.000438	1.000		
AS3 standard	1085	12.6	1018	329.0	1040	227.0	100.00	0.1711	0.05970	1.784	0.6220	0.07563	0.000476	1.000		
AS3 standard	1111	30.0	973	202.0	1016	144.0	99.92	0.1629	0.03650	1.721	0.3860	0.07662	0.001150	0.998		
AS3 standard	3581	25.9	1502	285.0	2577	200.0	99.95	0.2624	0.05570	11.660	2.5000	0.32230	0.005430	0.997		
AS3 standard	1093	9.2	1022	170.0	1044	117.0	100.00	0.1717	0.03080	1.797	0.3230	0.07591	0.000348	1.000		
AS3 standard	1090	14.0	1029	184.0	1049	126.0	99.99	0.1731	0.03340	1.809	0.3500	0.07580	0.000529	0.999		
AS3 standard	1132	21.5	985	182.0	1031	129.0	99.99	0.1650	0.03280	1.762	0.3510	0.07741	0.000838	0.999		
AS3 standard	1107	17.4	1000	186.0	1034	130.0	99.98	0.1677	0.03360	1.768	0.3550	0.07644	0.000665	0.999		
AS3 standard	1085	18.5	1321	234.0	1234	140.0	99.95	0.2274	0.04450	2.370	0.4650	0.07560	0.000698	0.999		
AS3 standard	1040	16.5	1209	215.0	1150	134.0	99.95	0.2063	0.04020	2.103	0.4100	0.07394	0.000603	0.999		
AS3 standard	1366	23.0	1149	542.0	1227	367.0	99.96	0.1952	0.10000	2.347	1.2100	0.08723	0.001040	1.000		
AS3 standard	1136	49.6	1050	388.0	1078	266.0	99.68	0.1768	0.07080	1.891	0.7570	0.07757	0.001930	0.998		
AS3 standard	1091	21.0	1057	425.0	1068	288.0	99.91	0.1782	0.07770	1.864	0.8130	0.07586	0.000793	1.000		
AS3 standard	1100	17.6	1262	447.0	1203	275.0	99.94	0.2163	0.08430	2.271	0.8860	0.07617	0.000669	1.000		
AS3 standard	1066	28.7	1149	435.0	1120	280.0	99.87	0.1950	0.08060	2.015	0.8330	0.07492	0.001070	0.999		
AS3 standard	1101	27.9	1014	193.0	1042	135.0	99.97	0.1703	0.03510	1.790	0.3700	0.07624	0.001060	0.998		
AS3 standard	1075	24.7	986	197.0	1014	139.0	99.98	0.1653	0.03570	1.714	0.3700	0.07523	0.000927	0.998		
AS3 standard	1100	16.4	996	199.0	1029	140.0	99.99	0.1671	0.03610	1.755	0.3790	0.07618	0.000626	0.999		
AS3 standard	1132	26.8	932	241.0	993	176.0	99.98	0.1555	0.04330	1.660	0.4620	0.07742	0.001040	0.999		
AS3 standard	1101	19.8	1017	228.0	1044	158.0	99.98	0.1709	0.04150	1.796	0.4360	0.07622	0.000756	0.999		
AS3 standard	1113	11.7	999	219.0	1035	154.0	99.98	0.1676	0.03970	1.772	0.4200	0.07668	0.000449	1.000		
AS3 standard	1266	7.4	1088	55.9	1149	38.9	99.98	0.1839	0.01030	2.100	0.1190	0.08285	0.000314	0.998		
AS3 standard	1245	8.1	1088	39.9	1142	27.3	99.92	0.1839	0.00733	2.079	0.0829	0.08199	0.000337	0.995		

AS3 standard	1303	14.5	1178	63.5	1223	42.8	99.88	0.2005	0.01180	2.334	0.1400	0.08445	0.000629	0.992	
AS3 standard	1256	4.9	1132	47.4	1175	32.1	99.97	0.1919	0.00877	2.182	0.1010	0.08243	0.000206	0.999	
AS3 standard	1253	3.9	1065	43.9	1128	30.5	99.98	0.1796	0.00804	2.038	0.0913	0.08231	0.000163	0.999	
AS3 standard	1291	7.9	1098	47.8	1165	32.6	99.92	0.1857	0.00880	2.150	0.1010	0.08394	0.000343	0.996	
AS3 standard	1274	6.6	1058	38.2	1131	26.5	99.94	0.1784	0.00698	2.046	0.0795	0.08321	0.000281	0.996	
AS3 standard	1270	6.3	1071	40.5	1139	27.8	99.95	0.1808	0.00742	2.070	0.0840	0.08304	0.000267	0.997	
AS3 standard	1256	10.3	1120	44.2	1168	31.1	99.90	0.1898	0.00816	2.158	0.0967	0.08245	0.000435	0.994	
AS3 standard	1262	10.2	1142	47.2	1184	31.4	99.83	0.1938	0.00873	2.209	0.0994	0.08271	0.000433	0.993	
AS3 standard	1254	8.5	1092	43.7	1148	30.2	99.91	0.1847	0.00803	2.096	0.0921	0.08234	0.000356	0.995	
AS3 standard	1238	11.5	1189	57.1	1207	36.7	99.96	0.2026	0.01070	2.282	0.1190	0.08168	0.000479	0.994	
AS3 standard	1270	13.5	1152	47.4	1194	32.2	99.91	0.174	0.00880	2.241	0.1030	0.08304	0.000573	0.989	
AS3 standard	1109	30.0	1085	39.2	1093	29.5	99.89	0.1834	0.00719	1.935	0.0851	0.07654	0.001150	0.941	
AS3 standard	1008	11.7	1147	40.1	1100	26.0	99.61	0.1947	0.00744	1.955	0.0756	0.07280	0.000420	0.989	
AS3 standard	1109	34.9	1087	35.3	1095	26.2	99.62	0.1838	0.00647	1.939	0.0758	0.07653	0.001340	0.895	
AS3 standard	1114	24.1	1083	42.0	1094	28.5	99.91	0.1830	0.00770	1.936	0.0824	0.07672	0.000928	0.959	
AS3 standard	1132	68.1	1095	37.8	1107	35.6	99.65	0.1851	0.00695	1.975	0.1040	0.07741	0.002650	0.763	
AS3 standard	1109	306.0	1134	43.1	1126	113.0	68.11	0.1924	0.00798	2.030	0.3370	0.07654	0.011700	0.423	
AS3 standard	1107	28.5	1109	39.0	1108	27.5	99.96	0.1877	0.00719	1.978	0.0807	0.07646	0.001090	0.937	
AS3 standard	1068	30.1	1142	51.7	1117	36.3	99.85	0.1937	0.00957	2.003	0.1070	0.07499	0.001120	0.961	
AS3 standard	1065	26.6	1029	38.6	1041	27.8	99.80	0.1731	0.00702	1.787	0.0763	0.07487	0.000989	0.951	
AS3 standard	1019	22.9	1067	37.2	1051	25.4	99.73	0.1800	0.00680	1.816	0.0704	0.07320	0.000827	0.957	
8-10-15	1916	227.0	9025	186.0	3981	145.0	59.30	3.0550	0.11700	49.410	7.2200	0.11730	0.014900	0.605	
8-10-16	4004	5.3	4002	288.0	4003	96.1	99.90	0.8604	0.08310	50.550	4.8800	0.42610	0.001510	0.999	
8-10-19	3993	5.3	3021	249.0	3635	103.0	99.80	0.5978	0.06170	34.870	3.6200	0.42310	0.001490	0.999	
8-10-2	4056	6.4	1689	107.0	3001	68.9	98.70	0.2995	0.02150	18.220	1.3000	0.44120	0.001910	0.998	
8-11-6	2343	16.6	1616	115.0	1959	71.0	98.40	0.2849	0.02300	5.883	0.4810	0.14980	0.001460	0.993	
8-11-8	3515	4.1	2094	127.0	2897	68.1	99.00	0.3837	0.02730	16.340	1.1600	0.30890	0.000812	0.999	
8-12-10	3514	3.5	3443	267.0	3488	98.3	99.90	0.7059	0.07070	30.030	3.0000	0.30860	0.000704	1.000	
8-12-16	3723	5.7	1836	136.0	2881	81.4	99.20	0.3295	0.02800	16.070	1.3700	0.35360	0.001330	0.999	
8-12-4	3625	11.0	2365	179.0	3104	87.0	99.50	0.4432	0.04020	20.260	1.8200	0.33160	0.002370	0.997	

8-13-12	3534	4.4	3665	306.0	3580	108.0	99.90	0.7656	0.08380	32.990	3.6200	0.31260	0.000886	1.000	
8-13-18	3761	6.2	899	51.7	2170	55.6	97.50	0.1496	0.00921	7.479	0.4640	0.36260	0.001470	0.998	
8-16-12	3727	5.5	840	49.5	2086	56.0	97.90	0.1391	0.00874	6.801	0.4300	0.35460	0.001280	0.998	
8-16-14	4051	6.7	4314	359.0	4136	114.0	99.90	0.9526	0.10900	57.760	6.5900	0.43970	0.001970	0.999	
8-16-3	4127	5.1	4180	291.0	4144	94.1	99.80	0.9126	0.08630	58.240	5.4900	0.46280	0.001600	0.999	
8-18-14	3536	19.0	-	-	-	-	99.90	-	-	-	-	0.31310	0.003860	1.000	
8-19-11	3855	4.8	4036	311.0	3916	103.0	100.00	0.8704	0.09040	46.320	4.8100	0.38600	0.001230	1.000	
8-19-15	3469	8.2	3440	248.0	3459	90.8	100.00	0.7052	0.06560	29.150	2.7000	0.29980	0.001590	0.998	
8-19-2	3521	4.8	2202	139.0	2957	71.5	99.60	0.4071	0.03030	17.400	1.3000	0.31000	0.000968	0.999	
8-2-1	3117	6.3	2962	213.0	3055	87.0	99.70	0.5833	0.05240	19.270	1.7400	0.23950	0.000941	0.999	
8-2-11	3979	6.6	3990	297.0	3983	99.7	99.90	0.8568	0.08540	49.520	4.9600	0.41910	0.001840	0.999	
8-2-12	3534	5.7	3444	248.0	3501	91.6	99.90	0.7061	0.06570	30.440	2.8400	0.31260	0.001160	0.999	
8-3-10	3331	37.8	359	33.5	1170	70.9	92.60	0.0573	0.00550	2.167	0.2210	0.27430	0.006630	0.972	
8-3-8	3603	10.4	3047	229.0	3393	92.9	99.60	0.6043	0.05700	27.250	2.5800	0.32710	0.002210	0.998	
8-5-9	3137	39.9	430	61.4	1214	112.0	95.10	0.0690	0.01020	2.306	0.3650	0.24250	0.006090	0.989	
8-6-11	3478	6.8	3295	240.0	3410	91.3	99.90	0.6672	0.06210	27.740	2.5800	0.30150	0.001330	0.999	
8-6-15	2870	13.8	1210	81.7	1954	65.1	97.90	0.2064	0.01530	5.849	0.4390	0.20550	0.001750	0.994	
8-6-16	1459	39.0	279	18.5	451	26.1	88.60	0.0443	0.00300	0.559	0.0401	0.09161	0.001880	0.958	
8-6-8	3756	8.4	1846	128.0	2907	76.2	98.90	0.3315	0.02640	16.520	1.3200	0.36130	0.002000	0.998	
8-7-9	2852	28.9	1310	82.5	2020	63.1	93.30	0.2253	0.01570	6.309	0.4550	0.20310	0.003610	0.969	
8-8-20	3954	5.1	4094	333.0	4000	109.0	99.80	0.8871	0.09750	50.410	5.5400	0.41220	0.001400	1.000	
8-8-3	3500	3.3	3151	226.0	3368	88.9	99.90	0.6303	0.05730	26.570	2.4100	0.30580	0.000643	1.000	
8-8-5	3217	7.2	346	20.8	1095	41.5	91.50	0.0552	0.00341	1.941	0.1200	0.25510	0.001170	0.997	
8-9-12	3323	14.0	2415	195.0	2940	95.9	99.60	0.4545	0.04390	17.100	1.7100	0.27290	0.002450	0.996	
8-9-3	3783	5.7	3635	264.0	3731	94.7	99.90	0.7576	0.07200	38.440	3.6800	0.36810	0.001390	0.999	
8-9-6	3906	4.4	2304	150.0	3254	75.0	99.00	0.4296	0.03320	23.650	1.8200	0.39920	0.001170	0.999	
8-9-7	4569	542.0	2463	768.0	3774	94.3	98.60	0.4653	0.17500	40.140	3.8200	0.62570	0.234000	0.143	
AS3 standard	1096	16.2	947	91.0	993	65.5	99.90	0.1582	0.01640	1.659	0.1710	0.07605	0.000616	0.997	
AS3 standard	1074	13.0	1049	92.2	1057	62.5	99.90	0.1768	0.01680	1.833	0.1740	0.07520	0.000485	0.998	
AS3 standard	1080	13.1	1044	91.1	1056	62.0	99.90	0.1758	0.01660	1.828	0.1730	0.07542	0.000491	0.998	
AS3 standard	1084	9.2	1137	111.0	1119	72.1	100.00	0.1929	0.02050	2.009	0.2140	0.07556	0.000347	0.999	

AS3 standard	269	544.0	913	62.3	745	139.0	83.20	0.1521	0.01110	1.082	0.2840	0.05162	0.012300	0.470	
AS3 standard	1102	4.5	1206	113.0	1169	71.3	100.00	0.2057	0.02110	2.163	0.2220	0.07626	0.000172	1.000	
AS3 standard	1093	6.6	1189	114.0	1156	72.1	100.00	0.2026	0.02120	2.121	0.2220	0.07594	0.000248	1.000	
AS3 standard	1008	19.0	991	130.0	996	90.3	99.20	0.1661	0.02360	1.667	0.2370	0.07278	0.000681	0.998	
AS3 standard	1119	25.8	1104	94.5	1109	63.8	99.90	0.1869	0.01740	1.982	0.1870	0.07693	0.000994	0.991	
AS3 standard	1100	15.6	1102	94.6	1102	62.6	100.00	0.1865	0.01740	1.959	0.1820	0.07619	0.000593	0.997	
AS3 standard	1087	11.4	1122	97.7	1110	63.9	100.00	0.1901	0.01800	1.984	0.1880	0.07569	0.000431	0.998	
9-10-3	229	3950.0	1703	1920.0	1154	1530.0	80.00	0.3023	0.38700	2.116	4.6900	0.05075	0.086800	0.639	
9-11-2	3493	23.3	2755	374.0	3200	163.0	98.90	0.5331	0.08890	22.380	3.7400	0.30450	0.004590	0.996	
9-12-6	4165	6.1	3930	254.0	4087	85.8	99.70	0.8398	0.07240	55.000	4.7300	0.47500	0.001960	0.999	
9-13-12	1807	52.2	1153	252.0	1403	184.0	98.70	0.1958	0.04670	2.984	0.7210	0.11050	0.003180	0.993	
9-13-15	3216	19.1	825	68.4	1785	78.8	98.40	0.1365	0.01210	4.799	0.4500	0.25500	0.003090	0.993	
9-14-16	3467	7.4	2589	162.0	3111	74.2	99.70	0.4943	0.03760	20.410	1.5700	0.29950	0.001430	0.998	
9-14-3	4292	597.0	-	-	-	63.10	-	-	-	-	0.51760	0.210000	0.937		
9-14-9	3124	28.7	2511	151.0	2865	71.4	99.20	0.4762	0.03460	15.800	1.1800	0.24060	0.004340	0.971	
9-15-12	3630	7.8	1514	81.2	2616	56.1	98.60	0.2648	0.01590	12.150	0.7260	0.33290	0.001700	0.996	
9-18-12	1084	28.3	1068	84.8	1073	56.7	100.00	0.1802	0.01550	1.877	0.1610	0.07556	0.001070	0.987	
9-18-8	5353	343.0	1443	6160.0	3709	4670.0	-55.90	0.2509	1.20000	37.570	177.0000	1.08600	0.266000	0.999	
9-2-13	3493	22.3	2618	255.0	3140	110.0	99.40	0.5009	0.05930	21.030	2.3800	0.30450	0.004390	0.993	
9-2-16	3214	10.3	1564	101.0	2401	67.0	99.20	0.2746	0.01990	9.643	0.7020	0.25470	0.001660	0.996	
9-20-1	3487	10.6	813	57.4	1919	65.4	96.00	0.1344	0.01010	5.620	0.4270	0.30330	0.002070	0.996	
9-20-11	3763	25.9	313	18.1	1268	47.3	91.10	0.0497	0.00295	2.487	0.1630	0.36320	0.006190	0.967	
9-3-11	3340	69.4	888	173.0	1919	183.0	94.10	0.1477	0.03080	5.621	1.1900	0.27600	0.012200	0.978	
9-3-19	5773	652.0	585	824.0	3055	1170.0	-31.80	0.0951	0.14000	19.270	23.3000	1.47000	0.696000	0.957	
9-3-6	3943	12.6	2642	421.0	3439	193.0	99.40	0.5066	0.09840	28.570	5.6400	0.40910	0.003430	0.999	
9-4-3	4941	200.0	1483	835.0	3451	611.0	-928.00	0.2586	0.16300	28.920	18.0000	0.81100	0.114000	0.975	
9-5-18	4324	907.0	895	812.0	2511	936.0	-136.00	0.1489	0.14500	10.860	10.9000	0.52880	0.327000	0.805	
9-7-6	3470	16.5	1489	150.0	2502	105.0	98.70	0.2599	0.02940	10.750	1.2200	0.30000	0.003200	0.996	
9-9-9	3268	26.0	2087	362.0	2742	193.0	98.40	0.3822	0.07760	13.890	2.8300	0.26360	0.004350	0.997	
AS3 standard	1085	8.6	1144	90.9	1124	58.8	100.00	0.1943	0.01680	2.025	0.1750	0.07561	0.000324	0.999	

AS3 standard	1119	40.7	1080	66.7	1093	48.0	99.70	0.1825	0.01220	1.935	0.1390	0.07690	0.001570	0.959	
AS3 standard	1069	17.9	1094	66.9	1085	44.1	99.90	0.1849	0.01230	1.912	0.1270	0.07500	0.000670	0.991	
AS3 standard	1085	14.7	1142	76.4	1123	50.2	99.90	0.1939	0.01420	2.022	0.1500	0.07563	0.000555	0.995	
AS3 standard	1094	21.5	1092	68.0	1093	44.8	99.90	0.1847	0.01250	1.934	0.1290	0.07596	0.000815	0.987	
AS3 standard	1104	94.9	1064	65.9	1077	55.1	98.00	0.1795	0.01210	1.889	0.1570	0.07635	0.003620	0.820	
AS3 standard	1051	101.0	1113	77.8	1092	63.9	98.00	0.1884	0.01440	1.932	0.1840	0.07436	0.003740	0.852	
AS3 standard	1077	29.1	1075	85.5	1075	56.9	99.80	0.1814	0.01570	1.884	0.1610	0.07532	0.001090	0.986	
AS3 standard	1097	39.7	1018	93.1	1043	65.2	99.20	0.1710	0.01690	1.794	0.1790	0.07609	0.001510	0.980	
AS3 standard	990	77.1	818	87.8	866	70.6	98.20	0.1353	0.01550	1.346	0.1630	0.07213	0.002730	0.950	
AS3 standard	1070	10.0	1062	88.5	1064	59.5	99.90	0.1791	0.01620	1.853	0.1670	0.07504	0.000374	0.999	
AS3 standard	1080	17.6	1007	73.2	1030	51.5	99.90	0.1691	0.01330	1.758	0.1400	0.07542	0.000661	0.994	
AS3 standard	1118	20.2	1034	73.2	1061	51.3	99.90	0.1739	0.01330	1.843	0.1440	0.07688	0.000780	0.992	
AS3 standard	1056	49.6	1048	73.7	1051	52.9	98.90	0.1765	0.01350	1.814	0.1470	0.07455	0.001840	0.953	
AS3 standard	1032	29.8	1093	75.8	1073	50.9	99.60	0.1848	0.01390	1.876	0.1440	0.07364	0.001080	0.982	
11-10-16	3424	5.1	1025	63.4	2101	59.9	99.86	0.1724	0.01150	6.922	0.4670	0.29110	0.000959	0.999	
11-10-19	4132	9.7	4074	161.0	4113	53.5	99.92	0.8814	0.04710	56.460	3.0300	0.46460	0.003030	0.993	
11-10-3	3343	35.0	961	55.5	1994	57.1	98.06	0.1607	0.01000	6.124	0.4000	0.27640	0.006180	0.940	
11-12-2	3493	13.6	3569	199.0	3521	73.3	99.90	0.7396	0.05370	31.060	2.3100	0.30450	0.002680	0.993	
11-13-6	3599	6.2	732	42.4	1886	52.9	99.93	0.1203	0.00737	5.409	0.3340	0.32620	0.001310	0.998	
11-14-10	3498	10.6	2455	109.0	3068	51.4	99.89	0.4635	0.02470	19.520	1.0400	0.30550	0.002100	0.992	
11-16-15	5265	1430.0	-	-	-	-	9.99	-	-	-	-	-	-	0.981	
11-16-2	3161	19.6	201	12.3	740	31.9	95.71	0.0316	0.00197	1.073	0.0651	0.24620	0.003040	0.980	
11-20-10	6004	6340.0	531	4570.0	3120	4620.0	5.42	0.0859	0.77000	20.600	98.3000	1.73900	8.070000	0.955	
11-4-4	2546	38.5	777	48.4	1403	48.7	99.97	0.1281	0.00846	2.982	0.1910	0.16890	0.003880	0.938	
11-5-1	3525	8.0	2342	120.0	3030	58.0	99.88	0.4381	0.02670	18.770	1.1300	0.31080	0.001600	0.997	
11-8-12	3693	4.0	3634	191.0	3672	68.0	99.99	0.7573	0.05210	36.220	2.4900	0.34690	0.000904	0.999	
11-8-13	3502	4.4	3339	175.0	3442	65.8	99.98	0.6787	0.04550	28.660	1.9200	0.30620	0.000876	0.999	
AS3 standard	1051	17.3	1124	68.5	1100	44.9	99.66	0.1906	0.01270	1.953	0.1310	0.07435	0.000639	0.992	
AS3 standard	1092	38.5	1043	73.7	1059	51.7	99.70	0.1756	0.01340	1.838	0.1450	0.07588	0.001460	0.970	
AS3 standard	1365	22.3	1020	51.7	1136	39.3	99.96	0.1714	0.00940	2.060	0.1190	0.08718	0.001010	0.980	

AS3 standard	1098	8.6	1100	67.5	1099	45.0	99.98	0.1861	0.01240	1.953	0.1310	0.07611	0.000328	0.998	
AS3 standard	1101	8.6	1067	92.1	1079	62.3	99.95	0.1801	0.01690	1.893	0.1770	0.07624	0.000327	0.999	
12-1-15	3249	3.7	1792	43.4	2565	26.5	99.17	0.3205	0.00889	11.500	0.3260	0.26030	0.000608	0.997	
12-10-15	2797	510.0	7838	754.0	4243	377.0	63.02	2.3730	0.39500	64.300	24.3000	0.19650	0.061200	0.582	
12-10-6	3274	4.3	1692	51.0	2519	31.8	99.11	0.3002	0.01030	10.950	0.3740	0.26460	0.000730	0.997	
12-14-12	3989	4.8	4021	129.0	3999	42.1	99.86	0.8659	0.03730	50.360	2.1300	0.42180	0.001350	0.997	
12-14-17	2812	17.9	5998	28.0	3818	14.8	98.49	1.5360	0.01100	41.970	0.6260	0.19820	0.002170	0.721	
12-14-5	3966	3.5	4053	123.0	3995	40.3	99.84	0.8751	0.03590	50.120	2.0300	0.41540	0.000960	0.999	
12-15-3	3746	5.1	979	21.7	2244	22.5	98.18	0.1640	0.00391	8.119	0.2020	0.35900	0.001200	0.992	
12-17-6	4019	2.8	2346	55.9	3349	27.7	99.60	0.4390	0.01250	26.060	0.7380	0.43050	0.000816	0.998	
12-17-9	3822	2.6	2930	71.1	3486	29.8	99.64	0.5755	0.01740	29.960	0.9080	0.37760	0.000644	0.998	
12-2-8	3655	4.2	3698	103.0	3670	36.4	99.93	0.7747	0.02830	36.130	1.3300	0.33830	0.000921	0.997	
12-20-11	3768	8.3	2747	76.2	3372	32.3	99.64	0.5313	0.01810	26.690	0.8800	0.36430	0.001990	0.987	
12-20-12	3773	10.7	2757	56.2	3380	26.1	99.82	0.5338	0.01340	26.900	0.7180	0.36550	0.002590	0.965	
12-20-5	3918	6.5	3703	106.0	3843	37.7	99.79	0.7760	0.02930	43.040	1.6300	0.40230	0.001750	0.993	
12-3-11	3775	7.8	1769	56.0	2873	34.4	99.13	0.3159	0.01140	15.940	0.5730	0.36600	0.001890	0.990	
12-3-3	3978	4.8	1602	37.9	2894	26.2	98.86	0.2822	0.00754	16.300	0.4470	0.41890	0.001330	0.994	
12-6-13	3827	1810.0	-	-	-	-	22.21	-	-	-	-	0.37880	0.454000	0.891	
12-8-2	2788	12.0	1145	34.8	1859	29.5	97.17	0.1944	0.00645	5.238	0.1810	0.19540	0.001430	0.978	
12-9-3	3383	4.1	1781	39.2	2639	23.5	99.31	0.3183	0.00801	12.450	0.3120	0.28370	0.000751	0.995	
AS3 standard	1083	11.7	1143	39.3	1122	26.0	99.95	0.1939	0.00728	2.020	0.0774	0.07553	0.000439	0.989	
AS3 standard	1098	16.9	1059	30.2	1072	20.9	99.96	0.1786	0.00552	1.875	0.0593	0.07612	0.000644	0.964	
AS3 standard	1102	15.9	1098	37.2	1099	25.3	99.92	0.1856	0.00684	1.952	0.0734	0.07626	0.000607	0.977	
AS3 standard	1094	7.4	1080	30.6	1084	20.7	99.99	0.1823	0.00561	1.910	0.0592	0.07597	0.000282	0.993	
AS3 standard	1085	23.0	1050	31.7	1062	22.0	99.96	0.1770	0.00579	1.845	0.0617	0.07563	0.000867	0.940	
AS3 standard	1101	8.7	1144	39.2	1129	25.7	99.94	0.1942	0.00727	2.042	0.0770	0.07623	0.000333	0.993	
AS3 standard	1112	17.4	1125	37.3	1121	25.7	99.91	0.1907	0.00689	2.015	0.0764	0.07663	0.000668	0.973	
AS3 standard	1100	15.9	1092	38.1	1095	26.0	99.95	0.1846	0.00700	1.939	0.0752	0.07620	0.000604	0.979	
AS3 standard	1094	9.3	1049	35.4	1064	24.2	99.92	0.1767	0.00646	1.851	0.0680	0.07596	0.000352	0.992	
AS3 standard	1046	22.9	1049	55.0	1048	38.0	99.83	0.1766	0.01000	1.807	0.1050	0.07418	0.000842	0.981	

AS3 standard	1067	23.7	1090	36.0	1083	26.4	99.53	0.1842	0.00662	1.904	0.0756	0.07496	0.000884	0.956	
AS3 standard	1102	18.3	1076	40.7	1085	28.0	99.83	0.1817	0.00747	1.910	0.0803	0.07625	0.000696	0.976	
AS3 standard	1089	25.3	1150	44.6	1129	29.8	99.83	0.1954	0.00828	2.041	0.0894	0.07577	0.000958	0.958	
AS3 standard	1089	25.3	1150	44.6	1129	29.8	99.83	0.1954	0.00828	2.041	0.0894	0.07577	0.000958	0.958	
AS3 standard	1115	15.7	1104	34.6	1108	23.4	99.96	0.1868	0.00636	1.977	0.0686	0.07677	0.000603	0.974	
AS3 standard	1096	9.0	1090	34.1	1092	22.9	99.94	0.1842	0.00626	1.931	0.0660	0.07604	0.000343	0.991	
AS3 standard	1122	29.5	1080	38.0	1094	28.5	99.66	0.1823	0.00697	1.936	0.0825	0.07701	0.001140	0.939	
AS3 standard	1122	29.5	1080	38.0	1094	28.5	99.66	0.1823	0.00697	1.936	0.0825	0.07701	0.001140	0.939	
15-1-1	4219	4.7	3853	209.0	4097	73.0	99.70	0.8178	0.05900	55.540	4.0700	0.49260	0.001560	0.999	
15-1-11	3980	9.1	836	32.5	2231	37.6	94.70	0.1384	0.00573	8.004	0.3340	0.41930	0.002550	0.989	
15-1-12	3510	7.1	3044	177.0	3332	71.3	99.70	0.6034	0.04390	25.610	1.8700	0.30780	0.001420	0.998	
15-1-14	3147	14.3	548	22.3	1404	32.8	89.80	0.0887	0.00377	2.985	0.1290	0.24410	0.002200	0.978	
15-1-15	4065	8.8	888	39.9	2341	46.1	95.60	0.1476	0.00710	9.033	0.4550	0.44380	0.002610	0.994	
15-1-5	3347	5.3	3192	194.0	3288	74.8	99.70	0.6408	0.04930	24.490	1.8800	0.27720	0.000941	0.999	
15-1-7	4094	4.9	4072	213.0	4087	70.5	99.90	0.8808	0.06210	54.960	3.8900	0.45260	0.001500	0.999	
15-1-9	3662	60.7	278	15.6	1137	55.8	86.20	0.0440	0.00253	2.063	0.1680	0.33990	0.013500	0.893	
15-10-13	3448	18.5	900	65.7	1991	70.1	98.40	0.1497	0.01170	6.106	0.4910	0.29580	0.003540	0.989	
15-10-18	2147	69.1	89	3.1	231	11.7	60.30	0.0138	0.00049	0.255	0.0145	0.13370	0.005290	0.728	
15-10-20	3540	8.5	495	17.7	1517	29.4	84.40	0.0798	0.00296	3.454	0.1290	0.31380	0.001730	0.989	
15-10-9	3122	11.4	125	4.6	508	15.0	75.60	0.0196	0.00072	0.649	0.0243	0.24030	0.001730	0.982	
15-11-10	4038	3.7	633	25.6	2005	36.9	97.10	0.1032	0.00439	6.202	0.2620	0.43590	0.001080	0.998	
15-11-11	3532	3.6	3362	177.0	3469	66.4	99.90	0.6846	0.04630	29.460	1.9900	0.31220	0.000718	0.999	
15-11-14	2643	20.4	359	18.6	895	29.7	91.70	0.0573	0.00305	1.413	0.0706	0.17890	0.002200	0.974	
15-11-19	3925	27.9	3703	189.0	3849	69.7	99.80	0.7761	0.05200	43.270	3.0400	0.40440	0.007510	0.964	
15-11-20	3991	4.6	4214	259.0	4064	83.0	99.90	0.9227	0.07720	53.730	4.4800	0.42230	0.001310	0.999	
15-11-8	3391	4.5	1191	61.6	2228	51.1	95.50	0.2028	0.01150	7.974	0.4520	0.28510	0.000825	0.999	
15-12-11	3877	243.0	-	-	-	-	100.00	-	-	-	-	0.39160	0.063200	1.000	
15-12-12	2515	2550.0	139	55.5	411	636.0	52.30	0.0218	0.00879	0.498	0.9380	0.16580	0.252000	0.919	
15-12-15	3293	9.6	711	21.2	1694	26.9	95.70	0.1166	0.00367	4.304	0.1400	0.26770	0.001640	0.982	
15-12-19	3289	8.2	947	41.8	1951	42.4	96.70	0.1583	0.00750	5.828	0.2850	0.26700	0.001400	0.995	

15-13-11	3250	9.3	819	27.7	1797	30.5	86.20	0.1355	0.00487	4.868	0.1760	0.26050	0.001540	0.987	
15-13-12	3328	17.1	267	8.9	970	21.9	92.20	0.0424	0.00143	1.599	0.0560	0.27380	0.002990	0.950	
15-13-13	3329	20.6	1632	88.0	2513	56.7	97.60	0.2881	0.01760	10.890	0.6640	0.27410	0.003600	0.977	
15-13-14	3141	36.6	407	19.6	1177	38.8	89.00	0.0652	0.00325	2.186	0.1220	0.24320	0.005600	0.911	
15-13-18	3343	20.9	3072	171.0	3238	70.0	98.40	0.6106	0.04260	23.270	1.6700	0.27640	0.003690	0.983	
15-13-3	3278	5.8	512	18.6	1413	28.6	88.70	0.0826	0.00312	3.021	0.1130	0.26530	0.000979	0.995	
15-13-5	3872	6.6	699	31.6	1999	41.6	95.90	0.1145	0.00545	6.164	0.2930	0.39030	0.001700	0.996	
15-13-8	2981	11.2	414	14.9	1119	25.8	85.10	0.0663	0.00246	2.010	0.0764	0.22010	0.001530	0.983	
15-14-10	3585	6.0	3704	213.0	3627	74.4	99.90	0.7765	0.05860	34.590	2.6100	0.32310	0.001270	0.999	
15-14-14	3520	8.4	3285	211.0	3433	79.4	99.80	0.6647	0.05440	28.400	2.3000	0.30980	0.001690	0.998	
15-14-19	2921	17.0	630	26.3	1408	34.0	91.30	0.1027	0.00450	3.002	0.1340	0.21200	0.002220	0.972	
15-14-6	3268	21.4	540	18.0	1450	29.6	89.60	0.0873	0.00303	3.172	0.1210	0.26350	0.003590	0.935	
15-15-10	3687	4.1	3265	172.0	3532	65.7	99.70	0.6594	0.04440	31.420	2.1000	0.34550	0.000920	0.999	
15-15-12	3430	12.4	435	14.0	1359	27.1	94.00	0.0698	0.00232	2.814	0.1020	0.29230	0.002340	0.977	
15-15-15	4057	5.4	3543	199.0	3879	72.3	99.80	0.7325	0.05360	44.600	3.2500	0.44160	0.001610	0.999	
15-15-16	3518	3.3	3354	190.0	3458	71.7	99.80	0.6826	0.04970	29.130	2.1300	0.30950	0.000655	1.000	
15-15-2	3047	14.1	638	22.2	1478	29.7	86.80	0.1040	0.00380	3.288	0.1260	0.22930	0.002020	0.973	
15-15-5	3645	3.8	3685	211.0	3659	73.9	99.80	0.7710	0.05780	35.720	2.6700	0.33600	0.000838	0.999	
15-15-7	3528	3.7	3088	165.0	3361	65.2	99.70	0.6146	0.04120	26.400	1.7600	0.31150	0.000743	0.999	
15-16-1	3751	4.4	788	29.5	2040	35.2	95.90	0.1301	0.00517	6.460	0.2580	0.36020	0.001050	0.997	
15-16-12	3450	56.3	1082	133.0	2168	129.0	95.50	0.1827	0.02440	7.457	1.0700	0.29600	0.010700	0.969	
15-16-16	3533	4.0	3392	188.0	3481	70.2	99.90	0.6924	0.04940	29.820	2.1300	0.31240	0.000813	0.999	
15-16-17	3447	5.4	2494	129.0	3054	59.5	99.30	0.4724	0.02940	19.250	1.1900	0.29550	0.001040	0.998	
15-16-18	3444	5.7	1600	68.9	2561	45.2	98.70	0.2817	0.01370	11.460	0.5540	0.29500	0.001090	0.997	
15-16-19	3703	7.8	919	31.8	2158	33.7	95.00	0.1532	0.00569	7.375	0.2780	0.34920	0.001790	0.991	
15-16-6	3434	3.4	3181	156.0	3338	60.9	99.80	0.6380	0.03970	25.770	1.6000	0.29300	0.000642	0.999	
15-16-8	3492	4.3	1232	49.8	2321	40.1	98.70	0.2105	0.00936	8.832	0.3890	0.30420	0.000842	0.998	
15-17-12	3513	17.4	1775	142.0	2714	86.8	98.80	0.3171	0.02900	13.490	1.2400	0.30850	0.003470	0.993	
15-17-14	3583	8.5	792	35.0	1949	40.2	97.00	0.1307	0.00613	5.817	0.2700	0.32280	0.001780	0.993	
15-17-17	2502	29.2	236	8.7	621	19.5	73.70	0.0372	0.00141	0.844	0.0354	0.16440	0.002850	0.911	
15-17-18	3110	27.5	415	16.0	1176	31.9	81.10	0.0664	0.00264	2.184	0.1000	0.23860	0.004120	0.928	

15-17-3	3383	7.7	652	20.9	1666	27.9	96.50	0.1064	0.00359	4.158	0.1420	0.28350	0.001390	0.990		
15-17-5	3651	4.5	2629	134.0	3245	60.3	99.60	0.5036	0.03130	23.430	1.4500	0.33740	0.000999	0.999		
15-17-6	3036	21.2	329	9.9	987	21.6	83.80	0.0524	0.00161	1.643	0.0561	0.22770	0.003010	0.922		
15-17-8	3489	6.0	1410	60.0	2457	43.9	98.20	0.2446	0.01160	10.240	0.4860	0.30360	0.001180	0.997		
15-18-10	3449	5.3	1178	48.5	2251	40.9	97.70	0.2006	0.00903	8.182	0.3700	0.29590	0.001000	0.997		
15-18-13	3937	10.1	211	7.2	1070	23.7	81.10	0.0332	0.00115	1.868	0.0671	0.40760	0.002750	0.982		
15-18-15	2257	50.6	238	7.6	562	20.5	60.30	0.0376	0.00122	0.739	0.0351	0.14250	0.004180	0.795		
15-18-3	2882	10.5	570	21.4	1311	29.5	86.00	0.0924	0.00363	2.636	0.1060	0.20690	0.001340	0.987		
15-18-4	3875	4.2	1352	41.6	2649	31.9	95.20	0.2333	0.00797	12.580	0.4270	0.39100	0.001080	0.997		
15-18-6	2997	14.1	302	9.9	919	21.4	87.50	0.0480	0.00161	1.472	0.0521	0.22230	0.001950	0.969		
15-18-8	3527	6.9	3436	194.0	3494	71.8	99.80	0.7040	0.05120	30.220	2.2100	0.31130	0.001390	0.998		
15-18-9	3481	224.0	485	58.2	1471	141.0	100.00	0.0782	0.00974	3.256	0.5930	0.30200	0.043600	0.613		
15-19-14	3443	4.7	3211	101.0	3356	38.5	99.93	0.6457	0.02580	26.240	1.0300	0.29470	0.000890	0.997		
15-19-17	3464	5.3	1494	31.2	2502	21.7	96.43	0.2608	0.00610	10.750	0.2510	0.29880	0.001020	0.989		
15-19-2	3385	7.6	3076	117.0	3266	47.0	99.82	0.6115	0.02930	23.940	1.1500	0.28390	0.001390	0.995		
15-19-5	3256	8.1	856	20.3	1839	22.2	93.11	0.1419	0.00359	5.118	0.1340	0.26150	0.001350	0.980		
15-2-10	4007	23.6	2943	357.0	3612	152.0	99.60	0.5787	0.08740	34.070	5.2300	0.42690	0.006750	0.995		
15-2-16	3463	2.4	2976	157.0	3274	64.4	99.90	0.5866	0.03870	24.140	1.5900	0.29850	0.000469	1.000		
15-2-2	3537	6.2	2768	148.0	3234	64.1	99.70	0.5362	0.03530	23.160	1.5300	0.31320	0.001260	0.998		
15-2-3	3624	12.6	3552	216.0	3598	75.8	99.40	0.7351	0.05820	33.600	2.5800	0.33150	0.002730	0.995		
15-2-5	3736	9.7	3567	186.0	3676	66.4	99.70	0.7390	0.05020	36.340	2.4400	0.35670	0.002290	0.996		
15-2-7	3905	7.4	3941	222.0	3917	75.6	99.80	0.8430	0.06350	46.360	3.5300	0.39890	0.001960	0.998		
15-20-6	3902	7.6	853	23.8	2204	26.6	97.94	0.1414	0.00422	7.764	0.2300	0.39810	0.002020	0.986		
15-20-8	4082	3.8	3385	102.0	3837	38.2	99.76	0.6906	0.02660	42.750	1.6500	0.44900	0.001140	0.998		
15-3-15	3535	5.5	3634	224.0	3571	79.3	99.90	0.7572	0.06120	32.670	2.6300	0.31290	0.001120	0.999		
15-3-5	3417	9.1	2939	174.0	3230	73.5	99.60	0.5777	0.04250	23.080	1.7400	0.28980	0.001690	0.997		
15-3-6	3368	13.2	3300	188.0	3342	72.0	99.60	0.6686	0.04870	25.890	1.9100	0.28080	0.002380	0.993		
15-3-7	3229	10.8	1192	46.4	2136	39.3	90.20	0.2031	0.00866	7.197	0.3170	0.25710	0.001760	0.988		
15-4-1	3515	5.9	2989	151.0	3312	61.8	99.60	0.5898	0.03730	25.110	1.5900	0.30870	0.001180	0.998		
15-4-11	4140	14.2	3941	1030.0	4074	347.0	99.50	0.8428	0.29400	54.270	18.9000	0.46700	0.004470	1.000		
15-4-12	3538	6.6	3040	193.0	3348	77.5	99.80	0.6026	0.04790	26.040	2.0600	0.31340	0.001340	0.999		

15-4-13	3544	4.9	2349	120.0	3045	58.7	99.00	0.4396	0.02680	19.070	1.1600	0.31460	0.001000	0.999		
15-4-19	3570	3.3	2681	139.0	3217	62.0	99.40	0.5158	0.03270	22.760	1.4500	0.32000	0.000686	0.999		
15-4-20	3456	4.2	3043	188.0	3297	75.8	99.60	0.6032	0.04670	24.720	1.9200	0.29720	0.000810	0.999		
15-4-6	3491	5.9	3392	168.0	3454	62.6	99.90	0.6924	0.04420	29.030	1.8500	0.30410	0.001160	0.998		
15-4-7	3514	3.2	3324	169.0	3443	64.1	99.80	0.6746	0.04400	28.700	1.8800	0.30850	0.000645	1.000		
15-4-8	3852	5.5	3780	202.0	3827	69.1	99.80	0.7975	0.05630	42.350	2.9500	0.38520	0.001410	0.999		
15-5-12	3138	12.7	302	14.9	973	31.1	89.70	0.0480	0.00243	1.607	0.0799	0.24280	0.001930	0.988		
15-5-14	2960	16.3	430	17.4	1137	29.4	89.20	0.0689	0.00288	2.065	0.0887	0.21720	0.002190	0.972		
15-5-4	3339	8.4	1688	69.4	2555	43.4	98.40	0.2994	0.01400	11.380	0.5290	0.27580	0.001470	0.993		
15-5-5	4120	8.5	1752	75.9	3083	47.8	98.10	0.3122	0.01550	19.830	0.9800	0.46080	0.002640	0.993		
15-5-9	3142	9.9	451	15.4	1252	25.9	81.80	0.0724	0.00256	2.430	0.0875	0.24340	0.001520	0.985		
15-6-10	3397	40.4	3150	801.0	3303	306.0	99.10	0.6301	0.20300	24.860	7.8000	0.28610	0.007420	0.997		
15-6-12	2658	291.0	203	12.6	594	98.2	54.50	0.0319	0.00202	0.795	0.1740	0.18060	0.031700	0.758		
15-6-20	2580	31.4	272	10.6	715	23.0	86.50	0.0430	0.00172	1.022	0.0458	0.17230	0.003240	0.908		
15-6-3	1756	536.0	-	-	-	-	61.90	-	-	-	-	0.10740	0.031500	0.656		
15-6-4	3174	21.4	728	72.2	1653	81.8	95.20	0.1195	0.01250	4.092	0.4100	0.24830	0.003360	0.992		
15-6-8	3597	14.5	557	19.6	1644	32.5	91.40	0.0902	0.00332	4.050	0.1620	0.32560	0.003080	0.973		
15-7-10	3403	15.0	628	21.3	1645	30.9	87.70	0.1024	0.00364	4.056	0.1540	0.28730	0.002770	0.968		
15-7-11	2696	19.5	282	9.6	771	20.4	73.90	0.0447	0.00156	1.138	0.0429	0.18480	0.002180	0.950		
15-7-14	2512	44.7	248	6.8	650	20.0	63.10	0.0393	0.00110	0.896	0.0374	0.16550	0.004400	0.777		
15-7-18	3100	6.9	576	22.7	1421	31.3	94.80	0.0935	0.00384	3.053	0.1250	0.23700	0.001030	0.994		
15-8-5	4051	4.2	3763	218.0	3953	76.0	99.80	0.7927	0.06050	48.060	3.6700	0.43970	0.001250	0.999		
15-9-4	3224	6.8	724	25.0	1674	30.0	96.80	0.1188	0.00435	4.198	0.1540	0.25630	0.001100	0.993		
15-9-5	3298	15.8	2281	115.0	2860	59.8	99.20	0.4245	0.02550	15.720	0.9850	0.26860	0.002700	0.988		
15-9-8	3924	4.0	956	37.6	2328	38.7	95.00	0.1598	0.00676	8.901	0.3770	0.40400	0.001070	0.998		
AS3 standard	1078	19.6	1162	86.7	1133	56.0	99.90	0.1975	0.01610	2.051	0.1680	0.07535	0.000738	0.993		
AS3 standard	1056	17.6	1108	77.1	1090	50.6	99.90	0.1875	0.01420	1.927	0.1460	0.07453	0.000650	0.993		
AS3 standard	1104	16.1	1038	71.5	1060	49.3	100.00	0.1748	0.01300	1.839	0.1380	0.07634	0.000617	0.994		
AS3 standard	1058	24.1	1166	91.4	1129	58.5	99.80	0.1983	0.01700	2.040	0.1750	0.07461	0.000895	0.990		
AS3 standard	1081	13.6	1175	86.0	1142	54.8	99.90	0.1999	0.01600	2.080	0.1660	0.07546	0.000513	0.996		
AS3 standard	1066	22.0	1178	91.8	1139	58.1	99.90	0.2004	0.01710	2.070	0.1760	0.07490	0.000821	0.992		

AS3 standard	1093	11.9	1201	90.2	1163	57.3	100.00	0.2047	0.01690	2.143	0.1770	0.07593	0.000451	0.997		
AS3 standard	1092	28.0	1166	84.2	1140	55.6	99.90	0.1982	0.01570	2.074	0.1680	0.07590	0.001060	0.985		
AS3 standard	1081	11.3	1191	91.5	1152	57.6	100.00	0.2029	0.01710	2.111	0.1770	0.07547	0.000424	0.998		
AS3 standard	1099	25.3	1231	93.6	1184	58.0	99.90	0.2105	0.01760	2.210	0.1830	0.07617	0.000962	0.989		
AS3 standard	1089	16.7	1016	72.1	1039	50.1	99.90	0.1707	0.01310	1.783	0.1370	0.07575	0.000631	0.994		
AS3 standard	1063	38.6	1188	86.6	1144	54.4	99.70	0.2023	0.01610	2.086	0.1650	0.07479	0.001440	0.971		
AS3 standard	1102	28.7	1042	78.8	1062	55.0	99.90	0.1755	0.01440	1.845	0.1540	0.07626	0.001090	0.985		
AS3 standard	1083	5.3	1065	65.6	1071	44.4	100.00	0.1797	0.01200	1.871	0.1250	0.07554	0.000199	0.999		
AS3 standard	1065	12.6	1078	66.9	1074	44.8	99.90	0.1820	0.01230	1.879	0.1270	0.07489	0.000471	0.996		
AS3 standard	1084	23.7	1116	72.3	1105	49.1	99.80	0.1890	0.01330	1.969	0.1430	0.07557	0.000892	0.987		
AS3 standard	1095	11.2	1135	85.8	1121	55.8	100.00	0.1926	0.01590	2.017	0.1660	0.07598	0.000426	0.998		
AS3 standard	1080	20.3	1130	74.9	1113	48.8	99.90	0.1916	0.01380	1.993	0.1440	0.07543	0.000764	0.990		
AS3 standard	1103	19.2	1079	73.8	1087	49.4	99.80	0.1822	0.01350	1.916	0.1420	0.07629	0.000732	0.992		
AS3 standard	1116	26.0	938	68.6	992	49.4	99.90	0.1565	0.01230	1.657	0.1290	0.07679	0.000999	0.986		
AS3 standard	1065	27.0	1073	68.9	1070	46.9	99.80	0.1812	0.01260	1.870	0.1320	0.07485	0.001000	0.982		
AS3 standard	1062	15.1	1036	65.7	1044	45.8	99.90	0.1744	0.01200	1.797	0.1260	0.07475	0.000562	0.994		
AS3 standard	1091	29.4	1073	67.7	1079	47.0	99.90	0.1812	0.01240	1.894	0.1340	0.07583	0.001110	0.978		
AS3 standard	1095	18.4	1113	86.7	1107	57.2	99.90	0.1884	0.01600	1.975	0.1680	0.07601	0.000698	0.994		
AS3 standard	1124	17.8	1061	64.3	1082	43.6	99.60	0.1788	0.01180	1.902	0.1250	0.07713	0.000689	0.991		
AS3 standard	1052	23.1	1082	76.9	1072	51.6	99.70	0.1827	0.01410	1.874	0.1460	0.07438	0.000854	0.989		
AS3 standard	1035	13.4	1117	72.6	1089	47.3	99.90	0.1891	0.01340	1.923	0.1360	0.07375	0.000491	0.996		
AS3 standard	1102	11.2	1189	85.3	1158	54.0	99.90	0.2025	0.01590	2.129	0.1660	0.07626	0.000427	0.998		
AS3 standard	1086	7.8	1111	73.0	1102	48.1	100.00	0.1881	0.01340	1.962	0.1400	0.07565	0.000294	0.999		
AS3 standard	1075	8.8	977	58.1	1008	41.0	99.90	0.1637	0.01050	1.698	0.1090	0.07526	0.000330	0.998		
AS3 standard	1091	10.1	1079	59.5	1083	40.0	100.00	0.1822	0.01090	1.906	0.1150	0.07585	0.000382	0.997		
AS3 standard	1084	14.5	1066	66.5	1072	45.4	99.90	0.1798	0.01220	1.874	0.1280	0.07559	0.000548	0.994		
AS3 standard	1066	13.8	1046	70.6	1053	48.2	99.90	0.1763	0.01290	1.821	0.1340	0.07491	0.000512	0.996		
AS3 standard	1046	22.9	1049	55.0	1048	38.0	99.83	0.1766	0.01000	1.807	0.1050	0.07418	0.000842	0.981		
AS3 standard	1067	23.7	1090	36.0	1083	26.4	99.53	0.1842	0.00662	1.904	0.0756	0.07496	0.000884	0.956		
AS3 standard	1102	18.3	1076	40.7	1085	28.0	99.83	0.1817	0.00747	1.910	0.0803	0.07625	0.000696	0.976		
AS3 standard	1089	25.3	1150	44.6	1129	29.8	99.83	0.1954	0.00828	2.041	0.0894	0.07577	0.000958	0.958		

18-1-16	3392	8.1	3149	114.0	3299	44.5	99.87	0.6298	0.02890	24.770	1.1300	0.28530	0.001480	0.994		
18-1-17	3212	13.2	488	31.9	1344	45.2	99.97	0.0786	0.00534	2.757	0.1670	0.25440	0.002130	0.998		
18-1-18	3536	5.3	2676	84.1	3193	37.3	99.94	0.5145	0.01980	22.200	0.8530	0.31300	0.001070	0.996		
18-1-2	3466	4.2	3366	107.0	3429	40.1	99.96	0.6856	0.02810	28.280	1.1600	0.29910	0.000818	0.998		
18-10-11	4186	5.0	4188	139.0	4187	45.0	99.94	0.9148	0.04140	60.760	2.7400	0.48170	0.001620	0.997		
18-10-20	3547	5.8	2903	87.3	3297	37.0	99.97	0.5688	0.02120	24.720	0.9380	0.31520	0.001180	0.995		
18-10-7	3498	7.9	3642	148.0	3549	52.3	99.87	0.7593	0.04040	31.970	1.7000	0.30540	0.001550	0.995		
18-10-8	3476	6.6	3407	145.0	3451	54.0	99.85	0.6964	0.03820	28.910	1.5900	0.30110	0.001280	0.997		
18-11-11	3539	7.6	3576	115.0	3552	41.2	99.86	0.7416	0.03100	32.060	1.3400	0.31360	0.001540	0.993		
18-11-13	4138	7.5	3191	91.5	3800	36.5	99.98	0.6406	0.02330	41.190	1.5200	0.46640	0.002360	0.991		
18-11-18	3634	4.8	3213	102.0	3477	39.8	99.90	0.6460	0.02610	29.720	1.2000	0.33360	0.001050	0.997		
18-11-19	3453	5.7	3135	98.0	3332	38.5	99.94	0.6262	0.02470	25.610	1.0100	0.29660	0.001080	0.996		
18-11-20	3611	7.1	2860	86.5	3320	36.7	99.97	0.5585	0.02090	25.310	0.9520	0.32870	0.001520	0.992		
18-11-4	3892	4.5	1109	26.2	2456	23.3	99.93	0.1877	0.00483	10.240	0.2580	0.39550	0.001180	0.993		
18-11-6	3837	7.9	551	13.6	1766	21.9	99.91	0.0892	0.00231	4.691	0.1230	0.38130	0.002000	0.980		
18-12-11	3869	10.6	3762	129.0	3833	44.5	99.97	0.7925	0.03580	42.570	1.9100	0.38960	0.002750	0.988		
18-12-17	3513	5.5	1954	53.6	2819	30.1	99.96	0.3542	0.01130	15.060	0.4770	0.30840	0.001090	0.994		
18-12-6	4108	9.7	3377	151.0	3851	54.3	99.89	0.6886	0.03950	43.380	2.3800	0.45690	0.002990	0.994		
18-12-7	3747	6.5	964	33.8	2230	32.7	99.95	0.1614	0.00609	7.994	0.2900	0.35930	0.001530	0.994		
18-12-8	4104	7.6	4284	159.0	4162	50.1	99.91	0.9436	0.04790	59.290	2.9800	0.45570	0.002340	0.995		
18-13-14	3647	5.8	3603	119.0	3631	42.5	99.93	0.7489	0.03220	34.740	1.5000	0.33640	0.001280	0.996		
18-13-15	3537	4.5	2023	82.8	2872	46.3	99.96	0.3686	0.01760	15.920	0.7710	0.31330	0.000910	0.998		
18-13-19	3652	5.4	3662	127.0	3655	45.3	99.96	0.7649	0.03490	35.600	1.6300	0.33750	0.001190	0.997		
18-13-20	4011	5.0	4027	121.0	4016	40.5	99.90	0.8676	0.03520	51.220	2.0800	0.42820	0.001420	0.997		
18-13-5	3548	5.4	3462	108.0	3517	39.5	99.96	0.7110	0.02860	30.930	1.2400	0.31550	0.001100	0.996		
18-13-7	4136	8.2	1536	49.2	2950	35.2	99.80	0.2691	0.00968	17.270	0.6340	0.46560	0.002590	0.989		
18-14-12	3804	4.7	1046	28.8	2344	27.3	99.95	0.1761	0.00525	9.057	0.2700	0.37310	0.001150	0.995		
18-14-16	4103	9.4	3984	124.0	4063	43.1	99.89	0.8552	0.03570	53.700	2.3200	0.45540	0.002880	0.990		
18-14-2	4072	3.1	3319	92.1	3805	35.2	99.97	0.6735	0.02390	41.410	1.4700	0.44600	0.000928	0.998		
18-14-6	3592	7.3	3521	111.0	3566	40.7	99.91	0.7267	0.02980	32.520	1.3500	0.32460	0.001540	0.993		

18-15-13	3560	10.9	1265	47.1	2387	38.7	99.93	0.2167	0.00889	9.499	0.4010	0.31790	0.002250	0.986		
18-15-15	3576	4.6	499	16.1	1542	26.2	99.95	0.0805	0.00269	3.565	0.1180	0.32140	0.000957	0.996		
18-15-16	3518	6.8	2305	72.3	3007	36.1	99.95	0.4298	0.01600	18.330	0.6880	0.30940	0.001360	0.993		
18-15-17	3669	4.6	684	18.9	1863	23.4	99.89	0.1119	0.00326	5.267	0.1440	0.34130	0.001020	0.996		
18-15-18	4176	7.1	4203	135.0	4185	44.3	99.88	0.9194	0.04020	60.640	2.6900	0.47840	0.002300	0.994		
18-15-20	3523	11.7	3560	114.0	3537	41.2	99.95	0.7372	0.03080	31.560	1.3200	0.31050	0.002350	0.984		
18-15-5	3829	6.8	2123	54.8	3111	28.7	99.96	0.3900	0.01180	20.400	0.6050	0.37940	0.001710	0.989		
18-15-6	3864	8.6	472	13.7	1647	25.0	99.80	0.0759	0.00228	4.063	0.1250	0.38830	0.002210	0.983		
18-15-9	3479	10.1	1171	35.2	2263	29.8	99.88	0.1993	0.00654	8.287	0.2730	0.30160	0.001970	0.980		
18-16-14	3504	12.3	1098	44.8	2215	40.0	99.92	0.1858	0.00825	7.856	0.3480	0.30670	0.002440	0.984		
18-16-16	3482	9.8	3398	108.0	3451	40.3	99.92	0.6940	0.02840	28.920	1.1900	0.30220	0.001910	0.988		
18-17-1	3499	11.8	1286	40.9	2368	31.8	99.98	0.2207	0.00775	9.304	0.3220	0.30570	0.002330	0.976		
18-17-10	3531	6.8	3524	136.0	3528	48.8	99.88	0.7276	0.03640	31.290	1.5500	0.31190	0.001370	0.996		
18-17-11	4050	47.8	-	-	-	-	99.93	-	-	-	-	0.43940	0.014100	0.997		
18-17-12	3676	6.1	2327	62.4	3118	30.4	99.95	0.4347	0.01390	20.550	0.6460	0.34290	0.001360	0.992		
18-17-14	3862	3.1	2236	72.8	3191	37.8	99.96	0.4146	0.01600	22.160	0.8620	0.38760	0.000805	0.999		
18-17-3	3358	10.6	709	26.8	1727	29.7	99.95	0.1163	0.00463	4.476	0.1600	0.27910	0.001900	0.990		
18-17-9	3531	6.8	3524	136.0	3528	48.8	99.88	0.7276	0.03640	31.290	1.5500	0.31190	0.001370	0.996		
18-18-11	3508	9.4	1054	32.3	2176	30.5	99.97	0.1776	0.00590	7.526	0.2560	0.30740	0.001870	0.984		
18-18-13	3523	3.7	3183	96.3	3395	37.5	99.95	0.6385	0.02450	27.330	1.0500	0.31040	0.000738	0.998		
18-18-20	4184	4.7	3743	117.0	4035	42.0	99.95	0.7872	0.03250	52.190	2.2000	0.48080	0.001540	0.997		
18-18-5	3796	4.0	2817	92.3	3421	39.3	99.89	0.5481	0.02220	28.050	1.1200	0.37110	0.000967	0.998		
18-19-1	3583	23.0	518	14.9	1577	27.7	99.94	0.0837	0.00250	3.726	0.1290	0.32280	0.004830	0.903		
18-19-14	3494	4.4	3511	114.0	3500	41.6	99.95	0.7240	0.03050	30.410	1.2900	0.30470	0.000859	0.998		
18-19-16	3866	4.8	701	22.8	1998	29.3	99.79	0.1149	0.00394	6.156	0.2070	0.38870	0.001250	0.996		
18-19-19	4053	5.5	4022	127.0	4043	41.5	99.96	0.8663	0.03670	52.590	2.1900	0.44030	0.001610	0.996		
18-19-5	3380	6.1	2190	67.1	2864	35.0	99.96	0.4046	0.01460	15.790	0.5800	0.28310	0.001110	0.994		
18-19-6	3446	19.9	2389	71.6	3004	33.7	99.98	0.4486	0.01610	18.270	0.6390	0.29540	0.003790	0.935		
18-19-8	3868	12.1	3865	157.0	3867	52.1	99.82	0.8213	0.04420	44.070	2.3100	0.38910	0.003120	0.989		
18-19-9	3596	5.9	921	22.7	2097	23.4	99.86	0.1535	0.00405	6.890	0.1820	0.32550	0.001240	0.990		
18-2-1	3324	7.2	3121	108.0	3246	42.9	99.91	0.6228	0.02720	23.460	1.0300	0.27320	0.001250	0.995		

18-2-12	3949	43.8	2901	106.0	3556	43.8	99.56	0.5684	0.02580	32.190	1.4300	0.41070	0.012000	0.789		
18-2-20	3986	9.6	2377	43.9	3342	23.7	99.94	0.4460	0.00985	25.890	0.6270	0.42110	0.002710	0.966		
18-2-3	3268	10.5	2482	67.6	2938	32.0	99.87	0.4697	0.01540	17.060	0.5700	0.26350	0.001770	0.980		
18-2-6	4056	13.6	513	13.2	1825	22.3	99.87	0.0828	0.00222	5.034	0.1330	0.44120	0.004010	0.942		
18-20-11	3427	7.9	1387	40.3	2402	31.8	99.91	0.2400	0.00776	9.654	0.3330	0.29180	0.001490	0.991		
18-20-12	3410	8.7	2574	73.9	3069	32.9	99.93	0.4908	0.01710	19.530	0.6660	0.28860	0.001620	0.987		
18-20-14	3965	4.6	3651	113.0	3857	40.7	99.96	0.7617	0.03080	43.620	1.7900	0.41530	0.001260	0.997		
18-20-2	3712	4.5	1787	60.6	2845	37.4	99.94	0.3195	0.01240	15.470	0.6060	0.35110	0.001030	0.997		
18-20-6	3505	7.3	3507	106.0	3506	38.6	99.95	0.7230	0.02820	30.590	1.2000	0.30690	0.001450	0.993		
18-20-7	3366	6.3	1779	67.5	2627	39.9	99.93	0.3177	0.01380	12.290	0.5220	0.28050	0.001140	0.996		
18-3-1	4062	6.8	4097	135.0	4073	45.4	99.87	0.8880	0.03960	54.240	2.4700	0.44300	0.002030	0.995		
18-3-10	3449	6.1	3375	130.0	3422	49.0	99.96	0.6881	0.03410	28.080	1.4000	0.29600	0.001160	0.997		
18-3-3	3531	7.2	3404	110.0	3485	41.0	99.94	0.6957	0.02900	29.940	1.2500	0.31210	0.001460	0.994		
18-3-4	3963	6.6	2645	98.1	3454	44.8	99.94	0.5072	0.02290	29.000	1.3200	0.41470	0.001810	0.995		
18-3-5	4087	5.0	1015	35.6	2488	34.8	99.88	0.1706	0.00647	10.590	0.3970	0.45040	0.001520	0.996		
18-3-8	3640	4.7	3684	134.0	3656	47.0	99.93	0.7710	0.03680	35.620	1.7000	0.33500	0.001020	0.998		
18-4-11	3734	6.6	3617	129.0	3693	46.9	99.93	0.7526	0.03520	36.980	1.7500	0.35640	0.001540	0.996		
18-4-18	3752	5.2	2801	82.9	3385	35.7	99.94	0.5441	0.01990	27.040	0.9860	0.36050	0.001220	0.996		
18-4-8	4099	8.9	4068	167.0	4088	55.2	99.86	0.8794	0.04870	55.060	3.0500	0.45410	0.002710	0.994		
18-5-12	3390	11.7	3354	122.0	3377	46.0	99.94	0.6826	0.03180	26.820	1.2600	0.28500	0.002130	0.987		
18-5-8	3505	4.7	3513	153.0	3508	55.3	99.94	0.7245	0.04090	30.640	1.7200	0.30670	0.000932	0.999		
18-5-9	3467	6.0	1383	48.3	2424	35.2	99.93	0.2393	0.00928	9.880	0.3770	0.29940	0.001150	0.995		
18-6-10	3402	7.2	2245	72.7	2906	37.1	99.72	0.4167	0.01600	16.490	0.6390	0.28710	0.001320	0.993		
18-6-12	3559	4.5	721	25.7	1850	31.3	99.84	0.1184	0.00446	5.187	0.1910	0.31780	0.000932	0.997		
18-6-14	3497	6.0	427	13.4	1378	24.5	99.93	0.0685	0.00222	2.884	0.0937	0.30530	0.001190	0.993		
18-6-3	3539	5.1	2475	77.8	3103	36.6	99.93	0.4679	0.01770	20.240	0.7660	0.31380	0.001030	0.996		
18-6-6	3783	9.0	722	25.4	1977	32.1	99.87	0.1184	0.00441	6.010	0.2220	0.36800	0.002180	0.987		
18-7-10	4018	9.2	4017	141.0	4017	47.0	99.73	0.8648	0.04070	51.280	2.4200	0.43010	0.002660	0.991		
18-7-15	3647	5.1	3145	118.0	3459	46.1	99.94	0.6288	0.02980	29.170	1.3700	0.33650	0.001130	0.998		
18-7-17	3484	16.6	3455	125.0	3474	47.8	99.73	0.7091	0.03300	29.600	1.4400	0.30280	0.003240	0.976		
18-7-2	3634	3.4	1138	31.3	2326	27.7	99.89	0.1930	0.00578	8.881	0.2690	0.33370	0.000740	0.997		

18-7-8	3551	5.8	3624	143.0	3577	50.3	99.95	0.7544	0.03880	32.890	1.6800	0.31620	0.001190	0.997		
18-8-11	3498	10.8	1422	81.8	2470	57.3	99.82	0.2468	0.01580	10.390	0.6430	0.30540	0.002130	0.995		
18-8-12	4122	3.1	2891	76.5	3666	32.4	99.96	0.5659	0.01860	35.990	1.1800	0.46130	0.000965	0.998		
18-9-12	4139	13.2	3936	145.0	4072	51.8	99.76	0.8415	0.04140	54.150	2.8100	0.46670	0.004170	0.986		
18-9-8	3533	5.8	2549	101.0	3134	46.3	99.89	0.4850	0.02330	20.890	0.9990	0.31240	0.001170	0.997		
AS3 standard	1111	29.7	1061	51.6	1077	35.4	99.92	0.1788	0.00944	1.889	0.1010	0.07660	0.001140	0.961		
AS3 standard	1117	36.6	1081	45.9	1093	35.6	99.97	0.1826	0.00841	1.934	0.1030	0.07683	0.001410	0.942		
AS3 standard	1094	9.4	1096	50.6	1096	33.4	99.99	0.1854	0.00930	1.942	0.0967	0.07596	0.000357	0.996		
AS3 standard	1099	10.0	1123	51.6	1115	34.1	99.99	0.1903	0.00953	1.999	0.1010	0.07616	0.000380	0.995		
AS3 standard	1137	16.0	1052	43.6	1080	30.5	99.98	0.1772	0.00797	1.896	0.0869	0.07762	0.000625	0.985		
AS3 standard	1150	25.6	1100	44.9	1117	30.9	99.89	0.1860	0.00826	2.003	0.0915	0.07811	0.001010	0.960		
AS3 standard	1082	34.7	1074	48.0	1076	32.6	99.68	0.1812	0.00879	1.886	0.0927	0.07549	0.001310	0.937		
AS3 standard	1153	22.0	1181	64.6	1171	41.9	99.85	0.2011	0.01200	2.169	0.1310	0.07824	0.000869	0.983		
AS3 standard	1243	35.5	1153	47.5	1185	33.7	99.83	0.1959	0.00882	2.213	0.1070	0.08191	0.001480	0.927		
AS3 standard	1134	23.7	1078	58.3	1097	40.0	99.95	0.1821	0.01070	1.946	0.1160	0.07751	0.000922	0.980		
AS3 standard	1093	22.3	1131	56.6	1118	36.9	99.97	0.1918	0.01050	2.009	0.1090	0.07594	0.000847	0.979		
AS3 standard	1081	38.5	1054	41.6	1063	29.1	99.67	0.1777	0.00761	1.849	0.0818	0.07547	0.001450	0.903		
AS3 standard	1099	11.9	1091	42.6	1093	28.3	99.98	0.1843	0.00784	1.935	0.0819	0.07614	0.000455	0.990		
AS3 standard	1097	19.4	1121	45.1	1113	30.4	99.85	0.1899	0.00832	1.992	0.0897	0.07607	0.000738	0.977		
AS3 standard	1097	24.7	1078	41.9	1084	29.3	99.90	0.1820	0.00768	1.909	0.0838	0.07608	0.000940	0.960		
AS3 standard	1099	22.6	1102	41.5	1101	29.4	99.95	0.1864	0.00763	1.957	0.0856	0.07616	0.000861	0.967		
AS3 standard	1095	24.2	1106	39.8	1102	25.9	99.93	0.1872	0.00734	1.961	0.0756	0.07598	0.000918	0.952		
AS3 standard	1118	29.4	1061	41.7	1080	28.6	99.90	0.1789	0.00763	1.897	0.0816	0.07689	0.001130	0.941		
AS3 standard	1128	9.3	1042	39.8	1070	27.3	99.98	0.1755	0.00726	1.870	0.0771	0.07727	0.000361	0.994		
AS3 standard	1127	34.3	1233	43.8	1195	28.6	99.92	0.2108	0.00822	2.245	0.0914	0.07722	0.001330	0.908		
AS3 standard	1103	10.4	1093	42.0	1096	28.1	99.99	0.1847	0.00771	1.943	0.0814	0.07630	0.000397	0.992		
AS3 standard	1127	13.5	1108	40.6	1114	26.6	99.97	0.1875	0.00747	1.996	0.0784	0.07724	0.000522	0.986		
AS3 standard	1103	10.9	1071	41.3	1081	27.9	99.98	0.1807	0.00756	1.901	0.0798	0.07630	0.000416	0.992		
AS3 standard	1083	24.2	1095	42.8	1091	29.0	99.88	0.1851	0.00788	1.927	0.0836	0.07553	0.000910	0.961		
AS3 standard	1108	12.9	1106	44.8	1107	29.8	99.99	0.1871	0.00824	1.974	0.0872	0.07648	0.000492	0.989		
AS3 standard	1126	26.0	1104	46.8	1111	30.0	99.86	0.1867	0.00861	1.987	0.0884	0.07717	0.001010	0.959		

AS3 standard	1109	22.3	1066	41.9	1080	29.2	99.96	0.1798	0.00766	1.897	0.0834	0.07653	0.000856	0.967
AS3 standard	1114	13.5	1097	43.8	1103	29.4	99.98	0.1855	0.00806	1.962	0.0858	0.07674	0.000520	0.988
AS3 standard	1188	28.7	1060	47.4	1103	32.8	99.82	0.1788	0.00866	1.963	0.0958	0.07962	0.001160	0.955
AS3 standard	1106	7.6	1189	67.0	1160	42.7	99.95	0.2025	0.01250	2.133	0.1320	0.07640	0.000289	0.998

**Table S3. General information about the 77 grains paleomagnetically analyzed in this study.** The first column shows grain name (grains that fragmented have hole number “hxx” next to the name to different the fragments). The second column shows source rock. The third and fourth columns show age of the grain in Ma calculated from  $^{207}\text{Pb}/^{206}\text{Pb}$  and the standard error (1 sigma) in Ma. The fifth column shows the age of the grain in Ma calculated from  $^{206}\text{Pb}/^{238}\text{U}$ . The sixth column shows the discordance calculated between  $^{207}\text{Pb}/^{206}\text{Pb}$  and  $^{206}\text{Pb}/^{238}\text{U}$  according to equation (1). Seventh column shows if sample lack of visible cracks, metamictization and secondary deposits in BSE images and the presence of zonation in CL images interpreted as a primary igneous texture (“PASS” if sample passes the criterion; “FAILS” if sample fails the criterion; “?” if we do not have data for the criterion). Eighth column shows if sample has detectable primary Li zoning with thickness of  $<20\text{ }\mu\text{m}$  as observed by Li-ion imaging (“PASS” if sample passes the criterion; “FAILS” if sample fails the criterion; “?” if we do not have data for the criterion). The ninth column shows if sample was acid washed or not (“PASS” if sample passes the criterion; “FAILS” if sample fails the criterion; “?” if we do not have data for the criterion). The tenth column shows if samples passed the selection (“PASS” if sample passes the criterion; “FAILS” if sample fails the criterion; “?” if we do not have data for the criterion). The eleventh column shows if samples passed the selection criteria ignoring the Li criterion (“PASS” if sample passes the criterion; “FAILS” if sample fails the criterion; “?” if we do not have data for the criterion). The twelfth column contains the NRM in  $\text{Am}^2$ . The thirteenth, fourteenth, fifteenth and sixteenth columns show maximum pTRM check, and maximum pTRM check above 500°C, 530°C and 550°C. The seventeenth column shows the DRATS calculated according to equation (2). The eighteenth column shows the MAD calculated from in-field steps. The nineteenth column shows if sample passes the paleomagnetic criteria (the NRM component had a difference ratio sum (DRATS)  $\leq 25\%$  (15) and the sample gained a moment in the direction of the laboratory field during in-field steps with a maximum angular deviation (MAD)  $\leq 15^\circ$  over the same temperature range as the NRM component; “PASS” if sample passes the criterion; “FAILS” if sample fails the criterion; “?” if we do not have data for the criterion). The twentieth column shows if samples passed both the selection and paleomagnetic criteria (“PASS” if sample passes the criterion; “FAILS” if sample fails the criterion; “?” if we do not have data for the criterion). The twenty-first column shows if samples passed both the selection and paleomagnetic criteria ignoring the Li criterion (“PASS” if sample passes the criterion; “FAILS” if sample fails the criterion; “?” if we do not have data for the criterion). Dashed values (“-”) represent no measurements were obtained. Shaded columns constitute the three section and two paleomagnetic quality criteria.

Sample name	Source rock	Age $(^{207}\text{Pb}/^{206}\text{Pb})$ Selection Criterion (1)	Age unc. (Ma)	Age $(^{206}\text{Pb}/^{238}\text{U})$ Selection Criterion (1)	Discordance (%) Selection Criterion (1)	BSEM and CL no cracks? Selection Criterion (2)	Li band? Selection Criterion (3)	Acid wash?	Pass selection criteria?	Pass selection criteria? (no Li)	NRM ( $\text{Am}^2$ )	Max. pTRM check (%)	Max. pTRM check (%) >500°C	Max. pTRM check (%) >530°C	Max. pTRM check (%) >550°C	DRATS (%) Selection Criterion (a)	in-field (°C) Selection Criterion (b)	MAD	Pass paleomagnetic criteria?	Pass selection and paleomagnetic criteria?	Pass selection and paleomagnetic criteria? (no Li)
K1	D175C	3275	8	3071	7	FAIL	?	PASS	FAIL	FAIL	8.95E-13	63.0	63.0	63.0	17.3	47.9	22.7	FAIL	FAIL	FAIL	
K2	D175C	3123	10	2836	10	FAIL	?	PASS	FAIL	FAIL	2.84E-12	31.8	31.8	22.5	16.6	26.4	16.3	FAIL	FAIL	FAIL	
2-9-19	D175C	3738	10	3076	22	FAIL	PASS	PASS	FAIL	FAIL	1.96E-14	19355.1	19355.1	19355.1	19355.1	173.1	19.7	FAIL	FAIL	FAIL	
2-10-5	D175C	4164	4	3548	17	PASS	PASS	PASS	FAIL	FAIL	3.80E-14	668405.9	668405.9	170.7	16.3	16863.9	8.5	FAIL	FAIL	FAIL	
3-13-14	D175C	4171	5	4700	11	FAIL	PASS	PASS	FAIL	FAIL	1.38E-13	1114036.6	1114036.6	1114036.6	99.1	12833.0	15.5	FAIL	FAIL	FAIL	
1-13-6	D175C	3402	3	3049	12	FAIL	PASS	PASS	FAIL	FAIL	6.62E-15	367.8	367.8	56.5	48.2	21.1	33.9	FAIL	FAIL	FAIL	

1-10-11	D175C	3564	4	4174	15	PASS	PASS	PASS	FAIL	FAIL	1.09E-14	466.5	466.5	466.5	99.6	8232.0	10.6	FAIL	FAIL	FAIL
18-2-3	Cong14C	3268	11	2482	32	FAIL	FAIL	PASS	FAIL	FAIL	1.73E-13	1065.2	1065.2	61.8	30.0	3.3	11.7	PASS	FAIL	FAIL
18-3-1	Cong14C	4062	7	4097	1	FAIL	PASS	PASS	FAIL	FAIL	2.87E-14	7933.8	7933.8	100.0	100.0	1507359.5	7.2	FAIL	FAIL	FAIL
18-3-8	Cong14C	3640	5	3684	1	FAIL	PASS	PASS	FAIL	FAIL	6.42E-15	99.9	99.9	99.9	99.9	31236.8	38.4	FAIL	FAIL	FAIL
18-7-15	Cong14C	3647	5	3145	16	FAIL	PASS	PASS	FAIL	FAIL	3.37E-13	874.8	874.8	64.6	19.2	69.6	47.8	FAIL	FAIL	FAIL
18-8-12 (h03)	Cong14C	4122	3	2891	43	FAIL	PASS	PASS	FAIL	FAIL	6.65E-15	5553.8	5553.8	199.4	174.6	1817.8	36.6	FAIL	FAIL	FAIL
18-8-12 (h11)	Cong14C	4122	3	2891	43	FAIL	PASS	PASS	FAIL	FAIL	6.64E-15	7681.3	7681.3	93.7	93.7	137657.8	20.1	FAIL	FAIL	FAIL
18-10-8	Cong14C	3476	7	3407	2	FAIL	PASS	PASS	FAIL	FAIL	2.07E-13	130.9	130.9	48.4	48.4	34.6	24.3	FAIL	FAIL	FAIL
18-11-13 (h05)	Cong14C	4138	8	3191	30	FAIL	FAIL	PASS	FAIL	FAIL	6.80E-15	95.7	95.7	95.7	95.7	1446.4	30	FAIL	FAIL	FAIL
18-11-13 (h12)	Cong14C	4138	8	3191	30	FAIL	FAIL	PASS	FAIL	FAIL	2.22E-13	258.9	258.9	258.9	99.8	20166.2	26.1	FAIL	FAIL	FAIL
18-11-13 (h19)	Cong14C	4138	8	3191	30	FAIL	FAIL	PASS	FAIL	FAIL	1.88E-14	11511.9	11511.9	99.6	99.6	1271.6	40.4	FAIL	FAIL	FAIL
18-11-18	Cong14C	3634	5	3213	13	FAIL	PASS	PASS	FAIL	FAIL	2.76E-14	8961.1	8961.1	8961.1	8961.1	8828.5	13.1	FAIL	FAIL	FAIL
18-14-2	Cong14C	4072	3	3319	23	FAIL	PASS	PASS	FAIL	FAIL	6.51E-15	9070.7	9070.7	103.6	99.5	74487.0	30.8	FAIL	FAIL	FAIL
18-15-18 (h04)	Cong14C	4176	7	4203	1	FAIL	PASS	PASS	FAIL	FAIL	1.28E-14	1253.3	1253.3	103.5	81.7	50.8	43.9	FAIL	FAIL	FAIL
18-15-18 (h06)	Cong14C	4176	7	4203	1	FAIL	PASS	PASS	FAIL	FAIL	1.86E-13	238.8	238.8	71.8	71.8	41.2	38.3	FAIL	FAIL	FAIL
18-20-6	Cong14C	3505	7	3507	0	FAIL	PASS	PASS	FAIL	FAIL	4.61E-14	25877.8	25877.8	99.9	99.9	295006.3	37.3	FAIL	FAIL	FAIL
18-20-14	Cong14C	3965	5	3651	9	FAIL	PASS	PASS	FAIL	FAIL	4.44E-14	99.3	99.3	99.3	99.3	135107.2	31.6	FAIL	FAIL	FAIL
18-4-8 (h29)	Cong14C	4099	9	4068	1	FAIL	FAIL	PASS	FAIL	FAIL	3.53E-14	171.7	171.7	171.7	97.6	5727.2	24.5	FAIL	FAIL	FAIL
18-4-8 (h30)	Cong14C	4099	9	4068	1	FAIL	FAIL	PASS	FAIL	FAIL	5.43E-14	3174.3	3174.3	3174.3	99.0	5888.0	26.3	FAIL	FAIL	FAIL
2-20-3	D175C	4215	6	-	-	FAIL	?	PASS	FAIL	FAIL	9.86E-14	247.4	129.5	129.5	99.0	24301.8	33.9	FAIL	FAIL	FAIL
3-3-11	D175C	4061	14	-	-	FAIL	FAIL	PASS	FAIL	FAIL	6.37E-15	69576.4	69576.4	69576.4	116.6	6073.2	14.4	FAIL	FAIL	FAIL
1-1-9 (h31)	D175C	3256	9	-	-	FAIL	?	PASS	FAIL	FAIL	8.94E-14	100.0	100.0	100.0	100.0	148016.0	21.3	FAIL	FAIL	FAIL
1-1-9 (h32)	D175C	3256	9	-	-	FAIL	?	PASS	FAIL	FAIL	1.00E-13	393.0	393.0	128.1	100.0	38759.5	27.2	FAIL	FAIL	FAIL
18-11-19	Cong14C	3453	6	3135	10	FAIL	FAIL	PASS	FAIL	FAIL	1.53E-13	104263.7	99.9	99.9	99.9	36337.2	37.1	FAIL	FAIL	FAIL
18-10-11	Cong14C	4186	5	4188	0	FAIL	FAIL	PASS	FAIL	FAIL	6.68E-15	9909.1	9909.1	99.8	99.8	268258.8	18.8	FAIL	FAIL	FAIL
18-2-12 (h21)	Cong14C	3949	44	2901	36	PASS	FAIL	PASS	FAIL	FAIL	8.94E-14	148.2	148.2	148.2	118.6	252.4	28.8	FAIL	FAIL	FAIL
18-2-12 (h22)	Cong14C	3949	44	2901	36	PASS	FAIL	PASS	FAIL	FAIL	8.50E-14	324.8	324.8	324.8	62.2	46.9	23.6	FAIL	FAIL	FAIL
18-12-11	Cong14C	3869	11	3762	3	FAIL	FAIL	PASS	FAIL	FAIL	2.82E-13	1536.4	1536.4	1536.4	92.9	209.5	9.5	FAIL	FAIL	FAIL
1-13-18	D175C	3361	7	-	-	FAIL	?	PASS	FAIL	FAIL	4.15E-12	138.2	138.2	35.0	17.9	45.6	44.3	FAIL	FAIL	FAIL
1-17-15	D175C	3771	18	3452	9	FAIL	FAIL	PASS	FAIL	FAIL	6.64E-15	7179.7	132.9	100.0	100.0	36868.6	17.4	FAIL	FAIL	FAIL
6-20-16	D175H	4035	7	4128	2	FAIL	PASS	PASS	FAIL	FAIL	9.66E-13	411.5	70.3	32.6	27.2	17.5	38.3	FAIL	FAIL	FAIL

7-13-20	D175H	3973	1	3899	2	PASS	PASS	PASS	PASS	PASS	PASS	1.14E-12	40.5	40.5	40.5	40.5	17.4	12.3	PASS	PASS	PASS
7-8-16	D175H	4198	2	4063	3	FAIL	PASS	PASS	FAIL	FAIL	2.13E-13	97.6	51.8	51.6	51.6	469.8	9.9	FAIL	FAIL	FAIL	
8-2-11	D175H	3979	7	3990	0	PASS	PASS	PASS	PASS	PASS	1.46E-12	40.7	10.5	10.5	10.5	13.4	14.8	PASS	PASS	PASS	
8-2-1	D175H	3117	6	2962	5	FAIL	PASS	PASS	FAIL	FAIL	1.02E-12	21.9	21.9	21.9	5.7	2.4	19.2	FAIL	FAIL	FAIL	
11-8-12	D175L	3693	4	3634	2	FAIL	PASS	PASS	FAIL	FAIL	3.53E-13	183.1	183.1	21.2	10.6	14.8	26.1	FAIL	FAIL	FAIL	
11-8-13	D175L	3502	4	3339	5	FAIL	PASS	PASS	FAIL	FAIL	5.10E-13	26.6	25.7	25.7	10.9	3.1	20.8	FAIL	FAIL	FAIL	
11-10-19	D175L	4132	10	4074	1	FAIL	FAIL	PASS	FAIL	FAIL	3.84E-14	255.4	255.4	100.0	100.0	195.6	30.1	FAIL	FAIL	FAIL	
11-9-10	D175L	4245	6	-	-	FAIL	PASS	PASS	FAIL	FAIL	3.10E-14	134.7	134.7	53.3	53.3	24.2	46.8	FAIL	FAIL	FAIL	
11-12-2	D175L	3493	14	3569	2	FAIL	PASS	PASS	FAIL	FAIL	1.26E-12	67.4	67.4	23.8	12.3	22.2	8.5	PASS	FAIL	FAIL	
12-14-12	D175L	3989	5	4021	1	PASS	FAIL	PASS	FAIL	PASS	1.61E-13	13122.7	13122.7	13122.7	13122.7	70.2	32.5	FAIL	FAIL	FAIL	
12-2-8	D175L	3666	4	3698	1	PASS	FAIL	PASS	FAIL	PASS	3.54E-13	240.5	240.5	240.5	240.5	25.8	17.5	FAIL	FAIL	FAIL	
12-14-5	D175L	3966	4	4053	2	PASS	FAIL	PASS	FAIL	PASS	4.09E-14	6910.3	6910.3	6910.3	3499.8	169.3	33.3	FAIL	FAIL	FAIL	
15-1-7	Cong14C	4094	5	4072	1	PASS	PASS	PASS	PASS	PASS	3.22E-14	298.8	298.8	298.8	21.3	672.7	26.6	FAIL	FAIL	FAIL	
15-3-15	Cong14C	3535	6	3634	3	PASS	FAIL	PASS	FAIL	PASS	3.77E-14	730.0	99.9	99.9	99.9	66.3	34.1	FAIL	FAIL	FAIL	
15-4-7	Cong14C	3514	3	3324	6	PASS	FAIL	PASS	FAIL	PASS	1.98E-14	519.9	519.9	519.9	144.5	148.0	26.9	FAIL	FAIL	FAIL	
15-11-19	Cong14C	3925	28	3703	6	FAIL	FAIL	PASS	FAIL	FAIL	5.09E-13	83.9	83.9	83.9	58.7	56.9	40.1	FAIL	FAIL	FAIL	
15-2-3	Cong14C	3624	13	3552	2	FAIL	FAIL	PASS	FAIL	FAIL	1.05E-13	233.2	233.2	28.3	28.3	0.2	7.3	PASS	FAIL	FAIL	
15-11-20	Cong14C	3991	5	4214	5	FAIL	PASS	PASS	FAIL	FAIL	1.69E-12	177.7	177.7	177.7	30.3	34.7	12.2	FAIL	FAIL	FAIL	
15-18-8	Cong14C	3527	7	3436	3	FAIL	FAIL	PASS	FAIL	FAIL	6.82E-14	200674.4	200674.4	200674.4	145.5	4.1	6.9	PASS	FAIL	FAIL	
WGAW1	Cong14E	?	-	-	-	?	?	PASS	FAIL	FAIL	3.50E-13	675.5	675.5	28.1	28.1	2.1	15.4	FAIL	FAIL	FAIL	
WGAW2	Cong14E	3664	12	837	338	?	?	PASS	FAIL	FAIL	2.23E-12	5800.9	5800.9	21.5	6.7	63.2	7.2	FAIL	FAIL	FAIL	
WGAW3	Cong14E	?	-	-	-	?	?	PASS	FAIL	FAIL	2.12E-13	295.5	295.5	35.6	35.6	4.3	40.6	FAIL	FAIL	FAIL	
WGAW4	Cong14E	?	-	-	-	?	?	PASS	FAIL	FAIL	2.13E-13	89.8	89.8	89.8	89.8	50.7	25	FAIL	FAIL	FAIL	
WGAW5	Cong14E	?	-	-	-	?	?	PASS	FAIL	FAIL	1.44E-12	63.0	63.0	17.9	10.9	83.0	45.2	FAIL	FAIL	FAIL	
WGAW6	Cong14E	?	-	-	-	?	?	PASS	FAIL	FAIL	3.76E-14	1296.3	1296.3	172.0	172.0	107.5	22.4	FAIL	FAIL	FAIL	
WGAW7	Cong14E	?	-	-	-	?	?	PASS	FAIL	FAIL	3.11E-13	2015.9	2015.9	2015.9	31.3	868.0	23.3	FAIL	FAIL	FAIL	
WGAW8	Cong14E	?	-	-	-	?	?	PASS	FAIL	FAIL	3.79E-13	75.7	67.1	50.4	50.4	259.4	28.2	FAIL	FAIL	FAIL	
WGAW9	Cong14E	?	-	-	-	?	?	PASS	FAIL	FAIL	1.08E-12	47345.2	47345.2	47345.2	47345.2	53.6	33.6	FAIL	FAIL	FAIL	
WGAW10	Cong14E	?	-	-	-	?	?	PASS	FAIL	FAIL	1.19E-13	5842.5	5842.5	78.5	78.5	120.1	-	FAIL	FAIL	FAIL	
WGAW11	Cong14E	?	-	-	-	?	?	PASS	FAIL	FAIL	5.96E-14	87.6	87.6	87.6	87.6	611.6	7.1	FAIL	FAIL	FAIL	
WGAW12	Cong14E	2345	74	260	802	?	?	PASS	FAIL	FAIL	5.65E-14	19909.0	19909.0	76.2	20.9	65.5	6.4	FAIL	FAIL	FAIL	

WGAW13	Cong14E	?	-	-	-	?	?	PASS	FAIL	FAIL	1.64E-13	73.6	73.6	54.3	54.3	157.0	-	FAIL	FAIL	FAIL	
WGAW14	Cong14E	?	-	-	-	?	?	PASS	FAIL	FAIL	1.79E-13	858.7	858.7	858.7	101.0	51.7	8.9	FAIL	FAIL	FAIL	
WGAW15	Cong14E	?	-	-	-	?	?	PASS	FAIL	FAIL	6.00E-14	99.8	99.8	99.8	99.8	125747.9	44.6	FAIL	FAIL	FAIL	
WGAW16	Cong14E	?	-	-	-	?	?	PASS	FAIL	FAIL	3.01E-14	5059.6	5059.6	78.6	78.6	251.9	35.3	FAIL	FAIL	FAIL	
WGAW17	Cong14E	?	-	-	-	?	?	PASS	FAIL	FAIL	9.48E-14	476.9	476.9	476.9	476.9	94.3	39.2	FAIL	FAIL	FAIL	
WGNAW1	Cong14E	?	-	-	-	?	?	FAIL	FAIL	FAIL	1.06E-12	310.3	310.3	310.3	310.3	70.5	13.8	FAIL	FAIL	FAIL	
WGNAW2	Cong14E	?	-	-	-	?	?	FAIL	FAIL	FAIL	7.55E-13	855.1	855.1	855.1	855.1	1448.7	37.4	FAIL	FAIL	FAIL	
WGNAW3	Cong14E	?	-	-	-	?	?	FAIL	FAIL	FAIL	1.54E-12	215.4	215.4	215.4	215.4	5610.0	2.9	FAIL	FAIL	FAIL	
WGNAW4	Cong14E	?	-	-	-	?	?	FAIL	FAIL	FAIL	2.22E-13	1317.5	1317.5	1317.5	1317.5	33.0	52.4	3.3	FAIL	FAIL	FAIL

**Table S4. Summary of the paleomagnetic data for the 77 samples paleomagnetically analyzed in this study.** The first column shows the grain name (grains that fragmented have hole number “hxx” next to the name to differentiate the fragments). The second column shows the paleointensity fit range. The third and fourth columns show the calculated paleointensity and the standard error of the paleointensity (1 sigma). The fifth, sixth, seventh, eighth and ninth columns show, respectively, the paleointensity parameters  $f$ ,  $\beta$ ,  $q$ , maximum DRAT and CDRAT. Dashed values (“-”) represent no measurements were obtained or no magnetic signal from the grain.

Sample name	Fit range (°C)	Paleointensity (μT)	Std. error (μT)	$f$	$\beta$	$q$	Max. DRAT	CDRAT
K1	550-565	36.1	17.7	0.264	0.491	0.2	86	119.06
K2	550-565	65.9	16.6	0.233	0.251	0.6	42.2	59.5
2-9-19	550-565	-82.6	25.6	9.801	0.31	11.5	154	136.17
2-10-5	550-565	-95.9	36.1	0.101	0.377	-0.1	15649.6	4809.23
3-13-14	550-565	-33.9	17.6	6.886	0.52	5	122.4	91.5
1-13-6	550-565	19	10.5	0.604	0.555	0.2	68.8	22.69
1-10-11	550-565	-298	273.3	0.077	0.917	0	1877.4	1765.43
18-2-3	550-580	-14.6	7.9	12.35	0.544	5	20.5	4.23
18-3-1	550-580	-5.7	2	12.291	0.355	3.2	144.7	126.08
18-3-8	550-580	-19.1	6.8	6.032	0.358	6.2	228.9	274.14
18-7-15	550-580	38	18.7	0.563	0.493	0.2	52.1	82.81
18-8-12 (h03)	550-580	-22.9	4.1	1.385	0.179	1.7	183	69.29
18-8-12 (h11)	550-580	-66.3	25.2	6.306	0.381	6.2	112.1	189.22
18-10-8	550-580	20.1	11.5	0.179	0.572	-0.2	90.6	77.43
18-11-13 (h05)	550-580	-36.7	4.7	5.007	0.128	16.7	315.4	28.27
18-11-13 (h12)	550-580	-38.9	4.8	12.714	0.122	23.1	152.8	88.87
18-11-13 (h19)	550-580	-12.8	6.9	0.853	0.542	-0.2	161.1	21.19
18-11-18	-	-	-	-	-	-	-	-
18-14-2	550-580	-37.6	12.3	5.897	0.326	-9.6	156.2	98.38
18-15-18 (h04)	550-580	95.3	33.3	0.549	0.349	-1.4	58.7	37.74
18-15-18 (h06)	550-580	-26.4	8.7	8.759	0.331	-4.5	123.9	97.8
18-20-6	550-580	-39.2	4.8	79.203	0.123	38.6	132.6	170.61
18-20-14	550-580	-34.9	7.1	9.685	0.205	21.7	84.9	150.52

18-4-8 (h29)	550-580	-71.3	8.9	13.117	0.125	47.2	19.8	32.06
18-4-8 (h30)	550-580	-45.9	10.9	100.774	0.238	-532	103.1	24.61
2-20-3	550-580	-13.3	6	17.943	0.453	9.6	272.5	179.05
3-3-11	-	-	-	-	-	-	-	-
1-1-9 (h31)	550-580	-15.3	1.9	55.465	0.125	-12	109.8	71.21
1-1-9 (h32)	550-580	-22	6	22.573	0.271	43.7	88.3	43.98
18-11-19	550-580	-42.2	4.9	19.854	0.115	-30.3	122.9	70.55
18-10-11	550-580	-12.4	2.2	15.639	0.177	-21.4	105.6	88
18-2-12 (h21)	550-580	68.8	24.1	0.768	0.35	-0.5	197.7	107.65
18-2-12 (h22)	550-580	85.3	51.1	0.791	0.599	-0.5	108.9	41.82
18-12-11	550-580	55.7	3.8	0.914	0.068	-11.2	943.2	123.71
1-13-18	550-580	22.2	7.2	0.446	0.325	-1.9	211.1	183.33
1-17-15	550-580	-11.5	1.7	15.07	0.152	-46	178.9	156.16
6-20-16	550-580	61.7	24.1	0.585	0.391	1.1	16.7	14.07
7-13-20	550-580	23.3	5	0.402	0.213	1.2	61.7	44.86
7-8-16	550-580	-12	4.9	2.523	0.405	1.3	1667.1	1456.53
8-2-11	550-580	41.9	15.2	0.278	0.363	0.6	20.7	37.66
8-2-1	550-580	48.8	3.2	0.392	0.065	4.9	17	4.29
11-8-12	550-580	14.4	8.6	0.272	0.596	-0.5	100.8	34.61
11-8-13	550-580	-22.4	9.3	0.406	0.413	-0.4	100.5	17.96
11-10-19	550-580	-20.1	12.4	1.955	0.617	-4.1	731.1	651.5
11-9-10	550-580	-41	20.1	5.136	0.49	-12.9	143.6	41.91
11-12-2	550-580	6.7	3.8	0.609	0.566	0.5	17.3	37.61
12-14-12	550-580	-6	3.3	2.355	0.55	-4.6	73.2	80.89
12-2-8	550-580	-4.2	2.3	0.531	0.545	0.5	16	8.55
12-14-5	550-580	-54.3	18.5	4.288	0.341	4.2	164.8	131.18
15-1-7	550-580	-50.2	29.5	18.078	0.587	-10.3	216.3	358.11
15-3-15	550-580	-10	5.8	6.88	0.581	4.5	251.1	133.84
15-4-7	550-580	16.9	8.3	0.368	0.492	-0.3	377	269.34
15-11-19	550-580	-37.1	10.7	6.924	0.289	1.8	176.5	82.28
15-2-3	550-580	-5.4	2	2.408	0.38	3.9	7.5	0.19

15-11-20	550-580	23.4	14.2	0.302	0.605	-0.7	105.4	62.09
15-18-8	550-580	-2.5	0.6	1.486	0.246	2.1	6.6	4.27
WGAW1	550-580	-33.1	18.8	0.803	0.567	0.6	49.5	5.77
WGAW2	550-580	-4.8	2.4	0.312	0.503	0.4	165	253.28
WGAW3	550-580	-106.1	39	0.993	0.367	-0.8	512.3	12.44
WGAW4	550-580	-21.1	10.7	4.405	0.505	-2.1	113.7	121.88
WGAW5	550-580	-35.7	18.9	0.096	0.528	0	67.3	121.24
WGAW6	550-580	6.1	3.5	1.083	0.571	0.2	737.6	188.23
WGAW7	550-580	-32.7	8.2	25.699	0.251	18.8	1352.6	1116.1
WGAW8	550-580	-30.1	10.5	12.794	0.348	-39.4	161.2	340.63
WGAW9	550-580	-56.7	22.3	4.732	0.393	-0.8	77.7	44.72
WGAW10	-	-	-	-	-	-	-	-
WGAW11	550-580	4.6	2.7	1.108	0.586	-0.6	2208.2	1969.05
WGAW12	550-580	-3.9	1.8	6.699	0.463	6.9	40.8	132.23
WGAW13	-	-	-	-	-	-	-	-
WGAW14	550-580	-3.7	1.5	4.821	0.399	5.1	45	66.86
WGAW15	550-580	-0.2	0.1	0.079	0.501	-0.1	100	350.92
WGAW16	550-580	-60.9	25.3	3.653	0.416	-6.1	715.3	400.55
WGAW17	550-580	-45	28.2	5.414	0.626	-4.9	185.6	85.74
WGNAW1	550-580	-0.8	0.4	1.044	0.512	0.6	93.6	87.29
WGNAW2	550-580	-26.7	9.8	2.806	0.366	2.3	1670.2	1627.28
WGNAW3	550-580	0	0	1.554	0.618	-1.7	96.7	113.21
WGNAW4	550-580	1.6	1	0.393	0.626	0.2	33.4	85.31

**Table S5. Comparison of paleomagnetic data between 56 polished grains and 21 unpolished grains.** First row shows the values for range of the NRM. Second row shows the number of grains that fail paleomagnetic criterion (a) (DRATS  $\leq$ 25) showing that they altered. Third row shows the number of grains that fail paleomagnetic criterion (b) (sample gained a moment in the direction of the laboratory field during in-field steps with a maximum angular deviation (MAD)  $\leq$ 15° over the same temperature range as the NRM component) showing that they are bad recorders. Fourth row shows the amount of grains that pass both criteria. Fifth row contains the total amount of grains. These results ignore the selection criteria and only consider the paleomagnetic data. We do not observe any significant difference in the resulting data between non-polished and polished grains.

	Unpolished	Polished
NRM range ( $\text{Am}^2$ )	$3.01 \times 10^{-14}$ to $2.23 \times 10^{-12}$	$6.05 \times 10^{-15}$ to $4.15 \times 10^{-12}$
Alteration (fails paleomagnetic criterion "a")	19 (90%)	44 (79%)
Poor magnetic recorders (fails paleomagnetic criterion "b")	12 (57%)	42 (75%)
No signs of alteration (passes paleomagnetic criterion "a") and robust recorder (passes paleomagnetic criterion "b")	0 (0%)	6 (11%)
Total	21 (100%)	56 (100%)

**Table S6. Summary of principal component analysis and maximum angular deviation (MAD) of the 77 samples analyzed here.** The first column shows grain name (grains that fragmented have hole number “hxx” next to the name to differentiate the fragments). The second column contains component name (“LT” for low temperature component, “MT” medium temperature component, “HT” high temperature component). The third, fourth and fifth columns show, respectively, the range of the component, MAD value and if the component was forced through the origin (“Y” if forced).

Sample name	Component	Range (°C)	MAD (°)	Origin forced?
K1	LT	025-400	12.1	
	MT	400-510	4.8	
	HT	510-565	7.4	Y
K2	HT	025-565	3.8	Y
2-9-19	LT	025-400	35.3	
	HT	400-565	23.3	Y
2-10-5	HT	025-565	22.6	Y
3-13-14	HT	025-565	10.3	Y
1-13-6	HT	025-565	23.5	Y
1-10-11	HT	025-565	33.3	Y
18-2-3	HT	025-680	28.8	Y
18-3-1	HT	025-565	26.7	Y
18-3-8	HT	025-565	33.8	Y
18-7-15	LT	025-510	9.2	
	HT	510-680	30.7	Y
18-8-12 (h03)	HT	025-565	30.4	Y
18-8-12 (h11)	HT	025-565	27.2	Y
18-10-8	HT	025-680	18.3	Y
18-11-13 (h05)	HT	025-565	43.6	Y
	LT	0-200	32.3	
18-11-13 (h12)	MT	300-500	37.1	
	HT	500-565	39.6	Y
18-11-13 (h19)	HT	025-565	30.1	Y
18-11-18	-	-	-	-
18-14-2	HT	510-565	29.7	Y
18-15-18 (h04)	LT	0-565	27.5	
	HT	565-680	26.3	Y
18-15-18 (h06)	HT	025-680	48.0	Y
18-20-6	LT	025-535	40.3	
	HT	535-565	14.6	Y
18-20-14	HT	025-565	42.1	Y
18-4-8 (h29)	HT	025-565	23.8	Y

18-4-8 (h30)	HT	025-565	43.3	Y
2-20-3	HT	025-560	32.2	Y
3-3-11	-	-	-	-
1-1-9 (h31)	HT	025-565	34.9	Y
1-1-9 (h32)	HT	025-565	35.4	Y
18-11-19	HT	025-565	44.1	Y
18-10-11	HT	025-565	39.3	Y
18-2-12 (h21)	HT	025-630	13.5	Y
18-2-12 (h22)	HT	025-630	10.7	Y
18-12-11	HT	025-660	6.8	Y
1-13-18	LT	025-500	4.5	
	HT	500-660	36.6	Y
1-17-15	HT	25-565	29.1	Y
6-20-16	HT	025-580	11.6	Y
	LT	025-200	12.4	
7-13-20	MT	200-300 (?)	0.1	
	HT	300-680	10.6	Y
7-8-16	HT	025-680	39.1	Y
8-2-11	LT	025-510	13.3	
	HT	510-680	11.8	Y
8-2-1	LT	025-300	19.0	
	HT	300-680	10.0	Y
11-8-12	HT	025-680	32.9	Y
11-8-13	LT	025-400	11.1	
	HT	400-680	45.3	Y
11-10-19	HT	025-580	34.9	Y
11-9-10	HT	025-600	37.8	Y
11-12-2	HT	025-680	26.7	Y
12-14-12	HT	025-680	23.6	Y
	LT	025-500	23.5	
12-2-8	MT	500-580	45.0	
	HT	580-680	46.6	Y
12-14-5	HT	025-680	31.4	Y
15-1-7	HT	025-680	19.0	Y
15-3-15	HT	025-680	40.6	Y
15-4-7	HT	025-680	24.8	Y
15-11-19	HT	025-680	41.6	Y
15-2-3	HT	025-680	27.8	Y
15-11-20	HT	025-680	38.0	Y

15-18-8	HT	025-680	30.0	Y
WGAW1	HT	025-680	38.6	Y
WGAW2	HT	025-680	39.0	Y
WGAW3	HT	025-680	46.0	Y
WGAW4	HT	025-680	40.8	Y
WGAW5	HT	025-680	8.5	Y
WGAW6	HT	025-680	40.5	Y
WGAW7	HT	025-680	32.6	Y
WGAW8	HT	025-680	42.4	Y
WGAW9	HT	025-680	15.8	Y
WGAW10	-	-	-	-
WGAW11	HT	025-680	35.7	Y
WGAW12	HT	025-680	44.9	Y
WGAW13	-	-	-	-
WGAW14	HT	025-680	40.5	Y
WGAW15	HT	025-680	29.6	Y
WGAW16	HT	025-680	42.5	Y
WGAW17	HT	025-680	34.9	Y
WGNAW1	HT	025-680	37.9	Y
WGNAW2	HT	025-680	42.7	Y
WGNAW3	HT	025-680	30.0	Y
WGNAW4	HT	025-680	43.9	Y

**Table S7. Summary of maximum angular deviation (MAD) values of the in-field component acquired during paleointensity measurements by the 77 samples.** All in-field data points were used to calculate the MADs anchored to the origin. First column shows the grain name. Second column contains the in-field MAD value calculated using all temperature steps.

Sample name	MAD (°)
K1	22.7
K2	16.3
2-9-19	19.7
2-10-5	8.5
3-13-14	15.5
1-13-6	33.9
1-10-11	10.6
18-2-3	11.7
18-3-1	7.2
18-3-8	38.4
18-7-15	47.8
18-8-12 (h03)	36.6
18-8-12 (h11)	20.1
18-10-8	24.3
18-11-13 (h05)	30
18-11-13 (h12)	26.1
18-11-13 (h19)	40.4
18-11-18	13.1
18-14-2	30.8
18-15-18 (h04)	43.9
18-15-18 (h06)	38.3
18-20-6	37.3
18-20-14	31.6
18-4-8 (h29)	24.5
18-4-8 (h30)	26.3
2-20-3	33.9
3-3-11	14.4
1-1-9 (h31)	21.3
1-1-9 (h32)	27.2
18-11-19	37.1
18-10-11	18.8
18-2-12 (h21)	28.8
18-2-12 (h22)	23.6
18-12-11	9.5
1-13-18	44.3
1-17-15	17.4
6-20-16	38.3
7-13-20	12.3
7-8-16	9.9
8-2-11	14.8

8-2-1	19.2
11-8-12	26.1
11-8-13	20.8
11-10-19	30.1
11-9-10	46.8
11-12-2	8.5
12-14-12	32.5
12-2-8	17.5
12-14-5	33.3
15-1-7	26.6
15-3-15	34.1
15-4-7	26.9
15-11-19	40.1
15-2-3	7.3
15-11-20	12.2
15-18-8	6.9
WGAW1	15.4
WGAW2	7.2
WGAW3	40.6
WGAW4	25
WGAW5	45.2
WGAW6	22.4
WGAW7	23.3
WGAW8	28.2
WGAW9	33.6
WGAW10	-
WGAW11	7.1
WGAW12	6.4
WGAW13	-
WGAW14	8.9
WGAW15	44.6
WGAW16	35.3
WGAW17	39.2
WGNAW1	13.8
WGNAW2	37.4
WGNAW3	2.9
WGNAW4	3.3

## REFERENCES AND NOTES

1. W. Compston, R. T. Pidgeon, Jack Hills, evidence of more very old detrital zircons in Western Australia. *Nature* **321**, 766–769 (1986).
2. R. R. Fu, B. P. Weiss, E. A. Lima, P. Kehayias, J. F. D. F. Araujo, D. R. Glenn, J. Gelb, J. F. Einsle, A. M. Bauer, R. J. Harrison, G. A. H. Ali, R. L. Walsworth, Evaluating the paleomagnetic potential of single zircon crystals using the Bishop Tuff. *Earth Planet. Sci. Lett.* **458**, 1–13 (2017).
3. B. P. Weiss, A. C. Maloof, N. Tailby, J. Ramezani, R. R. Fu, V. Hanus, D. Trail, E. Bruce Watson, T. M. Harrison, S. A. Bowring, J. L. Kirschvink, N. L. Swanson-Hysell, R. S. Coe, Pervasive remagnetization of detrital zircon host rocks in the Jack Hills, Western Australia and implications for records of the early geodynamo. *Earth Planet. Sci. Lett.* **430**, 115–128 (2015).
4. J. A. Tarduno, E. G. Blackman, E. E. Mamajek, Detecting the oldest geodynamo and attendant shielding from the solar wind: Implications for habitability. *Phys. Earth Planet. Inter.* **233**, 68–87 (2014).
5. M. Sato, S. Yamamoto, Y. Yamamoto, Y. Okada, M. Ohno, H. Tsunakawa, S. Maruyama, Rock-magnetic properties of single zircon crystals sampled from the Tanzawa tonalitic pluton, central Japan. *Earth Planets Space* **67**, 150 (2015).
6. B. P. Weiss, R. R. Fu, J. F. Einsle, D. R. Glenn, P. Kehayias, E. A. Bell, J. Gelb, J. F. D. F. Araujo, E. A. Lima, C. S. Borlina, P. Boehnke, D. N. Johnstone, T. M. Harrison, R. J. Harrison, R. L. Walsworth, Secondary magnetic inclusions in detrital zircons from the Jack Hills, Western Australia, and implications for the origin of the geodynamo. *Geology* **46**, 427–430 (2018).
7. J. A. Tarduno, R. D. Cottrell, W. J. Davis, F. Nimmo, R. K. Bono, A Hadean to Paleoarchean geodynamo recorded by single zircon crystals. *Science* **349**, 521–524 (2015).

8. J. A. Tarduno, R. D. Cottrell, R. K. Bono, H. Oda, W. J. Davis, M. Fayek, O. van 't Erve, F. Nimmo, W. Huang, E. R. Thern, S. Fearn, G. Mitra, A. V. Smirnov, E. G. Blackman, Paleomagnetism indicates that primary magnetite in zircon records a strong Hadean geodynamo. *Proc. Natl. Acad. Sci.* **117**, 2309–2318 (2020).
9. B. P. Weiss, A. C. Maloof, T. M. Harrison, N. L. Swanson-Hysell, R. R. Fu, J. L. Kirschvink, E. Bruce Watson, R. S. Coe, S. M. Tikoo, J. Ramezani, Reply to comment on “Pervasive remagnetization of detrital zircon host rocks in the Jack Hills, Western Australia and implications for records of the early dynamo”. *Earth Planet. Sci. Lett.* **450**, 409–412 (2016).
10. F. Tang, R. J. M. Taylor, J. F. Einsle, C. S. Borlina, R. R. Fu, B. P. Weiss, H. M. Williams, W. Williams, L. Nagy, P. A. Midgley, E. A. Lima, E. A. Bell, T. M. Harrison, E. W. Alexander, R. J. Harrison, Secondary magnetite in ancient zircon precludes analysis of a Hadean geodynamo. *Proc. Natl. Acad. Sci. U.S.A.* **116**, 407–412 (2018).
11. D. Trail, D. J. Cherniak, E. B. Watson, T. M. Harrison, B. P. Weiss, I. Szumila, Li zoning in zircon as a potential geospeedometer and peak temperature indicator. *Contrib. Mineral. Petrol.* **171**, 1–15 (2016).
12. F. Corfu, J. M. Hanchar, P. W. O. Hoskin, P. Kinny, Atlas of zircon textures. *Rev. Mineral. Geochemistry* **53**, 469–500 (2003).
13. M. Tang, R. L. Rudnick, W. F. McDonough, M. Bose, Y. Goreva, Multi-mode Li diffusion in natural zircons: Evidence for diffusion in the presence of step-function concentration boundaries. *Earth Planet. Sci. Lett.* **474**, 110–119 (2017).
14. B. P. Weiss, E. A. Lima, L. E. Fong, F. J. Baudenbacher, Paleomagnetic analysis using SQUID microscopy. *J. Geophys. Res.* **112**, 1–20 (2007).
15. E. A. Lima, B. P. Weiss, Ultra-high sensitivity moment magnetometry of geological samples using magnetic microscopy. *Geochem. Geophys. Geosyst.* **17**, 3754–3774 (2016).
16. Y. Yu, L. Tauxe, A. Genevey, Toward an optimal geomagnetic field intensity determination technique. *Geochem. Geophys. Geosyst.* **5**, Q02H07 (2004).

17. L. Tauxe, H. Staudigel, Strength of the geomagnetic field in the cretaceous normal superchron: New data from submarine basaltic glass of the Troodos Ophiolite. *Geochem. Geophys. Geosyst.* **5**, Q02H06 (2004).
18. J. L. Kirschvink, The least-squares line and plane and the analysis of paleomagnetic data. *Geophys. J. Roy. Astron. Soc.* **62**, 699–718 (1980).
19. D. R. Glenn, R. R. Fu, P. Kehayias, D. Le Sage, E. A. Lima, B. P. Weiss, R. L. Walsworth, Micrometer-scale magnetic imaging of geological samples using a quantum diamond microscope. *Geochem. Geophys. Geosyst.* **18**, 3254–3267 (2017).
20. L. F. White, J. R. Darling, D. E. Moser, D. A. Reinhard, T. J. Prosa, D. Bullen, D. Olson, D. J. Larson, D. Lawrence, I. Martin, Atomic-scale age resolution of planetary events. *Nat. Commun.* **8**, 15597 (2017).
21. N. E. Timms, S. M. Reddy, J. D. Fitz Gerald, L. Green, J. R. Muhling, Inclusion-localised crystal-plasticity, dynamic porosity, and fast-diffusion pathway generation in zircon. *J. Struct. Geol.* **35**, 78–89 (2012).
22. S. Piazolo, A. La Fontaine, P. Trimby, S. Harley, L. Yang, R. Armstrong, J. M. Cairney, Deformation-induced trace element redistribution in zircon revealed using atom probe tomography. *Nat. Commun.* **7**, 10490 (2016).
23. T. Geisler, U. Schaltegger, F. Tomaschek, Re-equilibration of zircon in aqueous fluids and melts. *Elements* **3**, 43–50 (2007).
24. A. J. Cavosie, S. A. Wilde, D. Liu, P. W. Weiblen, J. W. Valley, Internal zoning and U-Th-Pb chemistry of Jack Hills detrital zircons: A mineral record of early Archean to Mesoproterozoic (4348-1576 Ma) magmatism. *Precambrian Res.* **135**, 251–279 (2004).
25. X. Quidelleur, M. Grove, O. M. Lovera, T. M. Harrison, A. Yin, F. J. Ryerson, Thermal evolution and slip history of the Renbu Zedong thrust, southeastern Tibet. *J. Geophys. Res.* **102**, 2659–2679 (1997).

26. C. Patterson, D. Settle, B. Glover, Analysis of lead in polluted coastal seawater. *Mar. Chem.* **4**, 305–319 (1976).
27. C. J. Spencer, C. L. Kirkland, R. J. M. Taylor, Strategies towards statistically robust interpretations of in situ U-Pb zircon geochronology. *Geosci. Front.* **7**, 581–589 (2016).
28. Q. Wang, S. A. Wilde, New constraints on the Hadean to Proterozoic history of the Jack Hills belt, Western Australia. *Gondw. Res.* **55**, 74–91 (2018).
29. E. A. Bell, P. Boehnke, M. D. Hopkins-Wielicki, T. M. Harrison, Distinguishing primary and secondary inclusion assemblages in Jack Hills zircons. *Lithos* **234–235**, 15–26 (2015).
30. M.-C. Liu, K. D. McKeegan, T. M. Harrison, G. Jarzebinski, L. Vltava, The Hyperion-II radio-frequency oxygen ion source on the UCLA *ims1290* ion microprobe: Beam characterization and applications in geochemistry and cosmochemistry. *Int. J. Mass Spectrom.* **424**, 1–9 (2018).
31. E. A. Bell, T. M. Harrison, M. T. McCulloch, E. D. Young, Early Archean crustal evolution of the Jack Hills zircon source terrane inferred from Lu-Hf,  $^{207}\text{Pb}/^{206}\text{Pb}$ , and  $\delta^{18}\text{O}$  systematics of Jack Hills zircons. *Geochim. Cosmochim. Acta* **75**, 4816–4829 (2011).
32. T. Berndt, A. R. Muxworthy, K. Fabian, Does size matter? Statistical limits of paleomagnetic field reconstruction from small rock specimens. *J. Geophys. Res. Solid Earth* **121**, 15–26 (2016).
33. G. A. Paterson, L. Tauxe, A. J. Biggin, R. Shaar, L. C. Jonestrask, On improving the selection of Thellier-type paleointensity data. *Geochem. Geophys. Geosyst.* **15**, 1180–1192 (2014).
34. P. W. Reiners, R. W. Carlson, P. R. Renne, K. M. Cooper, D. E. Granger, N. M. McLean, B. Schoene, *Geochronology and Thermochronology* (Wiley, 2017).